STUDY OF THE PHYSICOCHEMICAL PROPERTIES OF ORGANIC MOLECULES IN GEL AND AGGREGATED STATES USING MORPHOLOGICAL AND PHOTOPHYSICAL CHARACTERIZATION TECHNIQUES

A Thesis

Submitted for the Degree of

DOCTOR OF PHILOSOPHY

by

Soumya Sivalingam

School of Chemistry

University of Hyderabad

Hyderabad – 500 046

INDIA

December 2014

Dedicated

To

My Family

“A person who never made a mistake never tried anything new.”

Albert Einstein

“Educating the mind without educating the heart is no education at all.”

Aristotle

CONTENTS

STATEMENT

I hereby declare that the matter embodied in the thesis entitled "***Study of the Physicochemical Properties of Organic Molecules in Gel and Aggregated States using Morphological and Photophysical Characterization Techniques***" is the result of investigations carried out by me in the School of Chemistry, University of Hyderabad, India under the supervision of **Prof. Anunay Samanta**.

In keeping with the general practice of reporting scientific investigations, the acknowledgements have been made wherever the work described is based on the findings of other investigators. Any omission or error that might have crept in is regretted.

December 2014 **Soumya Sivalingam**

SCHOOL OF CHEMISTRY

UNIVERSITY OF HYDERABAD

HYDERABAD-500 046, INDIA

Phone: +91-40-2313 4813(O)
+91-40-2313 0715 (R)
Fax: +91-40-2301 1594
Email: assc@uohyd.ernet.in
anunay.samanta@gmail.com

Prof. Anunay Samanta

CERTIFICATE

Certified that the work embodied in the thesis entitled "***Study of the Physicochemical Properties of Organic Molecules in Gel and Aggregated States using Morphological and Photophysical Characterization Techniques***" has been carried out by **Ms. Soumya Sivalingam** under my supervision and the same has not been submitted elsewhere for any degree.

Anunay Samanta
(Thesis Supervisor)

Dean
School of Chemistry
University of Hyderabad

Acknowledgement

I express my sincere gratitude to Prof. Anunay Samanta, my research supervisor, for his constant cooperation, encouragement and kind guidance. He has been quite helpful to me in both academic and personal fronts.

I would like to thank the former and present Dean(s), School of Chemistry, for their constant support, inspiration and for the available facilities. I am extremely appreciative individually to all the faculty members of the school for their help, cooperation and encouragement at various stages.

I would like to acknowledge Dr. S. Venugopal Rao for the femtosecond Z-scan facility at Advanced Centre for Research in High Energy Materials (ACRHEM), University of Hyderabad, Hyderabad. I am thankful to Mr. Pavan Kumar, Dr. S. M. Ahmed and Miss. Nalini of Central Instrumentation Laboratory of University of Hyderabad, for helping with Scanning Electon Microscope (SEM) and fluorescence microscopy. I thank Mr. Durga Prasad for Transmission Electron Microscope (TEM) measurements at Centre for Nanotechnology, University of Hyderabad.

Financial assistance from DST and CSIR, New Delhi is greatly acknowledged. Special thanks are due to CSIR for providing me a research fellowship.

I am grateful to all my former teachers for their help and encouragement. I express my heartfelt appreciation to Krishnan Sir and Achamma Miss for the guidance and encouragement they have been giving to me till to date. No doubt that, today I am here due to them. I must not forget to thank my closest buddies ever, Soumya, Divya, Sreedevi, Midhun, Pramod, Maidhily and Pratheesh.

I value my association with my former lab-mates: Ravi, Dinesh, Santhosh, Tanmay, Sanghamitra, Uday and Praveen from whom I have learned many valuable aspects of research. I am extremely thankful to Santhosh anna for giving me useful advices. I acknowledge my present colleagues, Shalini, Satyajit, Ashok, Chandrasekhar, Navendu, Sudipta and Sneha for maintaining the friendly and cooperative atmosphere in the lab. I would also like to thank my project student, Chenthamizhan who helped me in my research projects. I am extremely thankful to Shalini di for the help and support she renders both, academically and personally. I had spent a wonderful time with her, Rudresh da and Ma.

I thank all the non-teaching staff of the school of chemistry for their time-to-time cooperation. They had all been quite helpful.

I had a wonderful time in this University with Ashitha, Anusha, Ambili, Prasanna, Simi, Greeshma and Megha. I never felt lonely in the hostel due to their company. They made my stay possible in Hyderabad during these years. Moments spent with Tulika, Nabamita and Iqra are precious. I will cherish each and every minute I spent with them throughout my life. I would like to thank Hari, Kesav, Srujana, Lasya, Chakri and Radha Krishna for the 'bindas' moments we spent together. I extend my thanks to Sandeep, Joby and Vimal for sharing the Chai time in shop com. I am really lucky to have friends like Viji, Prabhu, Prabha, Tamil Arazhi, Sajna, Venu Srinivas, Rajesh, Bheem, Pradipta, Dilip, Bagmi, Saritha, Arun, Salah, Rudro, Sreetamma, Sugatha, Tanmoy, Arpita, Debparna,Raziya, Murali, Sunil, Vignesh, Prasad, Sudheer, Anirban, Careena, Sherin and Sivaja. I wish the time spent with my little sisters, Meera, Mumul and Hamsa never ends. I should thank Krishnan Kartha for always sending me articles immediately.

I would like to thank all my relatives and neighbors for their close association with me.

Dedicating this thesis is just a small gift to my family. It gives me immense pleasure to thank Akku, Aliyan, Annu, Harshi chechi, Annan, Mithu chechi, Akka, Aliyan, Kimon, Lakshmi and Dili for the wonderful moments we had spent together. I am lucky to have them in my life. I am blessed with Chachi, Achu, Shreyu, Malu, Suddhu, Devu and Rudhroos. Without them life would have been colorless. I specially thank Periyamma, Periyappa, Brindhaunty, Chithappa, Kunju, Atha, Kala, Kailu, Maniyannan, Geetha Chechi, Vaishu and Mrinu for their care and understanding

This thesis would not have been completed without the selfless love, care and support of Amma and Achan. I don't have words to express my gratitude to them. Amma, I thank you for your selfless devotion to the family. No one can love and understand me as much as you can.

This thesis and my life will be incomplete without thanking you, Pavanu. You are so special to me. No words will be sufficient to express my gratitude to you for the love, care, encouragement and patience you have on me.

Soumya

List of Publications

1. "Fluorescence Quenching of CdS Quantum Dots by 4-Azetidinyl-7-Nitrobenz-2-Oxa-1,3-Diazole: A Mechanistic Study." K. Santhosh, S. Patra, **S. Soumya,** D. C. Khara and A. Samanta, ***ChemPhysChem***, 12 **(2011),** 2735-2741.
2. "CdTe Quantum Dots in Ionic Liquid: Stability and Hole Scavenging in the Presence of a Sulfide Salt." M. Chandra Sekhar, K. Santhosh, J. Praveen Kumar, N. Mondal, **S. Soumya,** and A. Samanta, ***J. Phys. Chem. C***, 118 **(2014)** 18481-18487.
3. "Contrasting Fluorescence Response of Two Dipolar Probe Molecules in a Leucine-based Organogel and Its Implications." **S. Soumya,** S. Seth, S. Paul and A. Samanta ***(submitted)***.
4. "Controlled Fabrication, characterization and (linear and non-linear) optical properties of phenazenium dye aggregates." **S.Soumya** and A. Samanta ***(manuscript under preparation).***
5. "Cyanine Dye Induced Fluorescence Quenching of an Oligo(p-phenylenevinylene)-based Self-Assembly: Presence of Multiple Aggregates and Selective Quenching." **S.Soumya** and A. Samanta ***(manuscript under preparation).***
6. "Förster Resonance Energy Transfer in Agarose Hydrogel." **S.Soumya** and A. Samanta ***(manuscript under preparation).***

Conference Presentations

Oral Presentation

1. "Contrasting Fluorescence Response of Two Dipolar Probe Molecules in a Leucine-based Organogel - Role of Hydrogen Bonding Interactions", **Chemfest-2014, 10th Annual In-House Symposium of the School of Chemistry,** University of Hyderabad, February 21st-22nd, **2014.**

Poster Presentations

1. "On the morphology, photophysical and nonlinear optical properties of phenazinium dye aggregates", **Third International Conference on Frontiers in Nanoscience and Technology, Cochin Nano,** Cochin, Kerala, August 14th-17th, **2011.**

2. "Organic Dye Induced Quenching of an Oligo (p-phenylenevinylene)-Based Self-Assembly: Presence of multiple aggregates and selective quenching", **4th Interdisciplinary Symposium on Materials Chemistry (ISMC)** organized by Bhabha Atomic Research Centre (BARC), Mumbai, Maharashtra, December 11th – 15th, **2012. (Best Poster Presentation Award)**

3. "Role of Hydrogen Bonding Interactions in a Leucine-based Organogel: A Fluorescence Study", **Trombay Symposium on Radiation and Photochemistry (TSRP),** Bhabha Atomic Research Centre (BARC), Mumbai, Maharashtra, January 6th – 9th, **2014.**

4. "Contrasting Fluorescence Response of Two Dipolar Probe Molecules in a Leucine-based Organogel - Role of Hydrogen Bonding Interactions", **Chemfest-2014, 10th Annual In-House Symposium of the School of Chemistry,** University of Hyderabad, February 21st-22nd, **2014.**

Thesis Layout

The thesis has been divided into seven chapters. ***Chapter 1*** starts with an introduction on organic nanoparticles, including their theory of aggregation, various methods of fabrication, mechanism of formation, optical and non-linear optical properties and photophysical applications. The chapter also discusses the disadvantages on organic nanoparticles, need for gels, various classifications of gels, their preparation and mechanism of formation followed by wide variety of properties and chemical and biological applications. Motivation behind the thesis and the systems studied are also discussed. ***Chapter 2*** provides the details of the materials, methods of synthesis, methods of purification of the solvents, various methodologies for the sample preparation for different experiments, instrumentation and methods of data analysis. ***Chapter 3*** compares the optical and non-linear optical response and morphology of phenazenium dye aggregates with self-aggregates formed at higher concentrations. ***Chapter 4*** explains the nature of aggregation and mechanism of fluorescence quenching in OPV self-assembly by OCY in benzonitrile. ***Chapter 5*** delineates the effect of specific interactions between guest molecules encapsulated in an organogel with the gelator. ***Chapter 6*** presents the use of Förster resonance energy transfer from C102 to Rh6G to understand the pore dimensions of in agarose hydrogel in 20% v/v ethanol-water mixture. ***Chapter 7*** summarizes the findings of the present investigations by touching upon the scope of further studies based on the present work.

Chapter 1

Introduction

This chapter provides a brief introduction on organic nanomaterials, presenting the different fabrication methods, mechanism of their formation, properties and applications. This chapter also introduces another important class of materials, gels. It discusses their preparation methods, applications, physicochemical and photophysical properties. A brief discussion of Förster resonance energy transfer is also included. The chapter is concluded by introducing the systems studied and the motivation behind the thesis.

1.1. Nanomaterials

Material science is a branch of science which investigates the relationships that exist between the structures and properties of materials.[1] Material engineering is a closely related branch which uses these structure–property correlations to design or engineer the structure of a material so as to obtain a predetermined set of properties in them.[1] Material chemistry combines both material science and material engineering to provide an overview of various types of materials, synthetic methodologies and relationships between the structures of materials and their overall properties.[2] Material chemistry mainly deals with nanomaterials which are defined as substances where at least one dimension is less than approximately 100 nanometers.[3] Nanomaterials exhibit significantly different and interesting properties from those of the constituent atoms/molecules as well as the

bulk materials. Suitable control of the properties of nanomaterials by material engineering can lead to the fabrication of new devices.[3]

One of the main advantages of nanomaterials is their high surface area to volume ratio compared to the bulk materials. This large surface to volume ratio significantly changes the role played by surface atoms in determining their thermodynamic properties. The reduced coordination number of the surface atoms increases the surface energy. This leads to dramatic changes in optical, electronic, magnetic, mechanical and catalytic properties of materials. For example, the melting temperature of gold nanoparticles (smaller than 5 nm) decreases to ~300 °C, where as the bulk melting temperature is 1063 °C.[4] Nanomaterials can be nanoscale in one dimension (rods or tubes), two dimensions (sheet), or three dimensions (cubes). They can exist as single, fused, aggregated or agglomerated forms. Nanomaterials can be broadly classified into inorganic and organic nanoparticles based on the materials used for the synthesizing the constituent building blocks. As the name indicates, organic nanoparticles are prepared using organic compounds. Nanoparticles formed from metals, alloys and semiconductors fall under inorganic nanoparticles. As this thesis is devoted to the study of organic nanomaterials/self-assemblies, the following sections will discuss about self-aggregation, advantages of organic nanoparticles over self-aggregates, various procedures for their preparation, mechanism of formation of organic nanoparticles and gelation.

1.1.1. Organic nanomaterials

In comparison to semiconductor and metal nanoparticles, the history of organic nanoparticles is not long. Even though close to 15 million kinds of

organic compounds have been synthesized so far in laboratories and are used in our day to day lives, the examples for organic nanoparticles are not many.[5,6] Like metals and semiconductors nanoparticles, it is expected that organic nanomaterials should also show interesting physical and chemical properties when their size is brought down to mesoscopic regime.[6] Before discussing organic nanoparticles further, it is important to discuss self-aggregation as it forms the foundation for the studies of organic nanoparticles. The self-association/aggregation of molecules is a frequently encountered phenomenon due to the strong intermolecular interactions between the molecules.

Cyanine dyes were well known before the discovery of aggregates and their unusual spectral behavior was observed independently by Scheibe *et al.* and Jelley. Later they concluded that these abnormalities in the spectra are due to a phenomenon called "aggregation". Thus the self-aggregation of dyes in concentrated aqueous solutions was first reported in cyanine dyes in 1936.[7,8] Later it was found that not only cyanine dyes, most of the dyes like squarine, merocyanine and perylene bisimide dyes also undergo self-aggregation.[9-14] Aggregation can be defined as a direct mutual attraction between particles (atoms or molecules) *via* van der Waals forces or chemical bonding. More commonly, it results in the self-association of particles in solution to form larger particles. The aggregates in solution exhibit distinct changes in the absorption band as compared to the monomeric species.[15,16] From the spectral shifts, various aggregation patterns of the dyes in different media have been proposed. The bathochromically shifted J-bands (named after Jelley, one of the first workers who investigated these shifts) and hypsochromically shifted H-bands (H for hypsochromic) of the

aggregates have been explained in terms of molecular exciton coupling theory, i.e., coupling of transition moments of the constituent dye molecules.[17-19] The J-aggregate can be defined as a one-dimensional molecular arrangement in which the transition moments of the individual monomers are aligned parallel to the line joining their centers (end-to-end arrangement). The H-aggregate is also a one-dimensional array of molecules with the transition moments of individual monomers aligned parallel to each other but perpendicular to the line joining their centers (face-to-face arrangement).

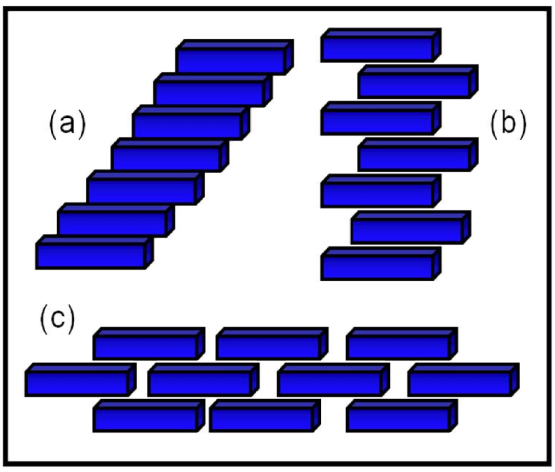

Figure 1.1. Schematic representation of the different arrangement of aggregates in solution. (a) Staircase-type, (b) Ladder-type and (c) Brickwork-type.

The aggregates that exhibit J-bands are called J-aggregates and H-aggregates exhibit H-band. The red-shifted J-aggregate is the most commercially important dye assemblage for photographic spectral sensitization.[20] Both these aggregates, can exist as a one-dimensional assembly in solution that could be in (a) staircase, (b) ladder, or (c) brickwork type of arrangement[21] as shown in Figure 1.1. This

arrangement depends on the type of interactions between the chromophores and also on the solvent-chromophore interactions, common of which are hydrogen bonding, π-π stacking, metal-ligand coordination (in case of porphyrin derivatives) etc.[22-24] All these interactions play an important role in deciding the final morphology of the aggregates as rod, cubes, spheres, octahedrons etc. The optical properties of the aggregates in turn depend on their morphology.[25]

According to the exciton theory, dye molecule is regarded as a point dipole. On irradiation, two identical molecules come close to each other and their transition dipole moments will start interacting. This, so called, excitonic coupling can be understood on the basis of Figure 1.2. When two dipoles are brought into close proximity, their relative orientation (parallel *vs.* antiparallel) will cause two things to happen: a) the energy of individual molecules, *E*, will split into two new states with the energies E_1 and E_2. The parallel dipoles repel each other and get the higher energy state, while the antiparallel dipoles attract, which lowers the energy of that state b) parallel dipoles make up an overall higher dipole moment, i.e. stronger absorption, while antipareallel dipoles cancel each other resulting in a weak absorption. The net result now is a blue-shift in the absorption. Similarly for head-to-tail arrangement, the lower energy state has larger transition dipole moment and the net effect is a red-shift of absorption. The intermediate, oblique orientation results in band splitting, i.e. two bands appearing at lower and higher energy.[26] The angle between the line of centers of a column of dye molecules and the long axis of any one of the parallel molecules is called the 'angle of slippage', α. Large molecular slippage ($\alpha < 54.7^{\circ}$) results in a bathochromic shift (J-

aggregate), and small slippage ($\alpha > 54.7^{o}$) results in a hypsochromic shift (H-aggregate).[18,19]

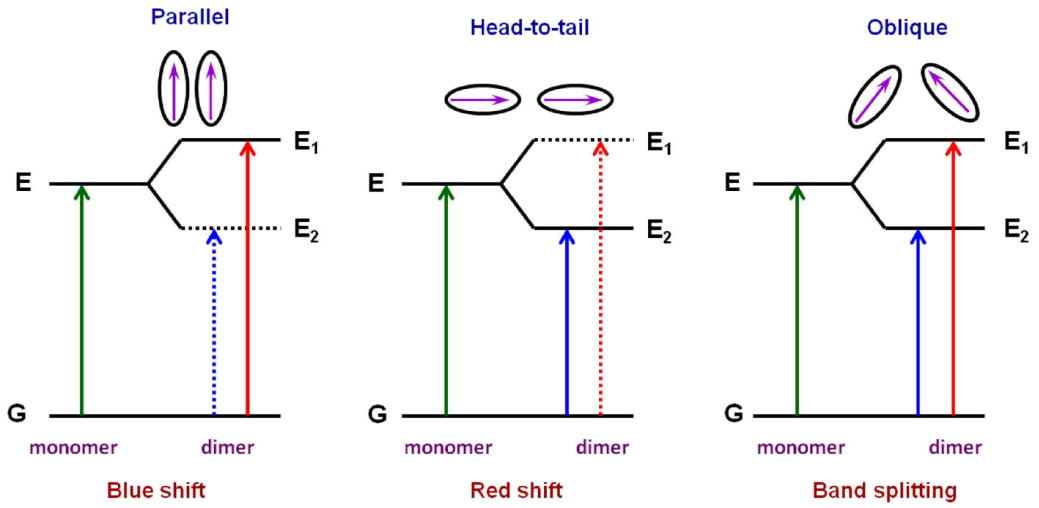

Figure 1.2. Scheme of the exciton band structure in molecular dimers with various geometrical arrangements of transition dipole moments.

H-aggregates are characterized by the large Stokes shift and decreased quantum yield where as J-aggregation results in a decrease in Stokes shift along with increase in quantum yield.[15] A new branch of chemistry has slowly evolved that designs molecules which will form only J-aggregates or seeks new aggregation methods for the existent organic compounds such that they will form only J-aggregates emerged and the resultant new class of materials are coined as organic nanoparticles. Therefore organic nanoparticles are nothing but the result of induced aggregation of organic compounds to enhance the optical properties. The conventional fabrication techniques used for semiconductor and inorganic nanoparticles cannot be applied in the case of organic nanoparticles due to the

instability of organic compounds at elevated temperatures. Hence, new synthetic methods need to be developed for the fabrication of organic nanoparticles. Some of the common fabrication methods of organic nanoparticles are discussed in the following section.

1.1.1.1. Fabrication methods

1.1.1.1.1. Reprecipitation method

Reprecipitation, which is a solvent displacement method, was first reported by Nakanishi and coworkers.[27-29] This is a very simple and versatile method to prepare organic nanoparticle dispersions. The method involves rapid mixing of a small amount of concentrated stock solution of the target compound dissolved in a good solvent (in terms of solubility) with excess of a poor solvent. The great difference in the solubility of the target compound in the good and poor solvents and the good miscibility of the two solvents are the necessary conditions for this method. The rapid mixing of the stock solution and the poor solvent, changes the micro-environment of the target compound molecules. The sudden exposure of the target molecules to the poor solvent surroundings in a very short time induces nucleation and growth of nanoparticles. In general, water is used as the poor solvent because of the low solubility of organic compounds in it. A series of organic nanoparticles were successfully fabricated using this method by several groups. Nanoparticles of β-carotene was prepared by Horn and coworkers and the influence of both supramolecular structure and particle size on the absorption spectra was studied.[30] Majima's group and Barbara's group prepared nanocrystals

from perylene and a perylene derivative, respectively, using this technique and studied the spectroscopy of the single nanoparticles.[31,32]

A modified version of reprecitation method is used for target molecules which are soluble in water. In this method the concentrated stock solution is prepared in water and then injected rapidly into large quantity of an organic solvent, which is miscible with water. This method is known as inverse reprecipitation[29] and illustrated in detail in Figure 2.1(chapter 2).

1.1.1.1.2. Chemical Reaction method

Though reprecipitation is a facile method for the preparation of organic nanoparticles, it is difficult to form kinetically stable nanoparticle dispersions using this method. Moreover, large-scale fabrication of nanoparticles is limited due to the solubility of the target compound in the good solvent. In addition to that, the heterogeneous environment of this method makes it difficult to precisely control the complicated nucleation process in the initial stages and the subsequent fast growth.[33] Consequently, there will be a broad distribution in both size and shape of the organic nanoparticles prepared using this method. Recently, Yao and coworkers developed a colloidal chemical reaction method to overcome these problems.[34] Using this method, the perylene nanoparticles were prepared by the reduction of perylene perchlorate by Br^- anions in the presence of cetyl trimethylammonium bromide (CTAB) in acetonitrile.[35] The large-scale synthesis of perylene nanoparticles ranging from 25 to 90 nm was achieved by changing the molar ratio of CTAB to perylene perchlorate. Furthermore, hierarchical self-organization of 25 nm perylene nanoparticles was observed, forming nanobelts

and/or square nanorods when the molar ratio was increased above 1.0. The homogeneous solution phase in this method provides several advantages, including facile separation of the nucleation and growth stages and better controllability of the growth parameters, through which control over the size of the organic nanoparticles could also be achieved.

1.1.1.1.3. Soft template assisted preparation

The template method is a straightforward way to fabricate nanostructures by inducing the target materials to grow according to the patterns of the employed templates. This strategy provides an easy way for the synthesis of nanomaterials with desired shape and size, and has been widely applied in the construction of 1D nanostructures. This method uses surfactant micelles, complexes, biomolecules, and copolymers as templates. It is well known that micelles or reverse micelles with different shapes, such as spherical or rod-like, will be formed in the surfactant solutions, above the critical micelle concentration (CMC). These can then be used as soft templates for the fabrication of nanostructures. Yao and coworkers reported nanofibers of 1,3-diphenyl-2-pyrazoline (DP) induced by CTAB micelles. They observed that the shape and size of the obtained nanostructures can be controlled by changing the molar ratio of DP to CTAB. At lower DP/CTAB molar ratios, CTAB tends to form spherical micelles, and increasing the DP/CTAB ratio will induce the sphere-to-rod transition of the micelles, which act as a template to direct the 1D growth of DP. Using the same method, Wan and coworkers also prepared nanotubes from zinc mesotetra-(4-pyridyl) porphyrin and constructed 3D arrays of the prepared

nanotubes on substrates. Zhang *et al.* used sodium dodecyl sulfate (SDS) micelles as templates to direct the 1D growth of pyrene molecules in an aqueous phase.

1.1.1.1.4. Vapor deposition

Vapor deposition (VD) is a facile and feasible method for preparing nanomaterials and has achieved great success in fabricating organic 1D nanostructures. In this method, a thin film of the precursor is coated on a suitable substrate by condensing its vapor. However, the monodispersity of the nanoparticles is hard to control when small organic molecules are selected as deposition sources. In this method, degree of saturation is the predominant factor in controlling the morphology and dispersity of the products, and it is possible to process most solid materials into 1D nanostructures by maintaining the vapor saturation at a low level.[36] Several techniques have been adopted to control the local supersaturation in the preparation of organic 1D nanomaterials by VD. For example, Lee *et al.* introduced anodized aluminium oxide (AAO) templates to the VD experiment.[37] Rubahn and coworkers and Perng and coworkers controlled the substrate temperatures to ensure the uniform 1D growth of organic molecules.[38,39] Yao and coworkers reported an adsorbent-assisted physical vapor deposition (PVD). Adsorbents such as neutral aluminum oxide or silica gel, used widely in column chromatography, were introduced into the VD method to control the degree of saturation, considering that there should exist an adsorption–desorption equilibrium between the adsorbents and the organic sources.[40-43] The length and diameter of the nanowires prepared using this method can be well controlled by varying the deposition conditions, such as time and temperature.

Few other methods like self-assembly with solvent evaporation,[25] hard template assisted preparation,[44-46] and self-assembly through organogelation[47-49] are also used for the preparation of organic nanoparticles, and they are not discussed here due to their limited utility. Among the various methods used, reprecipitation method is the most popular method for the fabrication of organic nanoparticles as it is simple, less expensive and has the ability to produce various morphologies under ambient conditions.

1.1.1.2. Nucleation and nanocrystallisation mechanism in reprecipitation and inverse reprecipitation method

For the preparation of dye aggregates we have used inverse reprecipitation method. Hence, it is important to illustrate the mechanism of nanoparticle formation in this method. Nakanishi *et al.* proposed a model for the growth mechanism of the microcrystals.[5] According to this, when the stock/probe solution of the target molecule in good solvent is injected into the poor solvent under sonication, the probe solution disperses and forms droplets. As both the solvents are miscible, the solvent shell around the droplets will be removed which results in the formation of amorphous clusters. Nucleation followed by growth of nanoparticles occurs through thermal collision between these clusters.[50-52] The size of the nanocrystals formed are governed by the size of the initial droplet formed. By reducing the amount of stock solution injected into the poor solvent and by using surfactants the size of the droplets can be controlled.

1.1.1.3. Optical properties

Organic nanoparticles exhibit unique and interesting optical properties due to aggregation of molecules in the nanostructures. These properties are however different form their inorganic counterparts as organic materials have weak interactions like hydrogen bonding, π-π stacking and van der Waals interactions. Besides exploring the fabrication methods, much effort has been made to investigate the optical properties of organic nanomaterials. As the bathochromic or hypsochromic shifts in the spectra depends on the solvent, structure of the organic compound used, nature of interactions and aggregation, a generalization of the spectral properties for all organic nanoparticles cannot be made.

1.1.1.3.1. Absorption

Nakanishi and coworkers first observed the size dependent optical properties in perylene nanocrystals (20-100 nm).[53-55] They observed a bathochromic shift with increasing particle size which was attributed to the lattice softening during the conversion from molecules to aggregates. Yao and coworkers prepared organic nanoparticles of a pyrazoline derivative, PDDP by reprecipitation method.[56] They observed that compared to the monomer the nanoparticles exhibit a red-shifted absorption along with a new peak at the higher wavelength region. With increasing particle size, the absorption spectra exhibited bathochromic shift and the new peak became more prominent. They concluded that the bathochromic shift is due to the increased overlap of the pyrazoline ring π-orbitals in the nanoparticles and also due to the increased intermolecular interactions between PDDP molecules with increasing size. The newly emerged peak was attributed to

the extended charge-transfer (CT) state of the aggregates resulting from the close stacking of PDDP molecules in the nanoparticles.

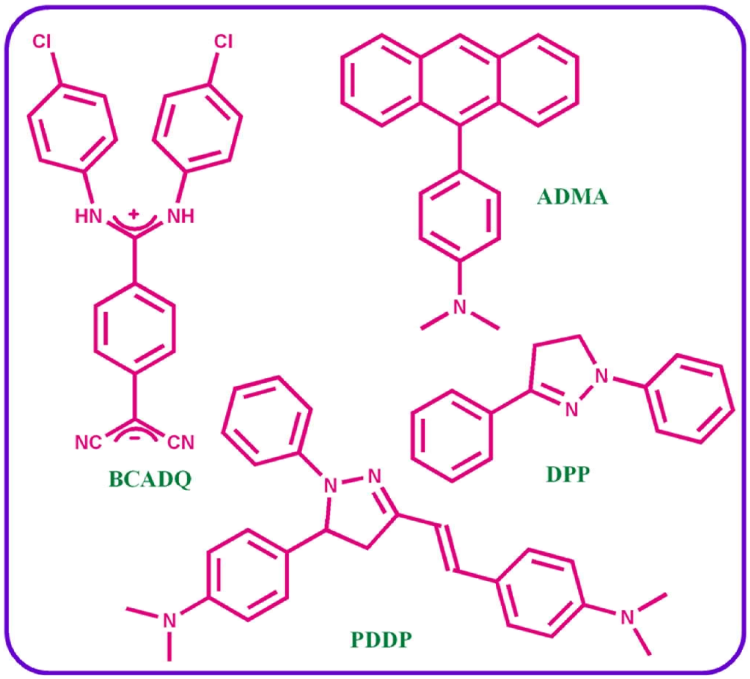

Chart 1.1. Structures of some organic compounds used for making organic nanoparticles.

1.1.1.3.2. Fluorescence

Organic nanoparticles exhibit size tunable emission behavior. The size dependent emission in perylene microcrystals has been explained by the lattice softening and the electric field effect of the surrounding media on the microcrystals.[53,57] With increasing particles size of PDDP, the intramolecular charge transfer (ICT) fluorescence is broadened and the peak position shifts towards longer wavelength compared to the monomer.[56] Same group have

reported multiple emissions from diphenyl pyrazole, DPP nanoparticles which are tunable from near UV to visible with change in morphology.[58] Patra *et al.* observed size dependent optical properties for BCADQ nanoparticles due to the structural rigidification of the molecules in the nano/microcrystals.[59] Structural rigidification of an electron donor-acceptor molecule ADMA has been observed by our group resulting in a size dependent emission of the nanoparticles.[60]

1.1.1.4. Nonlinear optical properties

Organic nanoparticles exhibit excellent non-linear optical properties. Non-linear optical properties of organic nano/microcrystals using techniques like third harmonic generation, Z-scan and degenerate four wave mixing was first explored by Nakanishi.[61] Colloidal solutions or thin films fabricated using organic nanoparticles were used for carrying out the measurements. The non-linear optical properties of nano/microcrystals are always found to be higher than the monomer.[62] This is due to the increased electron density in the aggregates due to close packing of constituent molecules. In aggregates, the electron clouds are localized and hence the perturbation of this electron cloud will be more by the electric field created by laser, in comparison to monomer.[63] Patra *et al.* have carried out Z-scan measurements in BCADQ nano/microcrystals and found the non-linear properties to be dependent on the particle size.[64] Open aperture Z-scan studies reveal appreciable 4-photon absorption in the colloidal materials.

1.1.1.5. Applications of organic nanoparticles

Organic nanoparticles are suitable candidates for various applications due to their unique optical properties.[38,65-67] Tubular organic nanoparticles have high

wave guiding performance.[68] A waveguide is a structure that guides light waves without much loss of energy. They have higher refractive indices than their environment and can guide light by total internal reflection at the interface. Rubahn and coworkers reported in 2003 that nanofibers of p-hexaphenyl fabricated by vacuum sublimation could act as effective waveguides for blue light.[38] Similarly H-aggregates of thiocyanine nanofibers can waveguide photoluminescence in the range of 520 to 560 nm over 250 μm without any loss of energy.[65] Nanobelts of 9, 10-diphenylanthracene (DPA) doped with Nile red (NR) acts as efficient acid vapor sensors.[69] This is accomplished by interrupting the charge transfer by protonating the N atoms by acids which leads to opening of energy transfer process between DPA and NR. Pentacene and rubrene nanocrystals are patterned in arrays to form single-crystal transistors.[70,71] Other than these applications, organic nanoparticles are widely used in logic gates, sensing hydrazine vapors, fluorescence signaling, multicolor and white light emission.[72,73]

Even though they have many advantages over self-aggregates formed at higher concentrations, one of the main disadvantage of organic nanoparticles is that, they exist in colloidal state. In colloidal state, they undergo Ostwald ripening which results in the formation of larger particles at the cost of smaller ones and hence losing the properties they acquired due to small size. This can be avoided to some extent by using surfactants, as the organic nanoparticles are then formed inside the pools of the surfactants. Special techniques are required to pattern or arrange organic nanoparticles on a solid surface in the required size and morphology, which are not very easy.[74,75] Therefore need for a material which

contain organic nanoparticles but in the solid state where there are no chances of Ostwald ripening is required to use them effectively for various applications.

From ancient times, gels were known to mankind as gels are commonly used in foods. Typical gelled food items like tofu were known from A.D. 20.[76] A brief descriptions of gels, their classifications, and mechanism of formation, properties and applications are discussed in the following sections.

1.2. Gels

Gels are solid, jelly-like material which can be defined as a dispersion of molecules of a liquid within a solid in which the solid is the continuous phase and the liquid is the discontinuous phase.[76] Gels are formed by the cross linking of one dimensional (1D) nanofibers to form a 3D network which can hold or trap large quantities of solvents thereby preventing its flow.[77] The fibers in turn are formed by the self-assembly/aggregation of monomer molecules through non-covalent interactions like π-π stacking, hydrogen bonding, co-ordination bonding, and van der Waals interactions.[78] Gels which have absorbed large quantities of solvents behave as materials in between solid and liquid state and their physical properties change from viscous liquids to hard solids according to the chemical composition.[79]

1.2.1. Classification of gels

Gels can be classified depending on the interactions between the molecules, solvents used for gelation, occurrence etc as follows:

1.2.1.1. Based on solvents

Classification of gels based on the nature of solvents used for gelation is one of the simplest and most basic classification.[76] When water is used as the solvent the gels are known as hydrogels and the use of organic solvents results in the name organogels. Xerogels are gels from which the solvent has been removed by freeze drying. When air is flushed into xerogel, then it is called as aerogel. Similarly if the gels are made using ionic liquids, then they are known as ionogels. Maruyama and coworkers reported a versatile supramolecular gelator which can form hydrogel, organogel as well as ionogel.[80]

1.2.1.2. Based on nature of the monomer

The gels formed by the polymerization of materials like agar and agarose are called polymer gels.[81] Low molecular weight (LMW) gels are formed by the gelation of low molecular weight organic compounds like phenylene vinylenes, lecithine etc.[82-84] The mechanisms of formation of these two gels are slightly different. Polymer gels forms nano/micro fibrils as a result of thermal polymerization of the monomers.[76] These fibrils entangle due to the physical interactions between them to form gels. In case of low molecular weight gels, due to physical interactions between the molecules, self-aggregates starts forming fibrils which form junctions or nodes from where further growth or Ostwald's ripening occurs ultimately resulting in a network structure.[78] The detailed mechanism of gelation of low molecular weight gelators will be discussed in later section.

1.2.1.3. Based on the type of cross-linking

Gels are classified into chemical and physical gels depending on the nature of cross linking. This is the most important classification which gives insight into the interactions in the gels and their properties.

Chemical gels are formed as the result of a chemical reaction. The molecules undergo chemical, mostly covalent bonding to form the gel. These gels cannot be converted into sol and are thus called as irreversible gels. The gels formed by polymerization reactions like that in the formation of silica gels are a classic example of chemically cross linked gels. The polymerization can occur *via* condensation, free radical, radiation or photo polymerization depending upon the molecules used.

Physical gels are also known as reversible gels due to the easy conversion of gel to sol under ambient conditions. Here, the cross linking is due to the weak physical interactions like hydrogen bonding, van der Waals interactions, hydrophobic interactions, π-π stacking and/or electrostatic interactions between the molecules leading to self-assembly/aggregates which results in the formation of fibrils.[81] These fibrils entangle to form a network resulting in gelation.

Physically cross linked gels are explored and understood well as these have more advantages than the chemically cross linked gels in view of their applications.[85-87] Physical gels are soft and gel to sol conversion can be achieved by simply changing the temperature, pH or composition of solvent.[82,88-91] These properties of physical gels makes them highly usable as media for drug transport

and delivery, chemical reactions, catalysis, sensors etc.[92-96] As gels provide a solid matrix and in most cases do not change the properties of the encapsulated guest molecules in it, physical gels can be used as very effective media in many fields of science. Gels which undergo transition to sol with varying temperature are known as thermo-reversible gels.[97]

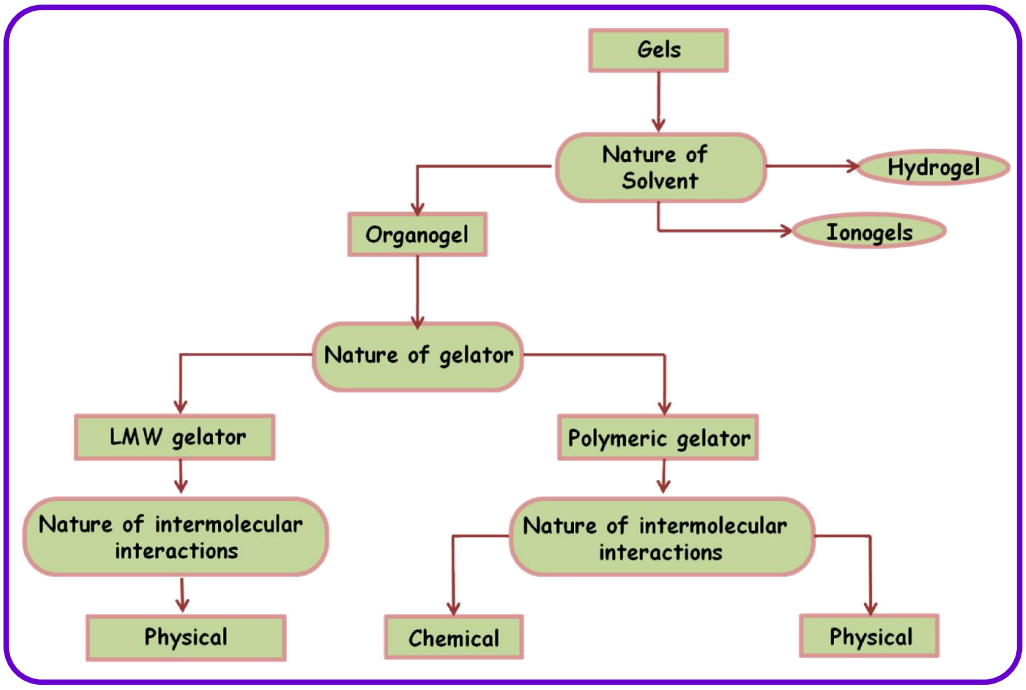

Figure 1.3. Classifications of gels

There are many other classifications in gels which are not very relevant to this thesis, but are worth mentioning. Gels can be classified into natural and synthetic gels depending on the origin of the monomers.[76] According to their emissive properties, gels can be called as fluorescent or non-fluorescent gels. The major classifications of gels can be pictorially represented as shown in Figure 1.3.

Here the classifications are shown only for organogels. Similar classifications follow for hydrogels also.

1.2.2. Preparation of thermo-reversible gels

As discussed earlier, gels can be prepared in numerous ways. However, in our studies since we have used thermo-reversible gels, importance is given to discuss their preparation method and mechanism of gelation. These gels are prepared by heating a weighed amount of the gelator in an appropriate quantity of the solvent in a sealed glass vial until the gelator is dissolved completely.[98-107] The solution was then allowed to cool down to room temperature and gel formation was confirmed by the failure of the transparent soft mass to flow by inverting the vial. An important thing to consider is the amount of gelator used for gel preparation; which depends on the critical gelator concentration (CGC) of the gel in the solvent used. CGC is the minimum amount of gelator required to form a stable gel. The CGC value depends on the gelator and solvent, as the type and extent of intermolecular interactions dictates the formation and stability of gel.[108,109]

1.2.3. Mechanism of gel formation

Gel formation involves two processes.[110] One is the formation of the fibrils and the other involves entanglement of these fibrils to form the gel network. In general, gel formation can occur in two ways. (1) The fibrils are formed and then entangle due to interactions between them or (2) both fibril formation and entangling occurs simultaneously. In the first case polymerization occurs through

condensation, free radical, radiative or photochemical mechanisms and then entangles to form gel. In the second case due to physical interactions fibrils are formed and then during the formation itself forms junctions from where they branch and entangle to form the gel.[76,108,109] In some cases, solvents also take part in gelation.[111] As there are numerous gelation mechanisms which are out of the scope of this thesis, we shall discuss in the following sections only gelation mechanisms of the gelators we used for our studies.

Both oligophenylene vinylene derivative (OPV) and leucine based gelator (OG-leucine) used in our studies, forms thermo-reversible gels. Initially the gelator is added to an appropriate solvent according to the CGC. The saturated solution formed is heated to dissolve the gelator completely. The clear solution is then allowed to cool at room temperature. As the solution cools, the gelator precipitates to form aggregates, which on further cooling entangles, to form gels. The alignment of molecules in the fibrils depends on the various interactions between the gelator molecules.[76,108]

Agarose forms a polymeric gel. Hence, its gelation mechanism is different from that of OPV and OG-leucine. Upon heating agarose polymerizes to form fibrils which exist as random coils in solution. In the initial stages of cooling, the coils form double helices due to hydrogen bonding. These double helical structures link in three dimensions to form interconnected bundles creating pores which can trap solvents.[112,113] The schematic representation is shown in Figure 1.4.

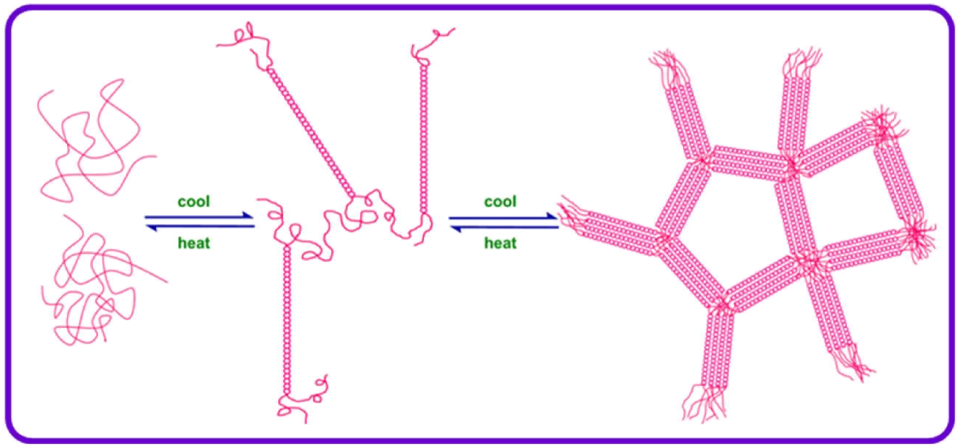

Figure 1.4. Gelation of agarose by formation of double helices.

1.2.4. Properties of low molecular weight (LMW) gels

1.2.4.1. Physicochemical properties

Gels exhibit properties of both liquids and solids. The various physicochemical properties of gels are discussed below.

Viscoelsticity: During gelation, the viscosity of the solution increases and shows maximum viscosity in the gel state. Gels behave like solids at lower shear rates and hence show elastic properties. With an increase in the shear stress, the physical interacting points among the fiber structures become weak. When the shear stress is high enough to disrupt the interactions amongst the fiber structures, the gels starts flowing.[114,115]

Thermo-reversibility: When gels are heated above a critical temperature it loses its solid matrix and starts flowing. This has been attributed to the disruption of the

physical interactions amongst the gelator molecules due to the increasing thermal energy. On subsequent cooling, it reverts back to form gels.[116,117]

Optical Clarity: Depending on the size of fibrils (width and thickness), the gels may be transparent or opaque in nature. Lecithin organogels are transparent in nature while sorbitan monostearate organogels are opaque.[118]

Transport and permeation: Gels can perform simple and/or complex functions of filtration, permeation and transport. By varying the cross link density and tuning the pore size in gels, selectivity in these processes can be attained. An example of gels in which permeability is important is contact lenses. The oxygen permeability of contact lenses increases with increasing water content.[76]

Diffusion: As the pores of the gels are interconnected, the diffusion of guest molecules within the gel matrix is possible, making gel an efficient medium for various chemical and biological processes.[119,120]

Biocompatibility: Many biopolymers like agarose, peptides, sugars and starch forms gels. Due to their biocompatible nature, they can be used for drug delivery applications.[121]

1.2.4.2. Photophysical properties

Although fluorescent gels are widely used in various applications, non-fluorescent gels have attracted significant attention from researchers worldwide due to some of their unique properties, where physical chemists have intense interest in characterizing them through both simulation and experimental

studies.[89,121-128] Various photo-induced processes are being studied in gels primarily to obtain insight into their complex nature and also to exploit some of their properties to control the photochemical processes of various systems.[129,130] Photophysical studies in gels show that they are heterogeneous media in terms of polarity and viscosity.[124,127] The solvation dynamics, rotational dynamics, and energy transfer reactions carried out in these media offered a better understanding of the microenvironment inside the gel media.[129,131,132] Some important photophysical studies in gels are briefly discussed in the following sections.

1.2.4.2.1. Absorption and emission in gels

The absorption and emission of guest molecules (micro environment sensitive probes) in gel gives insight into the complex microenvironment of the gels. The shift in the spectral properties of the guest molecules in comparison to the bulk solvent indicates a change in the microenvironment of the medium.[124,125,127] These spectral properties can be compared with that in solvents of varying polarity and viscosity to get an overall idea of the micro environment around the probe/guest molecules. A similar spectral property of guest molecules in gel and bulk solvent indicates the presence of guest molecules in the solvent pools of the gels which provides a microenvironment identical to that in bulk.

1.2.4.2.2. Excitation wavelength dependent fluorescence

According to Kasha's rule, irrespective of the excitation energy, fluorescence of molecules originates from lowest vibrational energy level of the lowest excited state of the same multiplicity.[133] Therefore, emission spectrum is expected to be independent of excitation wavelength. However, under specific

conditions emission spectrum is found to be dependent on the excitation wavelength. When fluorescent guest molecules are incorporated in non-fluorescent gels, the guest molecules are expected to show an emission spectrum independent of excitation wavelength due to diffusion of guest molecules in gels. But this is not the case in all gels.[125] If the guest molecules (viscosity or polarity sensitive) interacts with the gelator through specific interactions or find regions of varying polarity or viscosity, then the emission of the guest molecule shows significant dependence on excitation wavelength in gel medium. This shows that the microenvironments in the gel media are heterogeneous in nature.[124,127]

1.2.4.2.3. Fluorescence anisotropy – Rotational dynamics

Fluorescence anisotropy is a measure of emission depolarization of a fluorescent molecule that absorbs polarized light.[134] Rotational motion in the excited state is the common cause of emission depolarization. Specific solute-solvent interactions, viscosity and temperature of the surrounding solvent medium are the major parameters, which control the dynamics of solute rotation.[135-137] Therefore, rotational relaxation of the guest molecules in gels through time-resolved fluorescence anisotropy studies can also provide information on the guest-gelator interactions and the properties of microenvironments of the medium. Interestingly, most of the rotational relaxation studies reveal that the rotational times of the guest molecules in gels are dependent on the viscosity of the medium and the specific interactions between the gelator and the guest molecules.[127] However, when the guest molecules are capable of hydrogen bonding interaction with the gels, the observed rotational times are found to be higher than the expected values based on the viscosity of the medium.

1.2.4.2.4. Fluorescence quenching

Any process which results in the reduction of fluorescence intensity of molecules is known as fluorescence quenching.[134] There can be various reasons for fluorescence quenching. One such process which results in diminishing the fluorescence of a molecule is Förster resonance energy transfer (FRET) which is discussed briefly in the next section.

1.2.4.2.4.1. Förster resonance energy transfer (FRET)

FRET is a very important photophysical process which occurs under certain conditions. Transfer of the excitation energy of an initially excited molecule (donor, D) to another (acceptor, A) is possible if the emission spectrum of the donor has an overlap with the absorption spectrum of the acceptor.[134,138,139] It can be represented as

$$^{*}D + A \rightarrow D + {}^{*}A$$

The rate of energy transfer mainly depends upon the extent of this spectral overlap [$J(\lambda)$] of the emission spectrum of the donor with the absorption spectrum of the acceptor, the quantum yield of the donor, the relative orientation (κ^2) of the donor and acceptor transition dipoles, and the distance between the donor and acceptor molecules (R_{DA}). The most common application of FRET is to measure distances between a donor and acceptor present at two sites of a macromolecule.

It is important to distinguish between radiative and non-radiative energy transfer. Radiative transfer corresponds to the absorption of a photon by a

molecule A, which is emitted by a molecule D.[138] Such a transfer does not require any interaction between the partners, but it depends on the spectral overlap and on the concentration. Radiative transfer results in a decrease of the donor fluorescence intensity in the region of spectral overlap. Such a distortion of the fluorescence spectrum is called the inner filter effect.

In contrast, non-radiative energy transfer occurs at distances less than 10 nm, without previous emission of photons, and results from long-range dipole-dipole interactions between the donor and acceptor molecules. For example, non-radiative energy transfer by dipole-dipole interaction is possible at distances up to nearly 10 nm. Consequently, such a transfer provides a tool for determining distances of a few nanometers between chromophores. It is worth noting that the transfer of excitation energy plays a major role in photosynthetic systems.

FRET generally occurs between a donor and acceptor which are separated by distances 10-100 Å. According to the Förster theory, the rate of FRET is inversely proportional to the sixth power of the donor-acceptor distance. FRET can be monitored by the quenching of the donor fluorescence and an enhancement in the acceptor emission. Care should be taken to excite the donor at a wavelength where acceptor has negligible absorption. Decrease in the fluorescence lifetime of the donor is observed in FRET. When monitored at a wavelength where the acceptor emits, and the donor does not show significant emission, a rise time in the acceptor decay profile is expected due to the increase in the excited state population of the acceptor. These life time values are important for calculating the efficiency of FRET. [134,138,139]

According to the Förster theory, the rate of FRET, k_{FRET} is given by

$$k_{FRET} = \frac{1}{\tau_D}\left(\frac{R_0}{R_{DA}}\right)^6,$$

At a donor-acceptor distance $R_{DA} = R_0$, the efficiency of energy transfer is 50% and $k_{FRET} = (1/\tau_D)$. This distance at which FRET is 50% efficient is called as Förster distance and is typically 20-60 Å.The Förster distance, R_0 (in angstroms) is given by

$$R_0 = 0.211[\kappa^2 \eta^{-4} Q_D J(\lambda)]^{1/6},$$

where Q_D is the quantum yield of the donor in the absence of acceptor, η is the refractive index of the medium, κ^2 is the orientation factor, and $J(\lambda)$ is the spectral overlap between the donor emission and acceptor absorption, which is schematically represented in Figure 1.5.

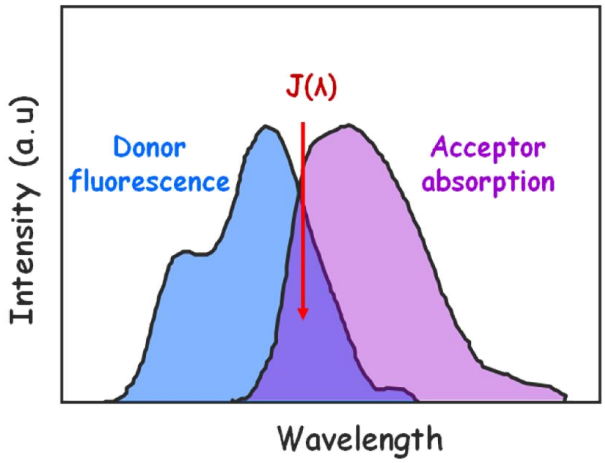

Figure 1.5. Typical spectral overlap between the emission spectra of the donor and the absorption spectra of acceptor.

J(λ) is related to the normalized fluorescence intensity (F_D) of the donor in the absence of the acceptor and the extinction coefficient of the acceptor (ε_A) as

$$J(\lambda) = \frac{\int_0^\infty F_D(\lambda)\varepsilon_A(\lambda)\lambda^4 d\lambda}{\int_0^\infty F_D(\lambda)d\lambda}$$

Non fluorescent gel media are an effective platform for photophysical reactions like FRET.[129] Rate of FRET can be increased by confining the D and A molecules within 100 Å. Hence, FRET in gels is an important area of research.

Various groups have explored FRET in heterogeneous media like micelles, vesicles, gels, room temperature ionic liquids and polymers.[129,140-146] Ultrafast FRET occurs in these media due to the confinement of the donor and acceptor molecules. From the donor-acceptor distance calculations using FRET, the fractal dimensions in a heterogeneous media can be calculated. Thus, FRET acts as an effective tool for understanding complex media.

1.2.5. Applications

Gels are widely used in day to day life in the form of tooth paste, cosmetics, contact lens, band aids and sanitary napkins.[77,80,89,91,93,95,110,122,126,147,148] China grass puddings, gel candies and cakes, which are made of gels, became part of our daily diet. Due to their solid matrix which can hold large quantities of solvents, scientists explored their use in drug delivery and in the preparation of ointments. In medicine, gels are also used in implantation surgeries and substitutes for soft

tissues.[91,95] Gel chromatography and electrophoresis are widely used techniques in laboratories. Moreover gels serve as good reaction media for catalysis and sensing. Dye sensitized solar cells using ionogels have recently gained interest due to their conducting properties. Research in hybrid systems like quantum dots (QDs) in gel media have attained recent attention due to the excellent optical properties of QDs in a solid matrix.[149,150]

1.3. Motivation behind the thesis

The work embodied in this thesis deals with investigation of photophysical properties of aggregates in a designed, induced aggregated state and in the self-assembled state and understanding of non-fluorescent gels using fluorescent probes. The present thesis comprises four distinct studies in this context; (1) exploration of linear and non-linear optical properties of specially fabricated dye aggregates, (2) investigation of the mechanism of fluorescence quenching of self-aggregates, (3) understanding the role of interactions between gelator and guest molecules in a guest incorporated gel and (4) exploitation of FRET for assessment of the pore dimensions in a polymeric gel using known FRET pairs. Photophysical studies have been made using UV-visible absorption and steady-state and time-resolved fluorescence measurements. Morphology characterizations were carried out using atomic force microscope (AFM), scanning electron microscope (SEM), transmission electron microscope (TEM), and confocal fluorescence microscope. The fluorescent molecules used in the studies are shown in Chart 1.2.

The morphology, linear and non-linear optical properties of phenazenium dyes, SFO, SFT and PSF, prepared by inverse reprecipitation method have been explored. This was compared with the self-aggregates of these dyes formed at higher dye concentrations.[151] Literature suggests that self-aggregates forms H–aggregates which results in the decrease in the optical properties of these aggregates. We could prove that by careful fabrication of nanoparticles, the photophysical properties and morphology of dye aggregates could be improved.

The nature of aggregation in oligophenylene vinylenes (OPVs) remains debatable as a red-shifted shoulder in the absorption spectra of the self-assembly indicates J-aggregation; but the decrease in their fluorescence quantum yield and the overall blue-shift in the absorption spectra of the self-assembly compared to monomer suggests H-aggregation.[102,107,152,153] Literature suggests different types of aggregation like β-sheet motif, J or H-aggregation, and pseudo J or H-aggregation various OPV derivatives considering the optical properties of each derivative.[102,107,152,153] Moreover the quenching of fluorescence in presence of organic dyes are explored only using steady-state spectral measurements. We investigated the nature of aggregation by quenching studies of OPV's using an organic dye, OCY, there by obtaining insight into the actual fluorescence quenching mechanism. Structures of the gelators used for the investigations were presented in Chart 1.3.

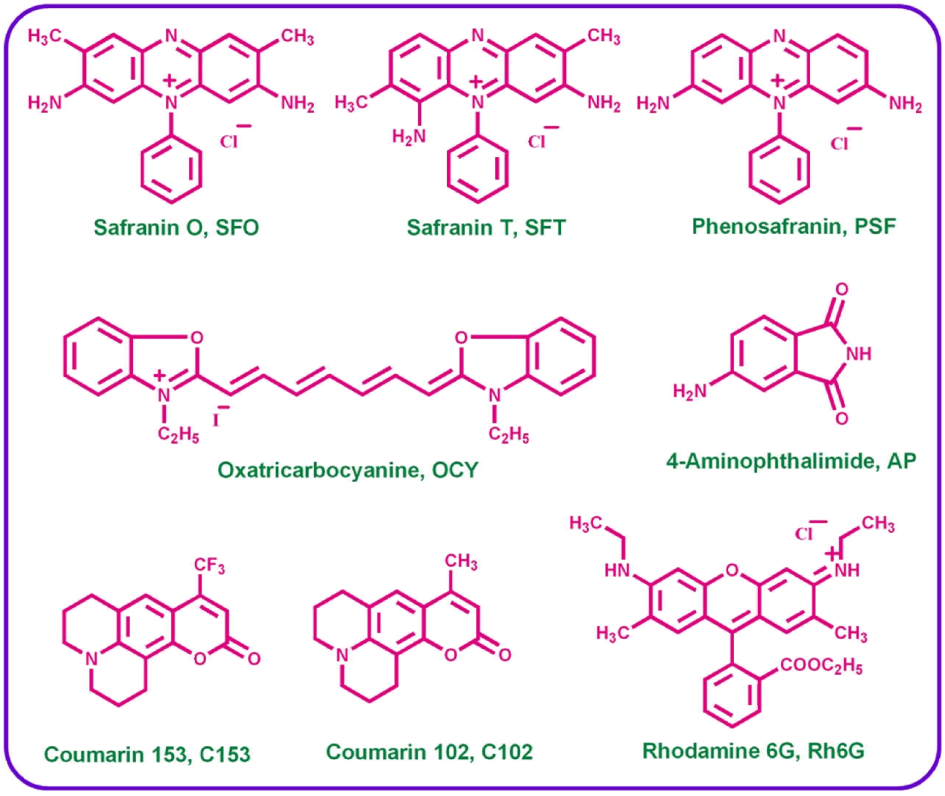

Chart 1.2. Structures and abbreviations of the fluorescent molecules used in this work.

Gels are effective medium for drug delivery, sensing and catalysis.[91,95,154] But the dogma is that any molecules encapsulated in gels stays in the solvent pools. Specific interactions in low molecular weight organogels remain unexplored and hence we were interested in understanding the interactions between the gelator and fluorescent guest molecules in OG-leucine gel, using steady-state and time-resolved fluorescence techniques. For this purpose we have employed C153 and AP, two polarity sensitive probes of comparable size, but different hydrogen

bonding capabilities.[155-165] The studies shows that specific interactions do takes place with molecules sensitive to hydrogen bonding and not always guest molecules stays in the pools of the gel. Moreover, the specific interactions can also affect gelation.

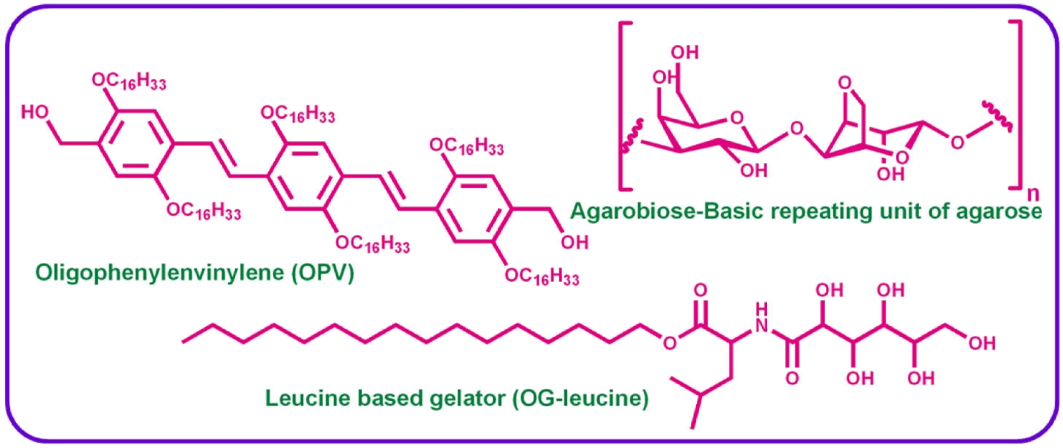

Chart 1.3. Structure and abbreviations of gelators used in this work.

FRET efficiency can be increased in gel medium due to confinement of donor and acceptor in the solvent pools of the gel.[129] Two important aspects can be understood using these studies. One is the effect of confinement on FRET efficiency and the second is the understanding of dimensions of the solvent pools in gel from the donor-acceptor distances calculated from FRET. As the heterogeneous media used in general, results in considerable shifts of the donor and acceptor spectra, resulting in the change of overlap integral, the actual reason for the increase in FRET efficiency in these media remains confusing.[144,146] To solve this, we have employed agarose gel, which does not alter the photophysics

of two well known FRET donor and acceptor, C102 and Rh6G, respectively. Efficient FRET was observed in the gel media, whereas the same donor-acceptor pair did not show FRET in the bulk solvent. Thus, only confinement of donor and acceptor in gel medium resulted in FRET from where the donor-acceptor distances were also calculated to understand the pore dimensions of the gel.

REFERENCES

(1) Callister, W. D., Jr. *Fundamentals of Materials Science and Engineering- An Interactive e-Text*; John Wiley & Sons, Inc.

(2) Fahlman, B. D. *Materials Chemistry*; Springer, 2007.

(3) *The Chemistry of Nanomaterials: Synthesis, Properties and Applications*; Rao, C. N. R.; Muller, A.; Cheetham, A. K., Eds.; WILEY-VCH Verlag GmbH & Co. KGaA, Weinheim.

(4) Buffat, P. H.; Borel, J. P. *Phys. Rev.* **1976**, *13*, 2287.

(5) *Single Organic Nanoparticles*; Masuhara, A.; Nakanishi, H.; Kasai, H., Eds.; Springer: Berlin, 2003.

(6) *Semiconductor Nanoparticles in Encyclopedia of Microfluidics and Nanofluidics*; Li, D., Ed.; Springer US, 2008.

(7) Jelley, E. E. *Nature.* **1936**, *138*, 1009.

(8) Scheibe, G. *Angew. Chem.* **1936**, *49*, 563.

(9) Chen, Z.; Lohr, C. R. *F. Chem. Soc. Rev.* **2009**, *38*, 564.

(10) Das, S.; Thanulingam, T. L.; Thomas, K. G.; Kamat, P. V.; George, M. V. *J. Phys. Chem.* **1993**, *97*, 13620.

(11) Johansson, L. B.-A.; Langhals, H. *Spectrochim. Acta. A.* **1991**, *47*, 857.

(12) Kalisky, Y.; Williams, D. J. *Chem. Phys. Lett.* **1982**, *86*, 100.

(13) Mizutani, F.; Iijima, S. I.; Tsuda, K. *Bull. Chem. Soc. Jpn.* **1982**, *55*, 1295.

(14) Wurthner, F.; Thalacker, C.; Diele, S.; Tschierke, C. *Chem. Eur. J.* **2001**, *7*, 2245.

(15) Mishra, A.; Behera, R. K.; Behera, P. K.; Mishra, B. K.; Behera, G. B. *Chem. Rev.* **2000**, *100*, 1973.

(16) Wurthner, F.; Kaiser, T. E.; Chantu, R.; Moller, S. *Angew. Chem.Int.Ed.* **2011**, *50*, 3376.

(17) Brooker, L. G. S.; White, F. L.; Heseltine, D. W.; Keyes, G. H.; Dent, S. G.; VanLare, E. J. *J. Photogr. Sci.* **1953**, *1*, 173.

(18) Kasha, M.; Rawis, H. R.; El-Bayoumi, M. A. *Pure. Appl. Chem.* **1965**, *11*, 371.

(19) McRae, E. G.; Kasha, M. *J. Chem. Phys.* **1958**, *28*, 721.

(20) Tani, T. *J-aggregates in Spectral Sensitization of photographic materials*; World Scientific Publish. Co. Ptc. Ltd.: Singapore, 1996.

(21) Harisson, W. J.; Mateer, D. L.; Tiddy, G. J. T. *J.Phys. Chem.* **1996**, *100*, 371.

(22) Holzwarth, A. R.; Schaffner, K. *Photosynth. Res.* **1994**, *41*, 41.

(23) Miyatake, T.; Tanigawa, S.; Kato, S.; Tamiaka, H. *Tetrahedron LEtt.* **2007**, *48*, 2251.

(24) Prokhorenkho, V. I.; Steensgard, D. B.; Holzwarth, A. R. *Biophys. J.* **2000**, *79*, 2105.

(25) Zhao, Y. S.; Yang, W.; Yao, J. *Phys.Chem.Chem.Phys.* **2006**, *8*, 3300.

(26) Katoh, T.; Inagaki, Y.; Okazaki, R. *Bull. Chem. Soc. Jpn.* **1997**, *70*, 2279.

(27) Kasai, H.; Nalwa, H. S.; Oikawa, H.; Okada, S.; Matsuda, H.; Minami, N.; Kakuta, A.; Ono, K.; Mukoh, A.; Nakanishi, H. *Jpn. J. Appl. Phys.* **1992**, *31*, 1132.

(28) Nalwa, H. S.; Kasai, H.; Kamatani, H.; Okada, S.; Oikawa, H.; Matsuda, H.; Kakuta, A.; Mukoh, A.; Nakanishi, H. *Adv. Mater.* **1993**, *5*, 758.

(29) Kasai, H.; Oikawa, H.; Nakanishi, H. *Organic Mesoscopic Chemistry*; Oxford, 1999.

(30) Auweter, H.; Haberkorn, H.; Heckmann, W.; Horn, D.; Lu ¨ddecke, E.; Rieger, J.; Weiss, H. *Angew. Chem. Int. Ed.* **1999**, *38*, 2188.

(31) Gesquiere, A. J.; Uwada, T.; Asahi, T.; Masuhara, A.; Barbara, P. F. *Nano.Lett.* **2005**, *5*, 1321.

(32) Tachikawa, T.; Chung, H.-R.; Masuhara, A.; Kasai, H.; Oikawa, H.; Nakanishi, H.; Fujitsuka, M.; Majima, T. *J.Am.Chem.Soc.* **2006**, *128*, 15944.

(33) Bertorelle, F.; Lavabre, D.; Fery-Forgues, S. *J.Am.Chem.Soc.* **2003**, *125*, 6244.

(34) Kang, L.; Wang, Z.; Cao, Z.; Ma, Y.; Fu, H.; Yao, J. N. *J.Am.Chem.Soc.* **2007**, *129*, 7305.

(35) Ristagno, C. V.; Shine, H. J. *J.Org.Chem.* **1971**, *36*, 4050.

(36) Dai, Z. R.; Pan, Z. W.; Wang, Z. *Adv.Funct.Mater.* **2003**, *13*, 9.

(37) Lee, J. K.; Koh, W. K.; Chaeb, W. S.; Kim, W. S. *Chem.Commun.* **2002**, *138*.

(38) Balzer, F.; Bordo, V. G.; Simonsen, A. C.; Rubahn, H. G. *Appl.Phys.Lett.* **2003**, *82*, 10.

(39) Chiu, J. J.; Kei, C. C.; Perng, T. P.; Wang, W. S. *Adv.Mater.* **2003**, *15*, 1361.

(40) Zhao, Y. S.; Di, C.; Yang, W.; Yu, G.; Liu, Y.; Yao, J. *Adv. Funct. Mater.* **2006**, *16*, 1985.

(41) Zhao, Y. S.; Xiao, D.; Yang, W.; Peng, A.; Yao, J. *Chem. Mater.* **2006**, *18*, 2302.

(42) Zhao, Y. S.; Fu, H.; Hu, F.; Peng, A.; Yao, J. *Adv. Mater.* **2007**, *19*, 3554.

(43) Zhao, Y. S.; Fu, H.; Hu, F.; Peng, A.; Yang, W.; Yao, J. *Adv. Mater.* **2008**, *20*, 79.

(44) Martin, C. R. *Science* **1994**, *266*, 1961.

(45) Possin, G. E. *Rev. Sci. Instrum.* **1970**, *41*, 772.

(46) Martin, C. R. *Acc. Chem. Res.* **1995**, *28*, 61.

(47) Ajayaghosh, A.; George, S. J. *J.Am.Chem.Soc.* **2001**, *123*, 5148.

(48) Terech, P.; Weiss, R. G. *Chem. Rev.* **1997**, *97*, 3133.

(49) van Esch, J. H.; Feringa, B. L. *Angew. Chem.Int.Ed.* **2000**, *39*, 2263.

(50) Kasai, H.; Oikawa, H.; Okada, S.; Nakanishi, H. *Bull. Chem. Soc. Jpn.* **1998**, *71*, 2597.

(51) Katagi, H.; Kasai, H.; Kamatani, H.; Okada, S.; Oikawa, H.; Matsuda, H.; Nakanishi, H. *J. Macromol.Sci.Pure & Appl.Chem.* **1997**, *A34*, 2013.

(52) Katagi, H.; Kasai, H.; Okada, S.; Oikawa, H.; Matsuda, H.; Liu, Z. F.; Nakanishi, H. *Jpn.J.Appl.Phys.* **1996**, *35*, 1364.

(53) Kasai, H.; Kamatani, H.; Okada, S.; Oikawa, H.; Matsuda, H.; Nakanishi, H. *Jpn. J. Appl. Phys.* **1996**, *35*, L221.

(54) Kasai, H.; Yoshikawa, Y.; Seko, T.; Okada, S.; Oikawa, H.; Matsuda, H.; Watanabe, A.; Ito, O.; Toyotama, H.; Nakanishi, H. *Mol.Crys.Liq.Cryst.* **1997**, *294*, 173.

(55) Nakanishi, H.; Katagi, H. *Supramole.Science* **1998**, *5*, 289.

(56) Fu, H.; Yao, J. *J.Am.Chem.Soc.* **2001**, *123*, 1434.

(57) Kasai, H.; Kamatani, H.; Yashikawa, Y.; Okada, S.; Oikawa, H.; Watanabe, A.; Ito, O.; Nakanishi, H. *Chem. Lett.* **1997**`, 1181.

(58) Fu, H.; Loo, B. H.; Xiao, D.; Xie, R.; Ji, X.; Yao, J.; Zhang, B.; Zhang, L. *Angew. Chem. Int. Ed.* **2002**, *41*, 962.

(59) Patra, A.; Hebelkar, N.; Sreedhar, B.; Sarkar, M.; Samanta, A.; Radhakrishnan, T. P. *Small.* **2006**, *2*, 650.

(60) Kanaparthi, R. K.; Sarkar, M.; Samanta, A. *J. Phys. Chem. B.* **2009**, *113*, 15189.

(61) *Organic Mesoscopic Chemistry.*; Masuhara, H.; De Schryver, F. C., Eds.; Blackwell Science., 1999.

(62) Matsuda, H.; Van Keruren, E.; Masaki, A. *Nonlinear Opt.* **1995**, *10*, 123.

(63) Huang, C.; Li, Y.; Song, Y.; Li, Y.; Liu, H.; Zhu, D. *Adv. Mater.* **2010**, *22*, 3532.

(64) Patra, A.; Venkatram, N.; Rao, D. N.; Radhakrishnan, T. P. *J. Phys. Chem. C.* **2008**, *112*, 16269.

(65) Takazawa, K. *J.Phys. Chem.C* **2007**, *111*, 8671.

(66) Takazawa, K.; Kitahama, Y.; Kimura, Y.; Kido, G. *Nano Lett.* **2005**, *5*, 1293.

(67) Zhao, Y. S.; Peng, A.; Fu, H.; Ma, Y.; Yao, J. *Adv.Mater.* **2008**, *20*, 1661.

(68) Zhao, Y. S.; Xu, J.; Peng, A.; Fu, H.; Ma, Y.; Jiang, L.; Yao, J. *Angew. Chem.Int.Ed.* **2008**, *47*, 7301.

(69) Zheng, J. Y.; Zhang, C.; Zhao, Y. S.; Yao, J. *Phys. Chem. Chem. Phys.* **2010**, *12*, 12935.

(70) Briseno, A. L.; Mannsfeld, S. C. B.; Ling, M. M.; Liu, S.; Tseng, R. J.; Reese, C.; Roberts, M. E.; Yang, Y.; Bao, Z. *Nature Lett.* **2006**, *444*, 913.

(71) Luo, L.; Liu, G.; Huang, L.; Cao, X.; Liu, M.; Fu, H.; Yao, J. *Appl.Phys.Lett.* **2009**, *95*, 263312.

(72) Zhang, Y. S.; Fu, H.; Peng, A.; Ma, Y.; Xiao, D.; Yao, J. *Adv. Mater.* **2008**, *20*, 2859.

(73) Zhao, Y. S.; Fu, H.; Peng, A.; Ma, Y.; Liao, Q.; Yao, J. *Acc. Chem. Res.* **2010**, *43*, 409.

(74) An, B. K.; Kwon, S. K.; Park, S. Y. *Angew. Chem.Int.Ed.* **2007**, *46*, 1978.

(75) Zhao, Y. S.; Wu, J.; Huang, J. *J.Am.Chem.Soc.* **2009**, *131*, 3158.

(76) Osada, Y.; Kajiwara, K. *Gels Handbook: The Fundamentals*; Academic Press., 2001; Vol. 1.

(77) Vintiloiu, A.; Leroux, J. C. *Journal of Controlled Release* **2008**, *125*, 179.

(78) Babu, S. S.; Praveen, V. K.; Ajayaghosh, A. *Chem. Rev.* **2014**, *114*, 1973.

(79) Flory, P. J. Principles of Polymer Chemistry.; Cornell University Press.: New York, 1973; pp 347.

(80) Minakuchi, N.; Hoe, K.; Yamaki, D.; Ten-no, S.; Nakashima, K.; Goto, M.; Mizuhata, M.; Maruyama, T. *Langmuir.* **2012**, *28*, 9259.

(81) Vintiloiu, A.; Leroux, J.-C. *J. Control. Release.* **2008**, *125*, 179.

(82) Prasanthkumar, S.; Gopal, A.; Ajayaghosh, A. *J. Am. Chem. Soc.* **2010**, *132*, 13206.

(83) Praveen, V. K.; George, S. J.; Ajayaghosh, A. *Macromol. Symp.* **2006**, *241*, 1.

(84) van Esch, J. H.; Feringa , L. B. *Angew. Chem., Int. Ed.* **2000**, *39*, 2263.

(85) Dasgupta, D.; Srinivasan, S.; Rochas, C.; Ajayaghosh, A.; Guenet, J. M. *Soft Matter.* **2011**, *7*, 9311.

(86) Dasgupta, D.; Srinivasan, S.; Rochas, C.; Thierry, A.; Schroder, A.; Ajayaghosh, A.; Guenet, J. M. *Soft Matter.* **2011**, *7*, 2797.

(87) Weiss, R. G. *J. Am. Chem. Soc.* **2014**, *136*, 7519.

(88) Kawata, M.; Suzuki, T.; Kim, N. S. *J. Pharm. Sci.* **1991**, *80*, 1072.

(89) Komatsu, H.; Matsumoto, S.; Tamaru, S.; Kaneko, K.; Ikeda, M.; Hamachi, I. *J. Am. Chem. Soc.* **2009**, *131*, 5580.

(90) Krieg, E.; Shirman, E.; Weissman, H.; Shimoni, E.; Wolf, S. G.; Pinkas, I.; Rybtchinski, B. *J. Am. Chem. Soc.* **2009**, *131*, 14365.

(91) Robinson, R. C. *Bull. Sch. Med. Univ. Md.* **1955**, *40*, 86.

(92) Aratani, N.; Kim, D.; Osuka, A. *Acc. Chem. Res.* **2009**, *42*, 1922.

(93) Carrasco-Orozco, M.; Tsoi, W. C.; O'Neill, M.; Aldred, M. P.; Vlachos, P.; Kelly, S. M. *Adv. Mater.* **2006**, *18*, 1754.

(94) Kartha, K. K.; Babu, S. S.; Srinivasan, S.; Ajayaghosh, A. *J. Am. Chem. Soc.* **2012**, *134*, 4834.

(95) Pisal, S. S.; Paradkar, A. R.; Mahadik, K. r.; Kadam, S. S. *Int J Pharm.* **2004**, *270*, 37.

(96) Warman, J. M.; Piris, J.; Pisula, W.; Kastler, M.; Wasserfallen, D.; Mullen, K. *J. Am. Chem. Soc.* **2005**, *127*, 14257.

(97) Jha, S. *Journal of Current Pharmaceutical Research.* **2013**, *11*, 6.

(98) Vijayakumar, C.; Praveen, V., K.; Kartha, K.; Ajayaghosh, A. *Phys. Chem. Chem. Phys.* **2011**, *13*, 4942.

(99) Ajayaghosh, A.; George, S. J.; Praveen, V. K. *Angew. Chem., Int. Ed.* **2003**, *42*, 332.

(100) Ajayaghosh, A.; Praveen, V. K.; Srinivasan, S.; Varghese, R. *Adv. Mater.* **2007**, *19*, 411.

(101) Ajayaghosh, A.; Praveen, V. K.; Vijayakumar, C. *Chem. Soc. Rev.* **2008**, *37*, 109.

(102) Ajayaghosh, A.; Vijayakumar, C.; Varghese, R.; George, S. J. *Angew. Chem. Int. Ed.* **2006**, *45*, 456.

(103) Babu, S. S.; Kartha, K. K.; Ajayaghosh, A. *J. Phys. Chem. Lett* **2010**, *1*, 3413.

(104) Prasanthkumar, S.; Gopal, A.; Ajayaghosh, A. *J. Am. Chem. Soc.* **2010**, *132*, 13206.

(105) Prasanthkumar, S.; Saeki, A.; Seki, S.; Ajayaghosh, A. *J. Am. Chem. Soc.* **2010**, *132*, 8866.

(106) Praveen, V. K.; George, S. J.; Ajayaghosh, A. *Macromol. Symp* **2006**, *241*, 1.

(107) Praveen, V. K.; George, S. J.; Varghese, R.; Vijayakumar, C.; Ajayaghosh, A. *J. Am. Chem. Soc.* **2006**, *128*, 7542.

(108) Weiss, R. G. *Molecular Gels: Materials with Self Assembled Fibrillar Networks*; Dordrecht, Springer., 2006.

(109) Tokita, M.; Nishinari, K. *Gels: Structure, Properties and Functions*; Springer-Verlag: Berlin, 2009.

(110) Osada, Y.; Kajiwara, K. *Gels Handbook: The Fundamentals.* ; Academic Press., 2001; Vol. 1.

(111) George, S. J.; Ajayaghosh, A. *Chem. -Eur. J.* **2005**, *11*, 3217.

(112) Arnott, S.; Fulmer, A.; Scott, W. E. *J. Mol. Biol.* **1974**, *90*, 269.

(113) Rees, D. A. *Biochem. J.* **1972**, *126*, 257.

(114) Kumar, R.; Kotare, O. P. *AAPS PharmSciTech.* **2005**, *6*.

(115) Patil, K. D.; Bakliwal, S. R.; Pawar, S. P. *Ind j pharm edu res.* **2011**, *45*, 65.

(116) Dasgupta, D. *LAngmuir.* **2009**, *25*, 85.

(117) Guenet, J. M. *Macromolecular Symposia.* **2006**, *241*, 45.

(118) Murdan, S.; Gregoriadis, G.; Florence, A. *Journal of Pharmaceutical Sciences* **1999**, *88*, 608.

(119) Pluen, A.; Netti, A. P.; Jain, K. R.; Berk, A. D. *Biophys. J.* **1999**, *77*, 542.

(120) Golmohamadi, M.; Davis, A. T.; Wilkinson, J. K. *J. Phys. Chem. A*. **2012**, 6505.

(121) Motulsky, A. *Biomaterials.* **2005**, *26*, 6242.

(122) Bucsiova, L.; Hrdlovic, P. *J. Macromol. Sci., Pure Appl. Chem.* **2007**, *44*, 1047.

(123) Datta, A.; Das, S.; Mandal, D.; Pal, S. K.; Bhattacharyya, K. *Langmuir.* **1997**, *13*, 6922.

(124) Grant, D. C.; DeRitter, R. M.; Steege, E., K.; Fadeeva, A. T.; Castner, W. E. *Langmuir.* **2005**, *21*, 1745.

(125) Hattori, T.; Ishii, K.; Tominaga, T.; Osada, Y.; Tahara, T. *Chem. Phys.* **2013**, *419*, 172.

(126) Kawaguchi, H. *J. Oleo Sci.* **2013**, *62*, 865.

(127) Mukhopadhyay, S.; Ira.; Krishnamoorthy, G.; Maitra, U. *J. Phys. Chem. B.* **2003**, *107*, 2189.

(128) Rahmi; Itagaki, H. *J.Photopolym. Sci. Technol.* **2011**, *24*, 518.

(129) Ghosh, S.; Dey, S.; Adhikari, A.; Mandal, U.; Bhattacharyya, K. *J. Phys. Chem. B.* **2007**, *111*, 7085.

(130) Wenger, O. S. *Chem. Soc. Rev.* **2011**, *40*, 3538.

(131) Pal, S. K.; Sukul, D.; Mandal, D.; Sen, S.; Bhattacharyya, K. *J. Phys. Chem. B*> **2000**, *104*, 2613.

(132) Singh, M. P.; Singh, R. K.; Chandra, S. *Chem Phys Chem.* **2010**, *11*, 2036.

(133) Birks, J. B. *Photophysics of Aromatic Molecules*; Wiley, London, 1970.

(134) Lakowicz, J. R. *Principles of Fluorescence Spectroscopy*, Second ed.; Kluwer Academic/Plenum Publishers, 1999.

(135) Ito, N.; Arzhantsev, S.; Heitz, M.; Maroncelli, M. *J. Phys. Chem. B.* **2004**, *2004*, 5771.

(136) Ito, N.; Arzhantsev, S.; Maroncelli, M. *Chem. Phys. Lett.* **2004**, *396*, 83.

(137) Khara, D. C.; Samanta, A. *Phys. Chem. Chem. Phys.* **2010**, *12*, 7671.

(138) Valeur, B. *Resonance Energy Transfer and Its Applications, in Molecular Fluorescence: Principles and Applications*; Wiley-VCH Verlag GmbH, Weinheim, FRG., **2001**.

(139) van der Meer, B. W. Förster Theory, in FRET - Förster Resonance Energy Transfer: From Theory to Applications; Medintz, I., Hildebrandt, N., Eds.; Wiley-VCH Verlag GmbH & Co. KGaA, Weinheim, Germany., **2013**.

(140) Adhikari, A.; Das, D. K.; Sasmal, D. K.; Bhattacharyya, K. *J. Phys. Chem. A.* **2009**, *113*, 3737.

(141) Das, A. K.; Mondal, T.; Sasmal, D. K.; Bhattacharyya, K. *J. Chem. Phys.* **2011**, *135*, 074507.

(142) Das, D. K.; Das, A. K.; Mondal, T.; Mandal, A. K.; Bhattacharyya, K. *J. Phys. Chem. B.* **2010**, *114*, 13159

(143) Kenney-Wallace, G. A.; Flint, J. H.; Wallace, S. C. *Chem. Phys. Lett.* **1975**, *32,*, 71.

(144) Mandal, A. K.; Das, A. K.; Mojumdar, S. S.; Bhattacharyya, K. *J. Indian. Chem. Soc.* **2011**, *88*, 1917.

(145) Mandal, U.; Ghosh, S.; Das, D. K.; Adhikari, A.; Dey, S.; Bhattacharyya, K. *J. Chem. Sci.* **2008**, *120*, 15.

(146) Sahu, K.; Ghosh, S.; Mondal, S. K.; Ghosh, B. K.; Sen, P.; Roy, D.; Bhattacharyya, K. *J. Chem. Phys.* **2006**, *125*, 044714.

(147) Hanabusa, K.; Fukui, H.; Suzuki, M.; Shirai, H. *Langmuir.* **2005**, *21*, 10383.

(148) Ho, C.; Williams, W. B.; Stubbs, D. C. *Biochim. Biophys. Acta.* **1992**, *1104*, 273.

(149) Wadhavane, D. P.; Izquierdo, M. A.; Galindo, F.; Burguete, M. I.; S., L. V. *Soft Matter.* **2012**, *8*, 4373.

(150) Wadhavane, P. D.; Galian, R. E.; Izquierdo, M. A.; -Sigalat, J. A.; Galindo, F.; Schmidt, L.; Burguete, M. I.; -Prieto, J. P.; Luis, S. V. *J. Am. Chem. Soc.* **2012**, *134*, 20554.

(151) Sarkar, D.; Das, P.; Girigoswami, A.; Chattopadhyay, N. *J. Phys. Chem. A.* **2008**, *112*, 9684.

(152) Hulvat, F. J.; Sofos, M.; Tajima, K.; Stupp, I. S. *J. Am. Chem. Soc.* **2005**, *127*, 366.

(153) Wall, D. B.; Zhou, Y.; Mei, S.; Ardona, M. A. H.; Ferguson, L. A.; Tovar, D. J. *Langmuir.* **2014**, *30*, 375.

(154) Tellis, C. J.; Christopher, A.; Myers, M. M.; Kneas, A. K. *Anal. Chem.* **2011**, *83*, 928.

(155) Dobek, K.; Karolczak, J. *J. Fluoresc.* **2012**, *22*, 1647.

(156) Dobek, K.; Karolczak, J.; Kubicki, J. *Dyes and Pigments* **2014**, *100*, 222.

(157) Ito, N.; Arzhantsev, S.; Maroncelli, M. *Chem. Phys. Lett.* **2004**, *396*, 83.

(158) Jones II, G.; Jackson, W. R.; Choi, C., Y; Bergmark, W. *J. Phys. Chem.* **1985**, *89*, 294.

(159) Knut, R.; Spieles, M. *Anal. Chem.* **2011**, *83*, 1232.

(160) Krolicki, R.; Jarzeba, W.; Mostafavi, M.; Lampre, I. *J. Phys. Chem. A.* **2002**, *106*, 1708.

(161) Maroncelli, M.; Fleming, R. G. *J. Chem. Phys.* **1987**, *86*, 6221.

(162) Samanta, A.; Fessenden, R. W. *J. Phys. Chem. A.* **2000**, *104*, 8577.

(163) Soujanya, T.; Fessenden, R. W.; Samanta, A. *J. Phys. Chem.* **1996**, *100*, 3507.

(164) Soujanya, T.; Krishna, T. S. R.; Samanta, A. *J. Photochem. Photobiol. A: Chem.* **1992**, *66*, 185.

(165) Wagner, D. B. *Molecules.* **2009**, *14*, 210.

Chapter 2

Materials, Methods and Instrumentation

This chapter presents a brief description of the materials used in the studies, their procurement sources, methods of synthesis of the gelators and the purification of the conventional solvents. Methods of sample preparations for the spectral measurements and microscopic experiments have been provided. The instrumentation details, specially the time-correlated single photon counting (TCSPC) setup, time-resolved confocal fluorescence microscope and femtosecond Z-scan setup are discussed in detail. Various methodologies employed in the study, such as measurement of fluorescence quantum yield, analysis of TCSPC data, detailed procedures of obtaining the anisotropy decay profiles and calculation of non-linear absorption coefficient have also been discussed.

2.1. Materials

The dyes, Safranin O, Safranin T and Phenosafranin were purchased from Sigma Aldrich and used without any purification. Laser grade DOTC iodide (3-ethyl-2-[7-(3-ethyl-2(3H)-benzoxazolylidene)-1,3,5-heptatrienyl] benzoxazolium iodide) was procured from Exciton and used as received. 4-Aminophthalimide (AP) was obtained from TCI and recrystallized twice from ethanol in the presence of activated charcoal.[1] Laser grade coumarin 153 (C153) was procured from Eastman Kodak and used as received. Laser grade coumarin 102 (C102) and rhodamine 6G (Rh6G) were purchased from Exciton and used as received.

Diethylamine and 4-chloro-7-nitrobenz-2-oxa-1,3-diazole (NBD-Cl) for the synthesis of 4-N,N-diethyl-7-nitrobenz-2-oxa-1,3-diazole (NBD) were purchased from Sigma-Aldrich. 1-Bromohexadecane, paraformaldehyde and hydrogen bromide used for the synthesis of OPV were purchased from Sigma Aldrich. 1,4-dihydroxy quinone, sodium thiosulphate, potassium carbonate and tetra-n-butyl ammonium bromide were purchased from Merck Millipore. Lithium aluminium hydride, sodium borohydride, triphenyl phosphine, pyridinium chlorochromate, lithium ethoxide and iodine used for the synthesis of 2,5-Bis(hexadecyloxy)-1,4-bis[(2,5-hexadecyloxy-4 hydroxymethyl) phenylenevinylene]-benzene (OPV) were purchased from local companies. Magnesium sulphate, sodium carbonate and glucono-δ-lactone for the synthesis of Hexadecyl 4-Methyl (2-(2, 3, 4, 5, 6-pentahydroxy) hexanamido) pentanoate (OG-leucine) were purchased from Merck Millipore. Cetyl alcohol, p-toluenesulphonic acid and leucine were purchased from local companies. Agarose was purchased from Sigma Aldrich and used as received.

Deuterated solvents, chloroform-d and dimethyl sulfoxide-d_6 for NMR spectral measurements were obtained from Merck. GR and synthesis grade solvents for synthesis and spectroscopic grade solvents for spectral measurements were obtained from Merck. Various drying agents such as benzophenone, calcium chloride, calcium hydride, phosphorous pentoxide, iodine, magnesium turnings and sodium metal used at different stages of solvent purification, hydrochloric acid for cleaning Mg turnings and molecular sieves for the storage of dried solvents were purchased from local companies.

2.2. Synthesis of gelators and electron donor acceptor (EDA) molecules

2.2.1. OPV

OPV was synthesized according to a multi-step procedure [2-4] as shown in Scheme 2.1. Specifically, 1,4-hydroquinone (**1**) was refluxed with 1-bromohexadecane in acetonitrile for 36 hours in presence of K_2CO_3 to yield 88% 1,4-bis(hexadecyloxy)benzene (**2**). Subsequent bromomethylation using HBr and formaldehyde at 60 ºC for 2 hours provided a key intermediate (**3**). Direct conversion of this intermediate to the dialdehyde (**6**) was achieved by an acetylation-reduction-oxidation sequence. The triphenylenevinylene dialdehyde (**8**) was synthesized by a double Wittig reaction of (**6**) with a diphosphonium salt (**7**) which was made from compound (**3**). The reduction of (**8**) to form triphenylenevinylene bis alcohol-OPV (**9**) was accomplished using sodium borohydride in DCM-methanol mixture at room temperature for 30 minutes. The yield of OPV was 81%. Details of the synthesis are given in Scheme 2.1.

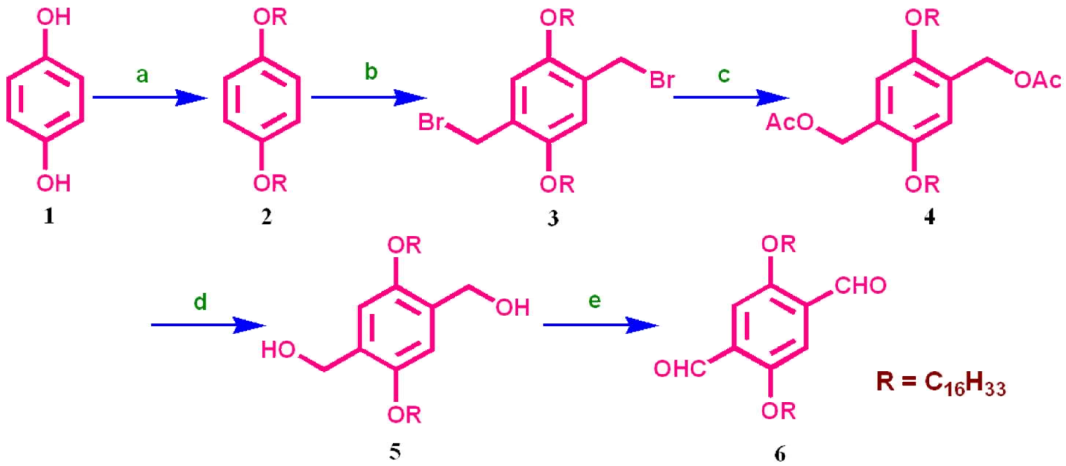

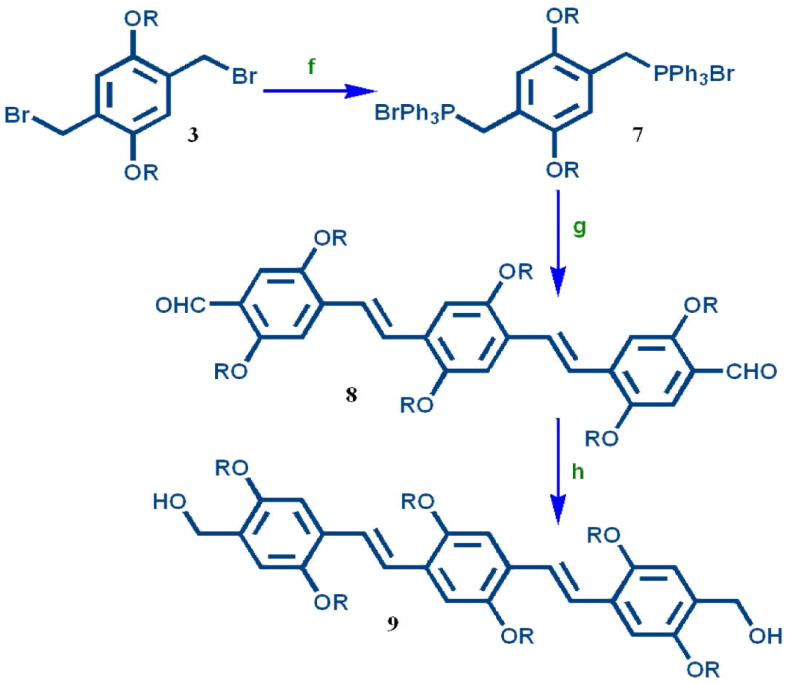

Scheme 2.1. (a) Bromohexadecane, K_2CO_3, acetonitrile, reflux, 36 hrs, 88%; (b) paraformaldehyde, HBr, 60 °C, 2 hrs, 83%; (c) KOAc, Bu_4NBr, acetonitrile, reflux, overnight, 97%; (d) $LiAlH_4$, THF, 25 °C , 2hrs, 95%; (e) pyridinium chlorochromate, CH_2Cl_2, 25 °C, 2 hrs, 81%; (f) PPh_3, toluene, reflux, 3 hrs; (g) (i) 6, LiOEt, CH_2Cl_2, 25 °C, 10 min; (ii) I_2, CH_2Cl_2, 25 °C, overnight, 78%; (h) $NaBH_4$, DCM/MeOH, room temperature, 30 min, 81%.

2.2.2. OG-leucine

OG-leucine was synthesized according to the two-step procedure reported by Maruyama and coworkers.[5] Details of the synthesis are given in Scheme 2.2. In the first step, a mixture of 1-hexadecanol (0.05 mol), p-toluenesulfonic acid monohydrate (0.06 mol), and leucine (0.05 mol) was refluxed in toluene (200 mL) for 5 hours in a Dean-Stark apparatus. After cooling the reaction mixture to room

temperature, toluene was evaporated, and the residue was dissolved in chloroform (200 mL). An aqueous solution of sodium carbonate was added to this and the organic phase was separated and dried over $MgSO_4$. Chloroform was evaporated and the residue was dissolved in 200 mL acetone containing 10 mL conc. HCl. The product of the first step, 1-hexadecyl-leucine ester hydrochloride, was precipitated at 4 ^{0}C. The precipitation process was repeated using 100 mL acetone to obtain the purified product. For neutralization, the precipitate dissolved in chloroform was mixed with 10% aqueous sodium carbonate solution. The separated organic phase was dried over anhydrous $MgSO_4$ and chloroform was evaporated.

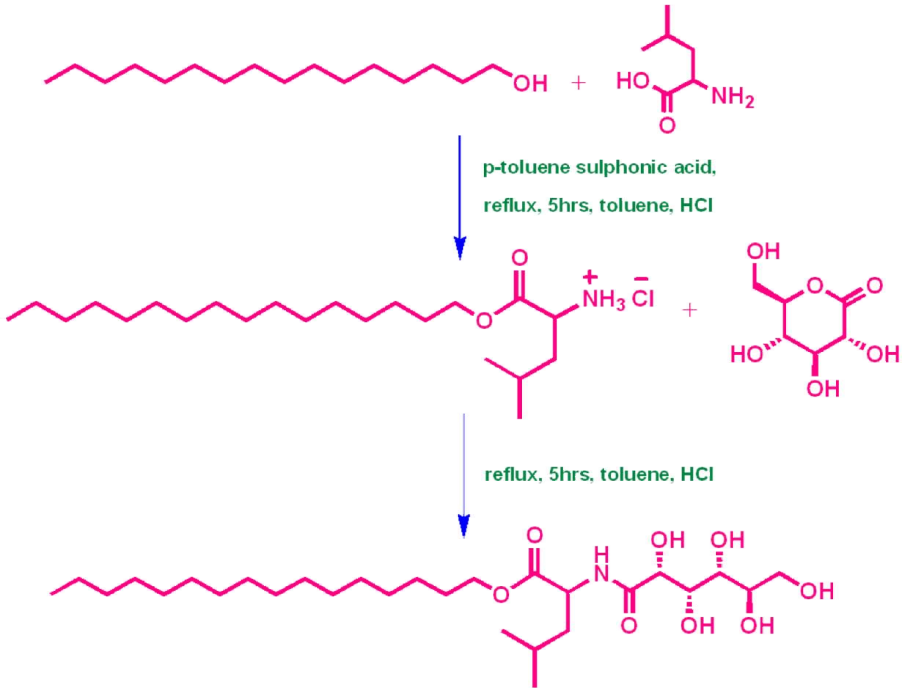

Scheme 2.2. Synthesis of OG-leucine

In the second step, the neutralized product was refluxed with glucono δ-lactone for 5 hours in ethanol (200 mL). After evaporating ethanol, the residue was dissolved in 1, 4-dioxane at 80 ^{0}C to remove the excess glucono δ-lactone and the hot solution was filtered immediately. The process was repeated thrice and 1, 4-dioxane was evaporated. The white powder obtained was recrystallised few times in acetonitrile until it was found free from 1, 4-dioxane. The yield of OG-leucine was 47%.

2.2.3. NBD

NBD was synthesized following a standard procedure as shown in Scheme 2.3, in which 2.0 mL ethyl acetate (EtOAc) solution of 1.2 mmol diethyl amine was added drop wise to 1 mmol of 4-chloro-7-nitrobenz-2-oxa-1,3-diazole (NBD-Cl) dissolved in 3 mL ethyl acetate at 0°C with stirring.[6] After stirring for 30 min at this temperature, the reaction mixture was further stirred for another 2 hrs at room temperature. The product, a red precipitate, was filtered out and purified by column chromatography using a silica gel column. Hexane and ethyl acetate were used as eluent for the purification of the compound. The purified compound was recrystallized from absolute ethanol.

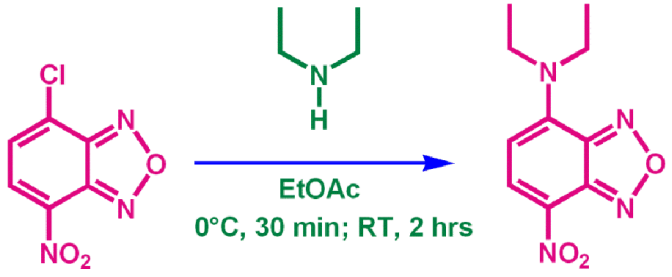

Scheme 2.3. Synthesis of NBD

2.3. Purification of conventional solvents

Conventional solvents used at different stages of the experiments were purified by following the procedures available in the literature.[7] After purification, molecular sieves were added to protect the solvents from moisture. The purified solvents were optically transparent in the region of the compounds of interest.

Ethyl acetate: After stirring with anhydrous P_2O_5 for 3-4 hours, the solvent was distilled out under dry atmosphere.

Benzonitrile: The solvent was refluxed with anhydrous P_2O_5 for an hour and distilled under reduced pressure.

Acetonitrile: After refluxing the solvent for 3-4 hrs with anhydrous P_2O_5, the solvent was distilled under dry condition.

Toluene and tetrahydrofuran (THF): The solvents were refluxed over metallic sodium for 3-4 hrs and then benzophenone was added after cooling. The dark solution was refluxed for another hour and distilled under dry condition.

Chloroform: The solvent was stirred overnight with $CaCl_2$ and then distilled under moisture free condition.

Dichloromethane: After stirring with CaH_2 for 5-6 hrs, the solvent was distilled under dry condition.

Ethanol and Methanol: The solvents were refluxed with Mg turnings and iodine for 3-4 hrs and then distilled under dry condition.

Water: Milli-Q water produced from Millipore, Synergy Pack was used for all the experiments.

2.4. Methods

2.4.1. Fabrication of nano/microparticles

Dye aggregates were prepared by the inverse reprecipitation method as illustrated in Scheme 2.4.[8] In a typical preparation, standard stock solution of the dye (in water) was prepared and small amounts of this aqueous stock solution was injected rapidly into large quantity of pure organic solvent (ethyl acetate) under ultra-sonication, which was continued for 2 min following completion of addition. The colloids were left as such for 1.5 hrs for stabilization/growth. Thus obtained particles were found to be stable for several weeks. The particle formation was confirmed by passing a beam of laser and the path was clearly visible due to scattering of light.

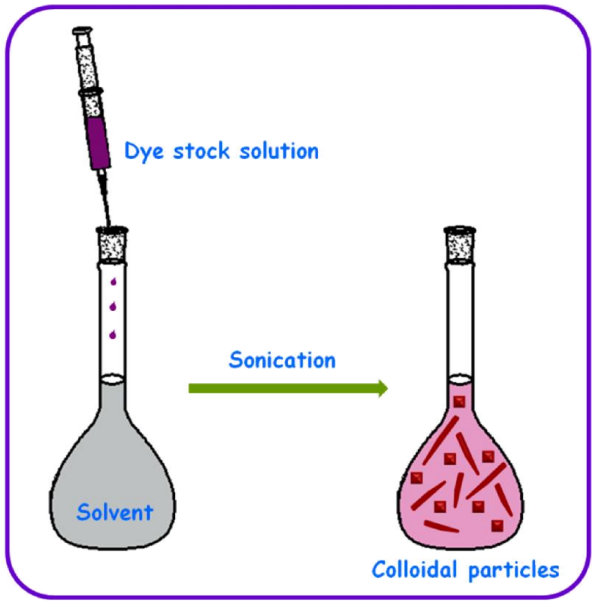

Scheme 2.4. Illustration of inverse reprecipitation method

2.4.2. Preparation of gels

All the gels used in the studies are thermo-reversible in nature and were prepared by a well known simple procedure.[2,4,5] Weighed amount of the gelator in an appropriate quantity of solvent was heated in a sealed glass vial until the gelator dissolved completely. The solution was then allowed to cool down to room temperature and gel formation was confirmed by the failure of the transparent soft mass to flow by inverting the vial. Various stages involved in the gelation process during the cooling process of the hot gelator solution is shown in Scheme 2.5. The probe incorporated gels were prepared following a similar procedure, the only difference being that the probe was dissolved in the solvent, prior to addition of the gelator and subsequent heating. The amount of gelator used for the preparation depends on the critical gelator concentration (CGC), which is the minimum amount of gelator required to form a stable gel. Details of the solvents and amount of gelator used are presented in the respective chapters.

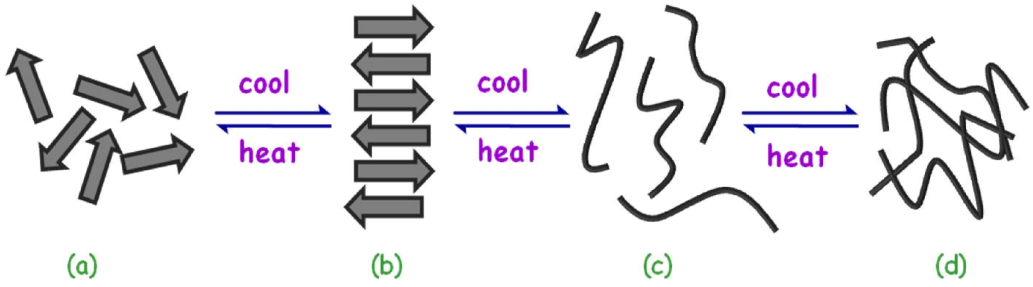

Scheme 2.5. Different stages of gel formation with decreasing temperature. (a) Free gelator molecules in a hot solution, (b) self- assembly of molecules, (c) random fibrils and (d) entangled fibrils or gel.

2.5. Sample Preparation

2.5.1. Spectral measurements

For the steady state and time resolved spectral measurements of the samples, the absorbance at the excitation wavelength was maintained around 0.05-0.3, to avoid problems due to inner filter effects. Cuvettes with various path lengths (0.1, 0.3 and 1 cm) were used depending upon the nature of the heterogeneous media employed, to minimize scattering. Care was taken to seal the cuvettes (for gel samples) with septum and parafilm, in order to avoid drying of the gel.

2.5.2. Microscopy analysis

The scanning electron microscopy (SEM), atomic force microscopy (AFM) and laser scanning confocal fluorescence microscopy samples were prepared by placing one or two drops of the colloidal solution onto a clean cover slip/glass plate and subsequent evaporation of the solvent under vacuum. For transmission electron microscope (TEM) measurements, the colloidal solutions were drop-casted on a carbon coated-copper grid and analyzed after drying. For fluorescence lifetime imaging microscopy (FLIM) measurements, one or two drops of the colloidal solution were placed on a neat cover slip and the solvent was evaporated under vacuum.

2.6. Instrumentation

The purity of the compounds was checked by single spot in thin layer chromatography (TLC) and also by the nuclear magnetic resonance (NMR) and UV-visible absorption and emission spectral data. NMR spectra were recorded

using Bruker AVANCE 400 MHz NMR spectrometer. The steady-state absorption and fluorescence spectra were recorded on a UV-visible spectrophotometer (Cary100, Varian) and a spectrofluorometer (FluoroLog-3, Horiba Jobin Yvon), respectively. Peltier temperature controller (Wavelength Electronics) was used with the spectrofluorometer for steady-state fluorescence measurements at different temperatures. The fluorescence spectra were corrected for the instrument response function.

Size and morphology of the nano/microparticles were examined by using a Solver Pro M (NT-MDT) atomic force microscope (AFM) in semi-contact mode using golden silicon probe (3.6×1.6×0.4 mm) having 5.5-22.5 N/m force constant and a Philips XL30 ESEM scanning electron microscope (SEM) using a beam voltage of 20 kV. Prior to SEM imaging, an ultra-thin layer of gold was coated using JEOL Fine coat Ion Sputter FC-1100 (operating at 1 kV and 10 mA for 5 minutes) to enhance the conductivity of the samples. FEI TECNAI G2 S-TWIN transmission electron microscope (TEM) was used for high resolution imaging at an accelerating voltage of 200 kV. The fluorescent nanostructures were characterized by using Leica TCS SP2 AOBS DM6000 B upright laser scanning confocal fluorescence microscope. Working principles and details of other instrumental setups employed in these studies are explained in the following sections.

2.6.1. Time-correlated single photon counting setup

Time-resolved fluorescence measurements were carried out using a time correlated single-photon counting (TCSPC) spectrometer (Horiba Jobin Yvon IBH) . The block diagram of the setup is shown in Scheme 2.6. Nano LEDs and

PicoBrite diode lasers were used as excitation sources, while a micro-channel plate (MCP) photomultiplier tube (Hamamatsu R3809U-50, 160-850 nm range) was used as the detector. Nano LED having output at 440 nm (FWHM = 120 ps) and two PicoBrite lasers with output at 375 nm (FWHM = 55 ps) and 405 nm (FWHM = 50 ps) were employed in the present study. While Nano LEDs were operated at a maximum pulse repetition rate of 1 MHz, PicoBrite laser sources were operated at 10 MHz repetition rate. Whenever needed, neutral density (ND) filters were used to reduce the excitation intensity. The experiment starts with simultaneous excitation of the sample and sending a signal to the electronics (Scheme 2.6).[9]

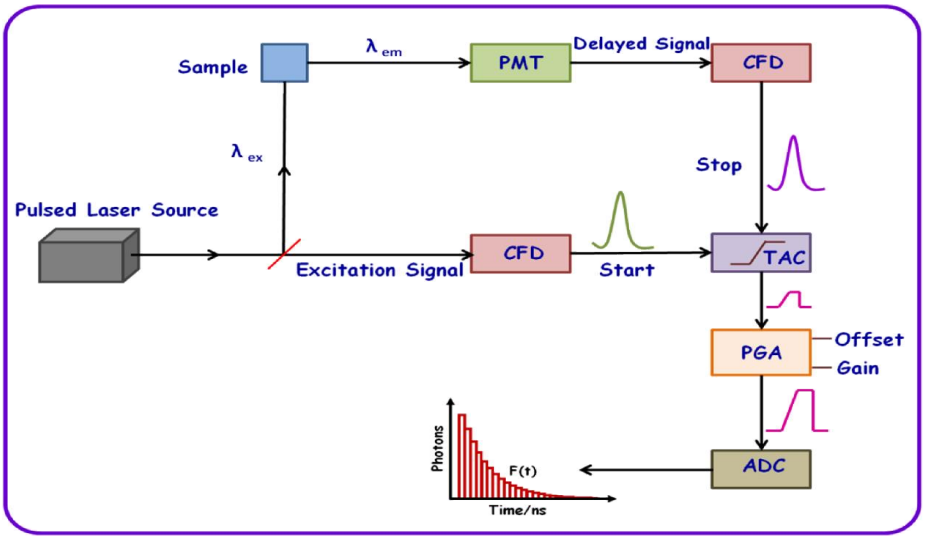

Scheme 2.6. Schematic diagram of the TCSPC setup

Constant fraction discriminator (CFD) receives the excitation signal and accurately measures the arrival time of the photon and then diverts the signal

towards the time to amplitude convertor (TAC) to start the voltage ramp. The second channel (CFD) which accurately measures the arrival time of the emitted photon makes TAC to stop the voltage ramp. The voltage ramp developed by TAC is proportional to the delay time between the excitation and emission signals. Programmable gain amplifier (PGA) amplifies the resultant voltage, which later be converted to a numerical value by analog-to-digital convertor (ADC). The numerical value with the measured time delay will be stored as a single event and by repeating the process several times with a pulsed excitation source, histogram of the fluorescence intensity decay with time can be constructed.

The lamp profile was recorded by placing a scatterer (dilute solution of Ludox in water) in place of the sample. For temperature dependent fluorescence decay profiles, a Julabo water circulator bath was used. The method of analysis of the decay curves are discussed in a later section.

2.6.2. Time-resolved confocal fluorescence microscope

The block diagram of the instrument is shown in Scheme 2.7. Olympus IX71 inverted microscope equipped with Olympus UPlansApo water immersion objective (1.2 NA, 60×) served as microscope body. A 405 nm picosecond pulsed diode laser pulse (fwhm of 176 ps) with a power of 1 μW was used as the excitation source, whose output was coupled into the main optical unit using polarization maintaining single mode optical fiber. After the reflection at the dichroic mirror, the collimated excitation beam entered into the entrance port of the inverted microscope. Water immersion objective focused the excitation laser beam on to the sample placed on the cover glass.

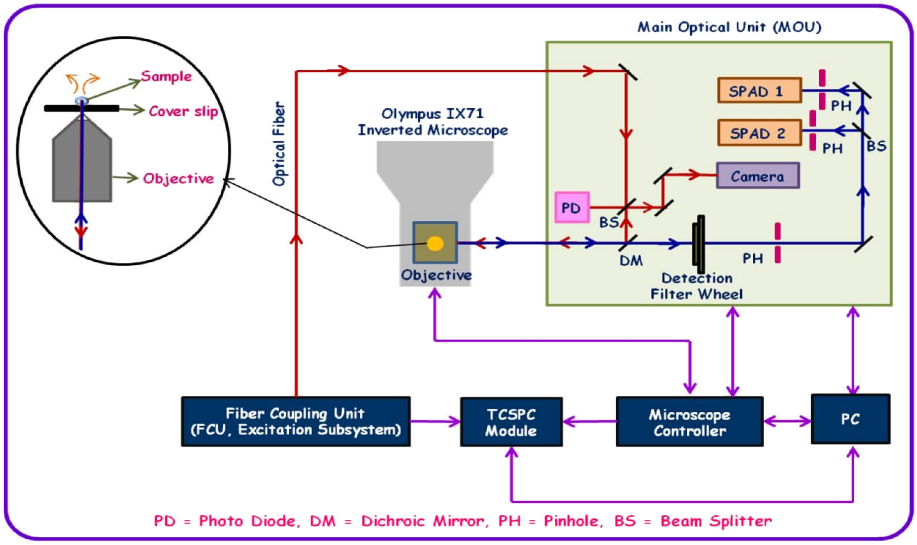

Scheme 2.7. Schematic diagram of the time-resolved confocal fluorescence microscope setup (Source: PicoQuant MicroTime 200 user manual)

Emission from the sample was collected by the same objective lens and directed back to the dichroic mirror, from where the fluorescence signal passed through a 430 nm long pass filter and entered into 50 µm diameter pinhole to cut off the out of focus light. Then the recollimated fluorescence signal was detected by single photon avalanche photodiode (SPAD). The data acquisition was performed with PicoHarp 300 TCSPC module in time-tagged time-resolved (TTTR) mode.

2.6.3. Femtosecond Z-scan setup

Z-scan measurements were performed using an amplified Ti:sapphire laser system (LEGEND, Coherent) delivering nearly transform-limited pulses of ~40 fs

(FWHM) with a repetition rate of 1 kHz at 800 nm. The amplifier was seeded with ~15 fs (FWHM), 55-60 nm (FHWM) pulses from an oscillator (MICRA, Coherent, 1 W average power, 80 MHz repetition rate, 800 nm central wavelength). A schematic diagram of the experimental set up is shown in Scheme 2.8.

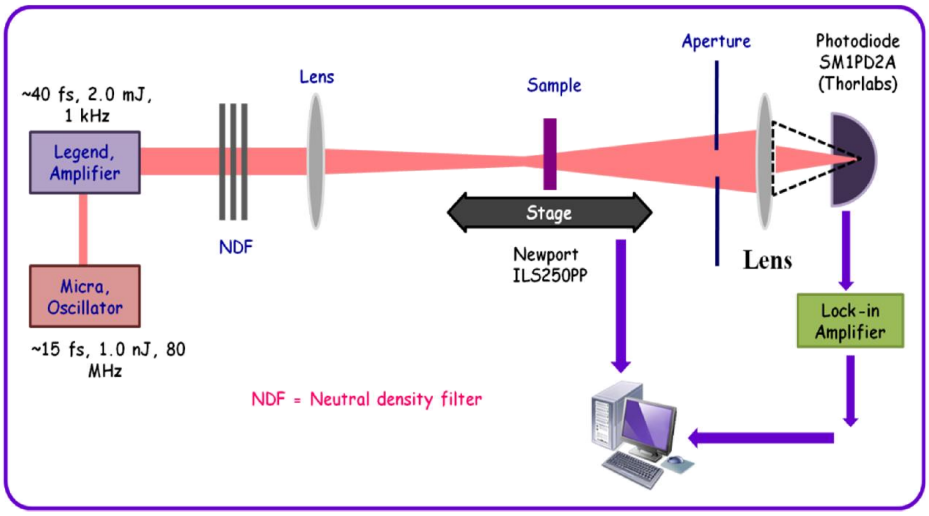

Scheme 2.8. Schematic diagram of the Z-scan experimental set up

Laser pulses with energy, typically less than 1 μJ were used for the experiments. The beam was focused into the sample using a 200 mm focal length lens. The beam waist (ω_o) estimated was about 28±2 μm ($FW1/e^2M$) with corresponding Raleigh range in the order of 3.1±0.4 mm. The transmittance changes of the sample placed on the translation stage (Newport, ILS250PP) was controlled by an ESP motion controller, measured with a sensitive photodiode (Thorlabs, SM1PD2A) in the far-field. An aperture was placed in front of the

collecting lens for closed aperture scans, while the open aperture scans were performed by removing the aperture. The photodiode output was fed to a lock-in amplifier (7265, Signal Recovery). Several neutral density filters were used to cut down the light intensity reaching the sample as well as the photodiode. The translation stage and the photodiode/lock-in were controlled by a personal computer using a Labview program. Since these ultra short pulses were passed through different optics (mirrors, filters, and lenses) before entering the sample, pulse duration near the sample was measured to be ~75 fs and this value was used for peak intensity calculations. For correction, the saturable absorption (SA) from solvents was also recorded. The solvents used, ethyl acetate and water, indicated low SA of 3.28×10^{-15} and 0.39×10^{-15} m/W, respectively.

2.7. Measurement of fluorescence quantum yield

For fluorescence quantum yield (Φ) measurements, optically matched solutions (or solutions with very similar optical density values) of the sample and the standard at a given absorbing/excitation wavelength were prepared. The Φ value was calculated by measuring the integrated area under the emission spectra and by using the following equation,[10]

$$\emptyset_{sample} = \frac{A_{sample}\times OD_{std}\times n^2_{sample}}{A_{std}\times OD_{sample}\times n^2_{std}} \times \emptyset_{std} \qquad (1)$$

where, A is the integrated area under the emission spectrum, OD is the optical density at the excitation wavelength and n is the refractive index of the solvent. The subscripts ‘sample’ and ‘std’ refer to the sample of unknown Φ and reference

sample of known Φ respectively. NBD was used as the standard (Φ = 0.48 in toluene)[6] for the Φ measurements employed in the present studies.

2.8. Fluorescence lifetime data analysis

The lifetimes of the samples were estimated from the measurements of fluorescence decay curves and the instrumental profiles using a nonlinear least-squares iterative fitting procedure (using decay analysis software IBH DAS6, Version 2.2). This program used a reconvolution method for the analysis of the experimental data.[11] When the decay time is long compared to the pulse width of the excitation pulse, the excitation may be described as a δ-function. However, when the lifetime is short, distortion of the experimental data occurs by the finite decay time of the lamp pulse and response time of the photomultiplier and associated electronics. Since the measured decay function is convolution of the true fluorescence decay and the instrumental pulse, it was necessary to analyze the data by deconvolution in order to get the actual fluorescence lifetime. The mathematical statement of the problem is given by the following equation:

$$D(t) = \int_0^t P(t')G(t - t')dt' \qquad (2)$$

where, D(t) is the fluorescence intensity at any given time t, P(t') is the intensity of the exciting light at time t' and G(t–t') is the response function of the experimental system. The experimental data D(t) and P(t') from the multi-channel analyzer (MCA) were fed into a personal computer (PC) to determine the lifetime. We used the IBH program to analyze the multi-exponential decays. An excitation pulse profile was recorded and then deconvolution started with mixing of the

excitation pulse and a projected decay to form a new reconvoluted set. The data was compared with the experimental set and the difference between the data points were summed, generating χ^2 functions for fitting. The deconvolution proceeded through a series of such iterations until an insignificant change of χ^2 occurred between iterations. The inspection of reduced χ^2, a plot of weighted residuals and autocorrelation function of the residuals allowed assessment of the quality of the fit.

2.9. Time-resolved anisotropy decay profiles

The anisotropy measurements were performed using two polarizers by placing one of them in the excitation beam path and the other in front of the detector.[9] An alternate collection of the fluorescence intensity in parallel (I_{II}) and perpendicular ($I_{\perp}$) polarization (with respect to the vertically polarized excitation laser beam) for equal interval of time was made until the count difference between the two polarizations (at t = 0) was ~5000. For G-factor calculation, the same procedure was followed, but with only 4 cycles and horizontal polarization of the exciting laser beam. The anisotropy measurements were performed at the respective fluorescence maxima of the probe using a monochromator with a bandpass of 2 nm. Time-resolved fluorescence anisotropy, r(t), is calculated using the following equation,

$$r(t) = \frac{I_{II}(t) - GI_{\perp}(t)}{I_{II}(t) + 2GI_{\perp}(t)} \tag{3}$$

where, G is the correction factor for the detector sensitivity to the polarization direction of the emission and $I_{II}(t)$ and $I_{\perp}(t)$ are the fluorescence decays

polarized parallel and perpendicular to the polarization of the excitation light, respectively. For all the systems studied, the estimated G factors are found to lie between 0.53 and 0.57. The initial anisotropies, r_0, are found to be within the limiting value of 0.4. The time dependence of the measured anisotropy profiles in the present study were found to be described by a single exponential function. A bi-exponential fit to the anisotropy data did not improve the quality of fitting and also, the average rotational time thus estimated was found to be identical with that obtained from the single exponential fit.

2.10. Z-scan data analysis

The open aperture Z-scan experimental data was fitted by time integration of sample transmittance assuming a Gaussian temporal profile. The fitting to experimental data was done using the equation,[12]

$$T_{OA}(z) = \frac{1}{\pi^{1/2} q_o} \int_{-\infty}^{\infty} \ln\left[1 + q_o e^{-x^2}\right] dx \tag{4}$$

where, $T_{OA}(z)$ is the normalized open aperture transmittance as a function of z, $q_0 = \beta I_0 L_{eff}$, β is the nonlinear absorption coefficient and I_0 is the intensity, $L_{eff} = \frac{1 - e^{\alpha_0 L}}{\alpha_0}$, are effective path lengths in a sample of length L and α_0 is the linear absorption coefficient.

The closed aperture data were fitted to the equation,

$$T_{CA} = 1 + 4\Delta\phi \frac{x}{(1 + x^2)(9 + x^2)} \tag{5}$$

where, T_{CA} is the normalized closed aperture transmittance, $\Delta\phi$ is the nonlinear phase shift, normalized position, x = Z/Z_0 where, Z is the position and Z_0 is the Rayleigh range.

$$\Delta\phi = \Delta\phi_0(z,t)\exp(\frac{-2r^2}{\omega^2}) \tag{6}$$

$\Delta\Phi_0(z,t)$ is the on-axis phase shift at the focus, r being the radius, ω is the spot size at Z.

$$\Delta\phi_0(z,t) = \frac{kn_2 I_{00} L_{eff}}{1+\frac{z^2}{z_0^2}} \tag{7}$$

where k = $2\pi/\lambda$, λ being the excitation wavelength, I_{00} is the on-axis peak intensity at focus calculated using the relation

$$I_{00} = \frac{2E}{\pi^{3/2}\omega_0^2 (HW\,1/e^2\,M)\tau_p (HW\,1/e\,M)} \tag{8}$$

E is the input pulse energy; τ_p is the pulse duration, $2\omega_o$ is the beam diameter at focus.

2.11. Standard error limits

Standard error limits involved in the experimental results were

λ_{max} (abs./flu.)	± 1 nm
Φ_f	± 10%
τ_f	± 5%
τ_r	± 5 - 10%

REFERENCES

(1) Soujanya, T.; Fessenden, R. W.; Samanta, A. *J. Phys. Chem.* **1996**, *100*, 3507.

(2) George, S. J.; Ajayaghosh, A. *Chem. Eur. J.* **2005**, *11*, 3217.

(3) Wang, S.; Gaylord, B. S.; Bazan, G. C. *J. Am. Chem. Soc.* **2004**, *126*, 5446.

(4) Ajayaghosh, A.; George, S. J.; Praveen, V. K. *Angew. Chem., Int. Ed.* **2003**, *42*, 332.

(5) Minakuchi, N.; Hoe, K.; Yamaki, D.; Ten-no, S.; Nakashima, K.; Goto, M.; Mizuhata, M.; Maruyama, T. *Langmuir.* **2012**, *28*, 9259.

(6) Saha, S.; Samanta, A. *J. Phys. Chem. A*. **1998**, *102*, 7903.

(7) Perrin, D. D.; Armerego, W. L. F.; Perrin, D. R. *Purification of Laboratory Chemicals.*; Pergamon Press: Newyork., **1980**.

(8) *Organic Mesoscopic Chemistry*; Masuhara, H.; De Schryver, F. C., Eds.; IUPAC, Black well Science Ltd: Malden, **1999**.

(9) Lakowicz, J. R. *Principles of Fluorescence Spectroscopy*, Second ed.; Kluwer Academic/Plenum Publishers, **1999**.

(10) Austin, E.; Gouterman, M. *Bioinorg. Chem.* **1978**, *9*, 281.

(11) Bevington, P. R. *Data Reduction and Analysis for the Physical Sciences.*; McGraw-Hill: New York., **1969**.

(12) Sheik-Bahae; Said, A. A.; Wei, T. H.; Hagan, D. J.; Stryland, E. W. V. *lEEE J. Quantum Electron.* **1990**, *26*, 760.

Chapter 3

Controlled Fabrication, Characterization and Linear and Non-Linear Optical Properties of Phenazenium Dye Aggregates

Following successful fabrication and morphological characterization, the linear and nonlinear optical properties of the aggregates of three cationic phenazinium dyes, namely safranin O, safranin T and phenosafranin have been probed. These studies reveal needle and cubic morphologies of the aggregates at higher and lower concentrations of the dyes, respectively. This difference is investigated by monitoring the morphology at various time intervals using atomic force microscopy (AFM). The findings suggest one dimensional Ostwald ripening of the cubic aggregates results in the formation of needles. The spectral data suggests that a J-type of interaction leads to the formation of the aggregates and hence, enhancements in the optical properties are observed. Z-scan studies reveal saturable absorption of the aqueous solutions and aggregates, with a five-fold enhancement of the non-linearity for the aggregates. Considering the one dimensional (1D) morphology, high fluorescence efficiency and nonlinear optical properties, the aggregates of these cationic phenazinium dyes appear to be potential candidates for opto-electronic applications.

3.1. Introduction

Nanomaterials based on low molecular weight organic molecules have attracted considerable attention during the past decade due to their interesting optical and electronic properties.[1-6] Organic nanomaterials show optoelectronic

properties, which are strikingly different from those of their inorganic counterparts due to weak intermolecular interaction of the van der Waals type.[7,8] These also have good processability, high reaction activity, good doping properties, and high photoluminescence efficiency.[9-12] Among the organic nanomaterials, those with crystalline one dimensional nanostructures find applications in color tunable display, field effect transistors, chemical sensors, optical waveguides and lasers due to their high charge transport properties and stability.[13-19] Aggregates of many small organic molecules also exhibit strong nonlinear optical (NLO) properties, offering great opportunities for applications in photonic devices.[20,21]

However, fluorescence quenching of the dye solutions at higher concentrations[22] render them unsuitable in photonic applications. Förster and Kasper observed the weakening of pyrene fluorescence with increasing solution concentration.[23] From further observations it was found that it was a general phenomenon for many aromatic compounds. The cause of this concentration-quenching effect was found to be the formation of excimers and exciplexes aided by the collisional interactions between the molecules in the excited and ground states. Much before Förster and Kasper's observation, Scheibe *et al.* and Jelley independently observed 'unusual' spectral behavior of cyanine dyes with increasing dye concentration.[24,25] Later they concluded that these abnormalities in the spectra are due to a phenomenon called "self-aggregation" which can be defined as a direct mutual attraction between particles (atoms or molecules) via van der Waals force or chemical bonding. Almost half a century later, it was found that not just cyanine dyes, many more dyes like squarine, merocyanine and

perylene bisimide derivatives also undergo self-aggregation.[26-30] From the absorption spectral shifts, various aggregation patterns of the dyes in different media have been proposed. The bathochromically shifted J-bands (named after Jelley, one of the first workers who investigated these shifts) and hypsochromically shifted H-bands (H for hypsochromic) of such aggregates have been explained in terms of molecular exciton coupling theory, i.e., coupling of transition moments of the constituent dye molecules.[31-33] H-aggregates are characterized by blue-shifted absorption and decreased quantum yield (compared to monomer), whereas J-aggregation results in a red-shifted absorption along with increase in quantum yield. Therefore, fluorescence quenching of dyes at higher concentration can also be due to the formation of H-aggregates. Aggregation induced emission enhancement (AIEE) first observed by Tang and coworkers offered a new path to address the 'notorious' aggregation-caused quenching of fluorescence at higher dye concentrations.[34] AIEE happens due to the restricted intramolecular vibrational and rotational motions in the aggregates which block the non-radiative pathways.

In the present work, we have studied the morphology, steady state and time-resolved fluorescence and NLO properties of the aggregated state of three cationic phenazinium dyes, namely, safranin O (SFO), safranin T (SFT) and phenosafranin (PSF) (Scheme 3.1). In recent years, phenazinium dyes have received considerable attention because of their use in diverse areas of research including biological stain in histology and cytology.[35-40] Chattopadhyay and coworkers explored the spectral behavior of SFT and PSF in polar protic and aprotic solvents at higher dye concentrations and attributed the unusual spectral behavior to the

self-aggregation of the dye molecules to form a mixture of H and J-aggregates.[41] Even though these studies were carried out carefully, they lack morphological characterization of the aggregates and the mechanism for the simultaneous formation of both H and J-aggregates was unclear. In this work, we have prepared the phenazenium dye aggregates through a facile inverse reprecipitation method and the morphologies are characterized using various microscopic techniques. The photophysical properties of these dye aggregates have been thoroughly studied and found to be very different from the earlier reports.

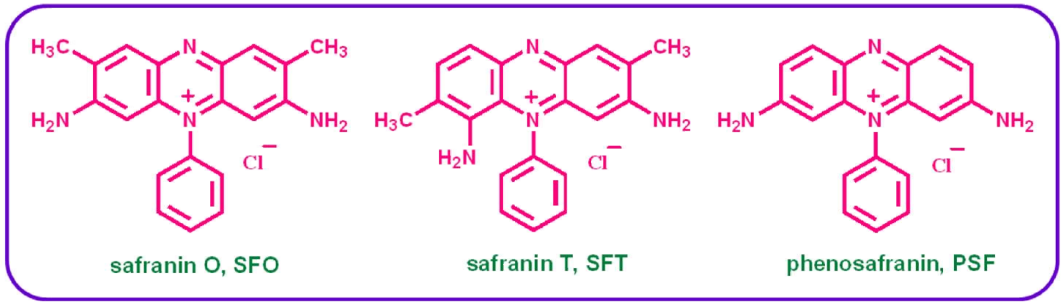

Scheme 3.1. Structures/Abbreviations of the dyes employed in the present study

3.2. Results and Discussion

3.2.1. Morphology characterizations of the dye aggregates

Figure 3.1 shows the SEM images of the SFO, SFT and PSF aggregates. As can be seen, when a small amount of stock solution (100 µL) was injected into ethyl acetate (10 mL), aggregates with cubic morphology and dimensions around 350 nm was observed. Interestingly, the morphology changed from cubes to needles with typical dimensions of ~5-14 µm in length and ~300 nm in width, when a larger quantity of stock solution (300 µL) was injected into 10 mL ethyl acetate. The morphology of the aggregates and their dimensions were further

confirmed by TEM images, Figure 3.1 (g)-(i). These images show that the surfaces of the needles are smooth and uniform. The formation of needle morphology for a higher quantity of stock solution is perhaps due to one dimensional growth of the cubes.

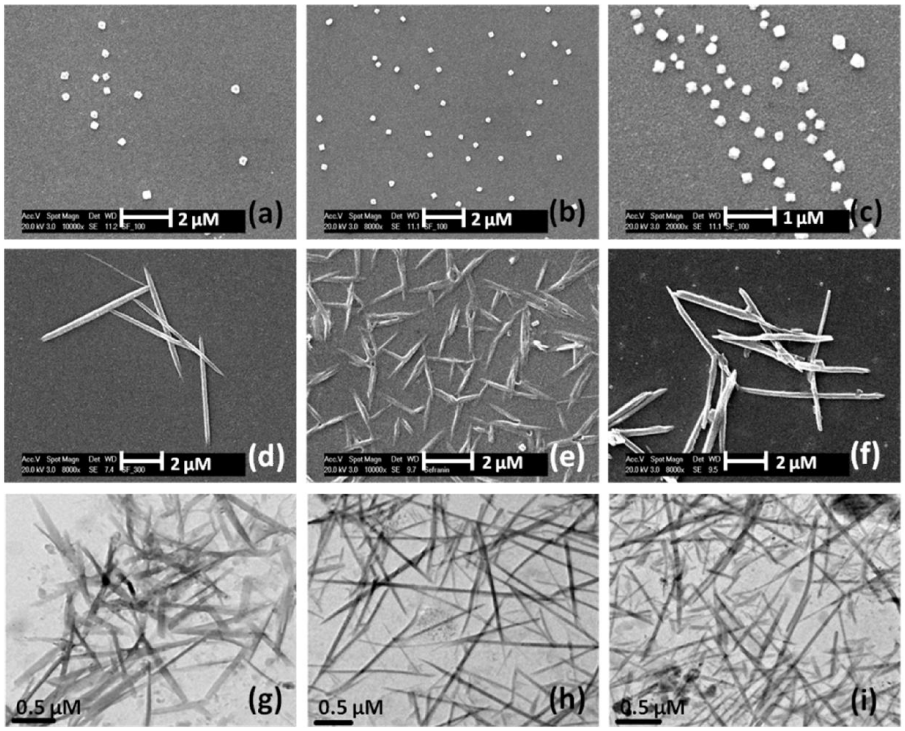

Figure 3.1. SEM and TEM images of the phenazenium dye aggregates at different concentrations of stock solution injected. Top panel- 100 µL injection, SEM, Middle panel- 300 µL injection, SEM, Bottom panel- 300 µL injection, TEM.

The morphologies were further characterized by AFM, Figure 3.2. The thickness of the aggregates measured using atomic force microscope is found to

be of ~350 nm for all the three dye aggregate needles and cubes. Therefore, the microstructures prepared by injecting 100 µL of the stock solution are cubic as all the dimensions are similar (~350 nm). As the thickness of the micro needles is also similar to that of the micro cubes, it is clear that the growth of micro cubes (seed) in one direction leads to the formation of micro needles when 300 µL of the stock solution is injected.

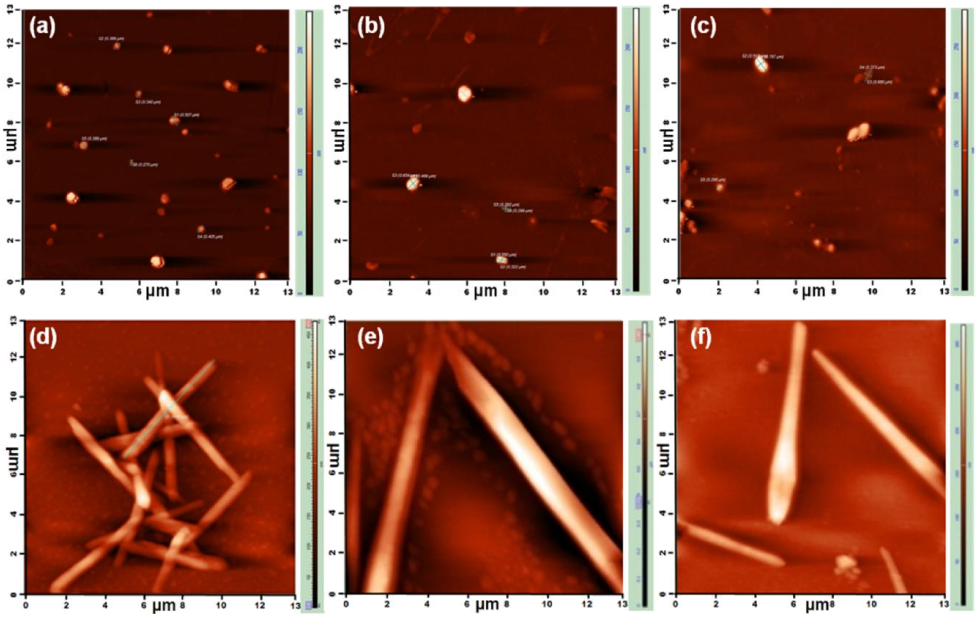

Figure 3.2. AFM images of micro cubes of (a) SFO, (b) SFT and (c) PSF, respectively. (d) – (f) are the corresponding micro needles.

Moreover the sharp edges of the needles were clearly visible in the AFM images which rules out the doubt of rod or tube morphology for phenazenium dye aggregates. The confocal fluorescence microscopy experiments were carried out

to understand the fluorescence behavior of the aggregates in the solid state as shown in Figure 3.3.

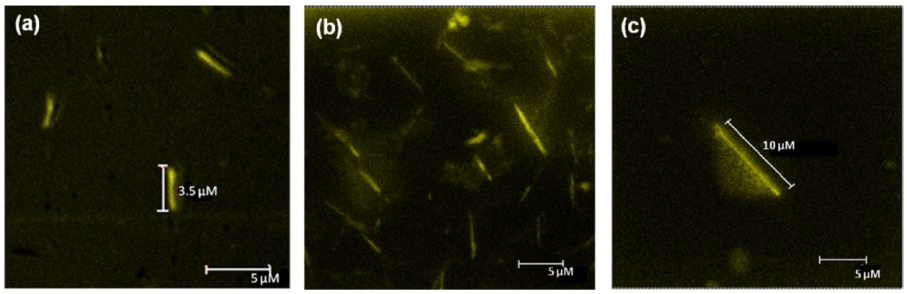

Figure 3.3. Laser scanning confocal fluorescence images of (a) SFO, (b) SFT and (c) PSF micro needles (λ_{exc}= 500-530 nm; λ_{exc} = 550-575 nm).

To understand the difference in the nature of aggregation as a function of the volume of stock solution injected, and also to confirm the one dimensional growth of micro cubes to needles as proposed before, we have studied the aggregation as a function of time. All the aggregate samples are stable for several weeks except for the initial stabilization time of 1.5 hours. In order to understand the initial stages of aggregation, the morphology of the aggregates immediately after preparation till the stabilization time, has been monitored using AFM as shown in Figure 3.4. Aliquots of the colloids (300 µL) are drop casted on the glass plate at intervals of 30 minutes and vacuum dried immediately to prevent further Ostwald ripening in the colloidal state. The images very clearly show gradual formation of needles by Ostwald ripening of the cubic particles. The size and morphology of the aggregates were found to be stable after 90 minutes.

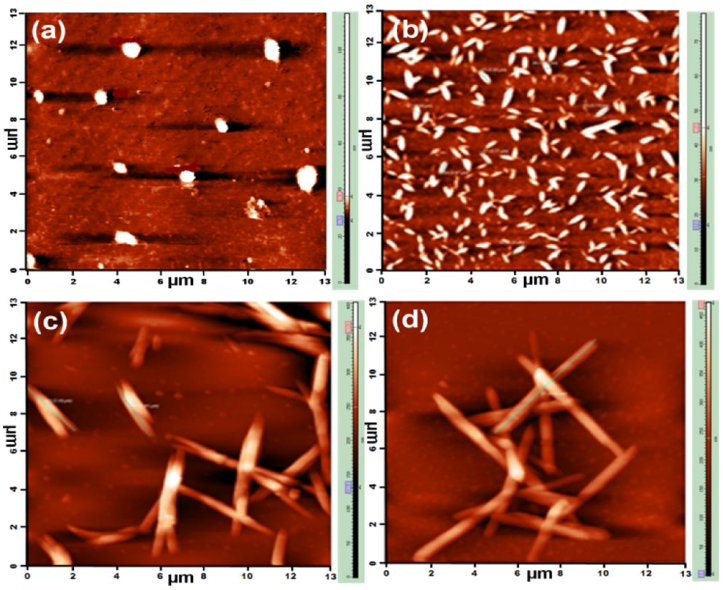

Figure 3.4. AFM images showing the growth sequence of SFO aggregates with time. (a) 0 (b) 30 (c) 60 and (d) 90 min after preparation.

3.2.2. Steady state and time-resolved spectral measurements

3.2.2.1. Absorption spectra

Figure 3.5 compares the absorption spectra of the molecular form of SFO, SFT and PSF in water with those in their aggregated states. All three molecules exhibit broad structureless absorption in water with λ_{abs}^{max} ~520 nm. This is in agreement with the literature.[39,42] The absorption spectra of the aggregates (100 and 300 µL) for all three dyes are similar to the monomer, except for the difference in absorbance and small variation of the λ_{max}. No deformity/broadening of the spectra were observed in the aggregated state in comparison to the homogeneous aqueous solution. A red-shift of the spectral maxima in the aggregated state indicates the formation of J-aggregates.

Deformity and broadening of the absorption spectra of phenazenium dyes at higher dye concentration observed by Sarkar *et al.* was attributed to the aggregation of the dyes.[41] Therefore, further optical studies are carried out to investigate the properties of the dye aggregates prepared by reprecipitation method.

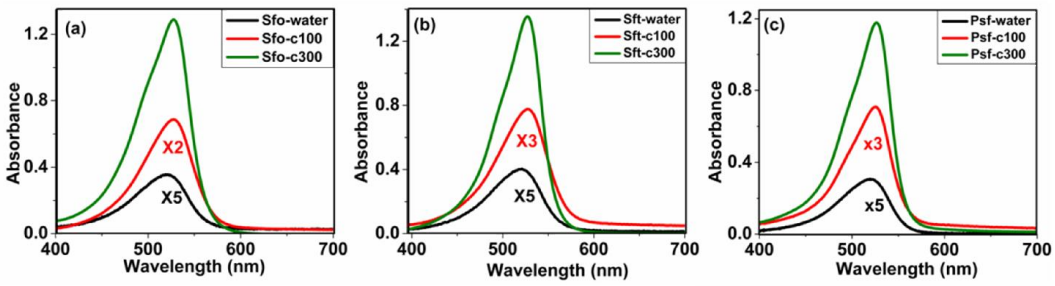

Figure 3.5. Absorption spectra of (a) SFO (b) SFT and (C) PSF in water (black), 100 µL colloid (red) and 300 µL colloid (green).

3.2.2.2. Fluorescence spectra

The emission spectra of the dyes are found to be similar with peak at ~590 nm in water (Figure 3.6). Dye aggregates exhibit 20-30 nm hypsochromic shift of the emission maxima compared to water. Worth noticing is the huge enhancement in the emission of the aggregates (100 and 300 µL) compared to the aqueous dye solution (monomer), which is observed for all the three phenazenium dye aggregates. This enhancement of fluorescence intensity and blue-shift of the emission peak with aggregation is very different from the literature data.[41]

The enhancement in emission is expected, as the aggregates formed are J-type. But, as a considerable enhancement in the absorption of the aggregates is also observed, it is important to know the contribution of aggregation to the

fluorescence enhancement. For this purpose, quantum yield measurements are performed which will be discussed later. But the blue-shift of the emission maxima is unexpected as J-aggregation leads to red- shifted emission. One can attempt to attribute the spectral shift of the emission with aggregation to the increasing structural rigidification of the molecule.[1,43,44] Another reason could be the change in environment of dyes from homogenous to aggregated state, the solvent shell of each participating dye molecule is removed during aggregation, creating a nonpolar/less polar environment compared to water, which leads to the observed blue-shift.[45,46] But a more appropriate explanation for the blue-shifted emission would be the later, *i.e.* change in the environment of the molecules from water to ethyl acetate resulted in the blue-shift. This reasoning is also substantiated by the fact that the emission of phenazenium dyes in ethyl acetate is ~555 nm.

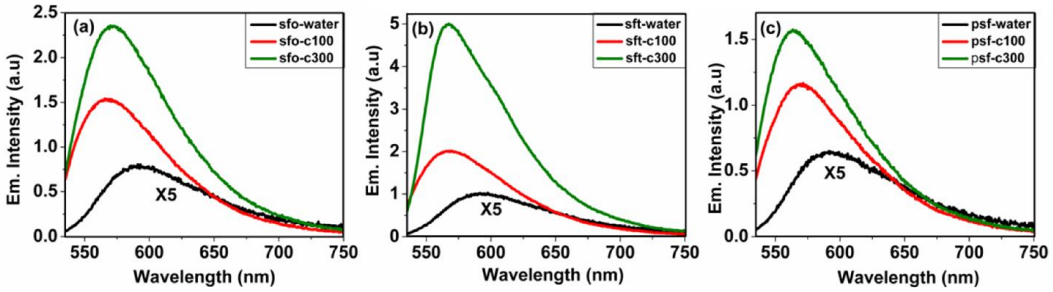

Figure 3.6. Emission spectra of (a) SFO (b) SFT and (C) PSF in water (black), 100 µL colloid (red) and 300 µL colloid (green), λ_{exc} = 405 nm.

3.2.2.3. Fluorescence quantum yield and lifetime studies

The quantum yields of the aggregates were measured and compared with that of the corresponding aqueous monomer dye solutions. For fluorescence quantum

yield measurements, ENBD (4-N,N-diethyl-7-nitrobenz-2-oxa-1,3-diazole-4-yl) in toluene ($\Phi = 0.48$) was used as the standard.[47] The fluorescence quantum yields of the aggregates were found to be 3-4 folds higher compared to the monomer in aqueous solution containing similar quantities of dye (Table 3.1). This enhancement in quantum yield can be attributed to structural rigidification of the molecule in the aggregated state, which blocks/decreases the non-radiative pathways leading to an increase in the quantum yield.[3,43] The increasing quantum yields once again prove J-aggregation of phenazenium dye aggregates.

Table 3.1. Photophysical parameters of SFO, SFT and PSF in water and in the colloidal state.

Sample	SFO			SFT			PSF		
	water	c100 µL	c300 µL	water	c100 µL	c300 µL	water	c100 µL	c300 µL
λ_{abs} (nm)	519	528	528	521	527	527	519	526	526
λ_{emi} (nm)	590	569	570	592	569	567	592	570	564
Φ	0.05	0.18	0.20	0.05	0.15	0.21	0.04	0.18	0.20
τ_1, ns	1.13	1.08	1.20	1.12	1.10	1.10	0.88	1.10	1.01
(a_1), (%)		62.6	50.9		66.3	40.8		64.9	45.7
τ_2, ns		3.07	3.06		3.10	3.02		3.16	3.01
(a_2), (%)		37.4	49.1		33.7	59.2		35.1	54.3
τ_{av}, ns (TCSPC)		1.85	2.11		1.78	2.23		1.82	2.09
τ_{fl} (FLIM)		0.55	0.83		0.63	0.95		0.51	0.73

The fluorescence lifetimes of the colloids and aqueous dye solutions were measured by recording the fluorescence decay profiles using nanosecond TCSPC

setup. The decay profiles of the dye and their corresponding aggregates were shown in Figure 3.7. The decay profiles of the colloids are found to be bi-exponential whereas the aqueous dye solutions exhibit single exponential decay. The decay parameters as well as the average lifetimes are listed in Table 3.1. As can be seen, the faster decaying component matches with that of the monomer and a new slow decaying component due to aggregation arises whose amplitude increases with increasing dye solution injected during colloid preparation. The average lifetimes of all the three dye aggregates are much higher when compared to that in water. A slight increase in the fluorescence lifetime is observed with increasing particle size.

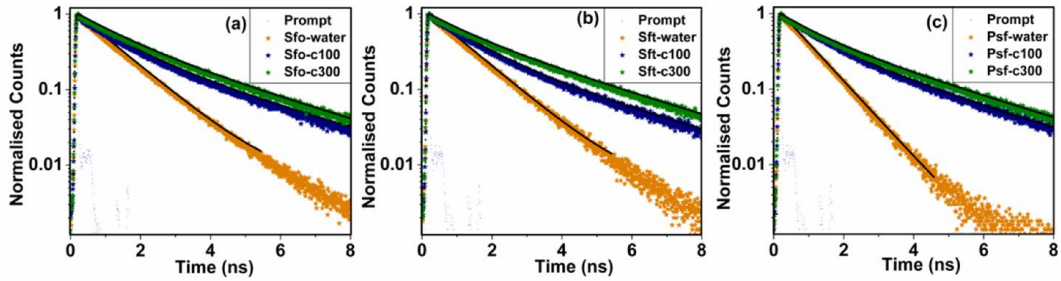

Figure 3.7. Fluorescence decay profiles of (a) SFO (b) SFT and (C) PSF in water (orange), 100 µL colloid (blue) and 300 µL colloid (green).

3.2.3. FLIM measurements

The lifetimes of the individual free standing nanoparticles are also measured with a picoseconds time-resolved fluorescence lifetime imaging microscope (FLIM), which gave spatially resolved fluorescence intensity and fluorescence lifetime images of the individual nano/microparticles. But the individual particles were found to possess single exponential decay with much lower fluorescence

lifetime than the colloids as listed in Table 3.1. FLIM images of the needle aggregates are shown in Figure 3.9. As the FLIM sample preparation involves drying of the solvent under high vacuum, the solvent interactions with the aggregates are eliminated in the samples used for these measurements. Perhaps, this could be the reason for the observed shorter lifetime of these aggregates from FLIM studies. Since only the aggregates are probed, the contributions from free dyes (dissolved) are eliminated which results in the single exponential decay. The same trend of increase in lifetime with increasing particle size is also observed in FLIM analysis which indicates structural rigidification in the aggregates on moving from cubic to needle morphology.

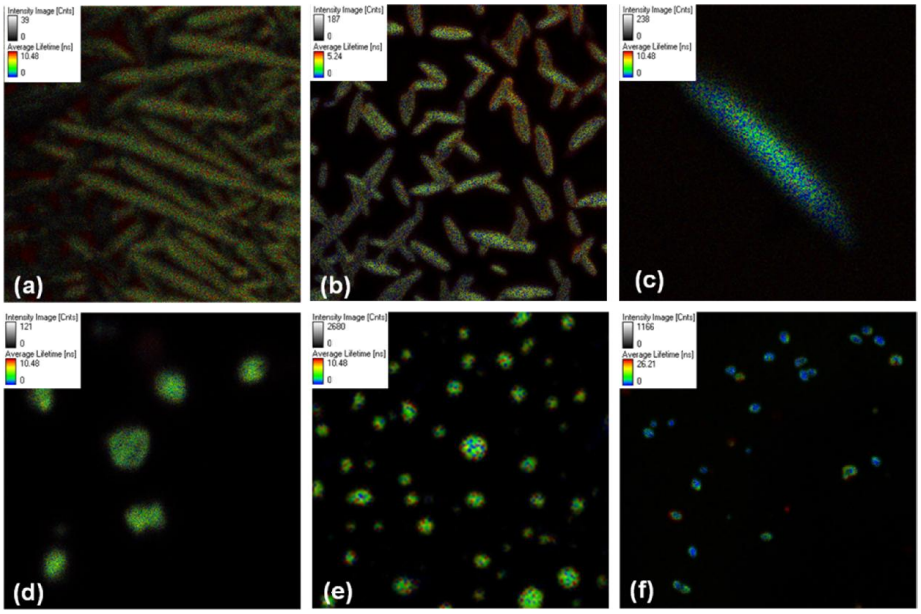

Figure 3.8. FLIM images of (a) SFO, (b) SFT and (c) PSF micro needles. (d)-(f) are FLIM images of the corresponding microcubes.

3.2.4. Z-scan measurements

Figure 3.9 (a)-(c) shows the open aperture Z-scan data for phenazenium dye colloids (300 µL). SFO, SFT and PSF colloids clearly demonstrated saturable absorption (SA) behavior with the magnitude of nonlinear absorption coefficients in the range of (3.6-5) $\times 10^{-15}$ m/W.

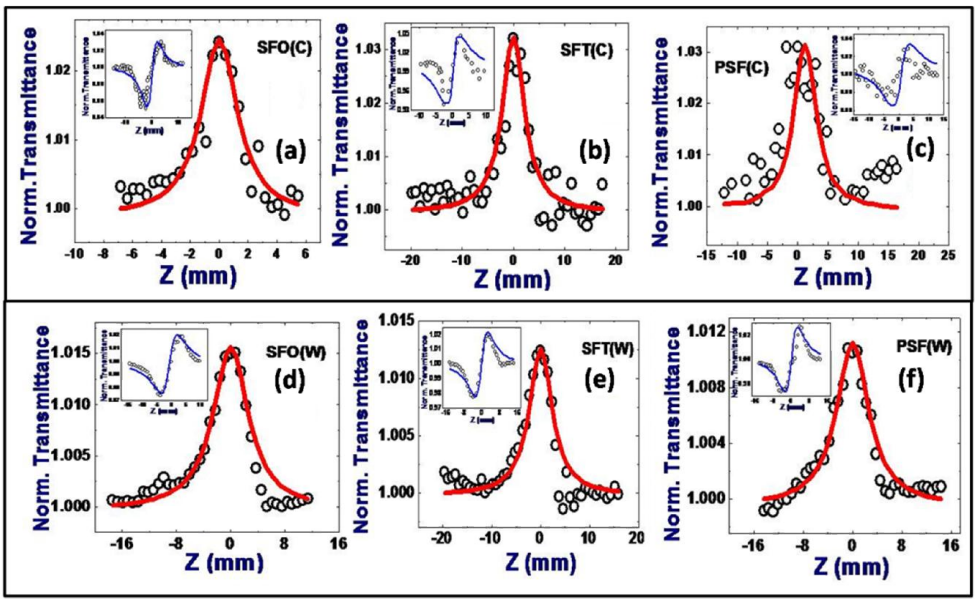

Figure 3.9. Open aperture Z-scan data of (a) SFO (b) SFT and (c) PSF colloids (300 µL). (d)-(f) are the Z-scan data of the corresponding dyes in water. Insets for each of them depict the closed aperture Z-scans. Open circles are the experimental data while the solid lines are theoretical fits.

Figure 3.9 (d)-(f) shows the open aperture Z-scan data for the aqueous dye solutions. SFO, SFT and PSF solutions again clearly demonstrated SA behavior with the magnitude of nonlinear absorption coefficients in the range of (0.95-1.5) $\times 10^{-15}$ m/W. All the values of NLO coefficients are tabulated in Table 3.2. The

values obtained for solutions were much lower compared to the colloids. The nanometric nature of the colloids in contrast to the homogenous dye solutions is responsible for this. Moreover, with the solutions we observed photo-degradation after 2-3 repeated scans. Therefore, we recorded the scans each time with fresh sample solutions.

Table 3.2. NLO coefficients obtained for dye colloids (300 μL) and solutions along with the solvents used.

Sample	n_2 m^2/W x 10^{-21}	Re $\lvert\chi^{(3)}\rvert$ (m^2/V^2) x 10^{-23}	β (m/W) x 10^{-15}	Im $\lvert\chi^{(3)}\rvert$ (m^2/V^2) x 10^{-24}	$\lvert\chi^{(3)}\rvert$ (m^2/V^2) x 10^{-23}	$\lvert\chi^{(3)}\rvert$ (esu) x 10^{-15}
EA	3.0	2.98	3.28	2.08	2.99	2.15
SFO (c)	5.9	5.88	4.89	3.10	5.88	4.21
SFT (c)	8.9	8.87	3.60	2.28	8.87	6.35
PSF (c)	4.0	3.98	5.05	3.20	3.99	2.86
Water	0.9	0.84	0.39	0.23	0.84	0.61
SFO (w)	1.1	0.10	1.45	0.86	0.13	0.09
SFT (w)	1.1	0.10	1.50	0.89	0.14	0.10
PSF (w)	1.3	0.12	0.95	0.56	0.13	0.09

The increase in the non linearity of the colloids can be due to the increased electron density of the aggregates as the molecules are more closely packed compared to the monomer solution. The increase in the non linearity of organic molecules assembled on polymer matrix in comparison to monomer solution has been well reported. This increase in non linearity is due to close packing of the molecules in films, there by the electron cloud is localized and therefore the perturbation of which is more by the electric field created by laser, compared to the monomer solution.[48] The NLO coefficients for phenazenium aggregates are in between the values observed for aromatic compounds and semiconductor/metal

nanoparticles.[49] Thus organic dye aggregates opens a new class of materials whose optical properties can be tuned according to the morphology and are in between the extremely high values of inorganic counterparts and extremely low/nil values of homogenous solutions of organic molecules.

3.3. Conclusions

In summary, three different dye aggregates were prepared through a facile inverse reprecipitation method and the nature of the intermolecular interactions were found to be J-type i.e. a head to tail interaction, from the spectral studies. The morphology of the aggregates could be tuned by changing the concentration of the colloids. We could compare the spectral properties of the as prepared aggregates with those of self-aggregates of SFT and PSF reported by Sarkar *et al.* and found that the deformity in the spectra was not due to aggregation. Also, irrespective of the positions of the methyl group all the three dye aggregates exhibited similar morphology and spectral behavior. The four-fold enhancement in the fluorescence quantum yield of phenazenium dyes on aggregation makes these dye aggregates potential candidates for opto–electronic applications. Increase in the fluorescence lifetime of the nanoparticles with increasing size is another important property which makes the phenazinium dye aggregates useful in the field of light emitting diodes and chemical sensing. Thus careful induced aggregation of phenazenium dyes into J-type aggregates by inverse reprecipitation method resulted in the enhancement of optical properties whereas the same “self-aggregates” formed by increasing dye concentration quenched the dye fluorescence. Moreover we could compare the fluorescence lifetimes of the nanoparticles in colloids with the individual particles using FLIM studies which

give insight into the effect of surrounding media on the lifetime of the aggregates. The Z-scan studies revealed that both the monomers as well as aggregates were saturable absorbers but with a five-fold enhancement in the nonlinearity for the colloids which can be useful in various Q-switching and mode-locking applications.

REFERENCES

(1) Kasai, H.; Nalwa, H. S.; Oikawa, H.; Okda, S.; Matsuda, H.; Minami, N.; Kakuta, A.; Ono, K.; Mukoh, A.; Nakanishi, H. *Jpn. J. Appl. Phys., Part 2,* **1992**, *31*, L1132.

(2) Kasai, H.; Yoshikawa, Y.; Seko, T.; Okada, S.; Oikawa, H.; Matsuda, H.; Watanabe, A.; Ito, O.; Toyotama, H.; Nakanishi, H. *Mol. Cryst. Liq. Cryst.* **1997**, *294*, 173.

(3) Kasai, H.; Kamatani, H.; Yoshikawa, Y.; Okada, S.; Oikawa, H.; Watanabe, A.; Itoh, O.; Nakanishi, H. *Chem. Lett.* **1997**, *26*, 1181.

(4) Debuigne, F.; Jeunieau, L.; Wiame, M.; Nagy, J. B. *Langmuir.* **2000**, *16*, 7605.

(5) Fu, H. B.; Yao, J. N. *J. Am. Chem. Soc.* **2001**, *123*, 1434.

(6) Zhao, Y. S.; Fu, H. B.; Peng, A.; Ma, Y.; Xiao, D.; Yao, J. N. *Adv. Mater.* **2008**, *20*, 2859.

(7) Alivisatos, A. P. *Science.* **1996**, *271*, 933.

(8) Halperin, W. P. *Rev. Mod. Phys.* **1986**, *58*, 533.

(9) An, B. K.; Kwon, S. K.; Jung, S. D.; Park, S. Y. *J. Am. Chem. Soc.* **2002**, *124*, 14410.

(10) An, B. K.; Kwon, S. K.; Park, S. Y. *Angew. Chem., Int. Ed.* **2007**, *46*, 1978.

(11) Zhao, Y. S.; Wu, J.; Huang, J. *J. Am. Chem. Soc.* **2009**, *131*, 3158.

(12) Peng, A.; Xiao, D.; Ma, Y.; Yang, W.; Yao, J. *Adv. Mater.* **2005**, *17*, 2070.

(13) Zhao, Y. S.; Fu, H.; Hu, F.; Peng, A.; Yang, W.; Yao, J. *Adv. Mater.* **2008**, *20*, 79.

(14) Zhao, Y. S.; Fu, H.; Hu, F.; Peng, A.; Yao, J. *Adv. Mater.* **2007**, *19*, 3554.

(15) Briseno, A. L.; Mannsfeld, S. C. B.; Lu, X.; Xiong, Y.; Jenekhe, S. A.; Bao, Z.; Xia, Y. *Nano Lett.* **2007**, *7*, 668.

(16) Che, Y.; Yang, X.; Loser, S.; Zang, L. *Nano Lett.* **2008**, *8*, 2219.

(17) Naddo, T.; Che, Y.; Zhang, W.; Balakrishnan, K.; Yang, X.; Yen, M.; Zhao, J.; Moore, J. S.; Zang, L. *J. Am. Chem. Soc.* **2007**, *129*, 6978.

(18) Takazawa, K.; Kitahama, Y.; Kimura, Y.; Kido, G. *Nano Lett.* **2005**, *5*, 1293.

(19) O'Carroll, D. L.; Lieberwirth, I.; Redmond, G. *Nt. Nanotechnol.* **2007**, *2*, 180.

(20) Wang, Y. *Chem. Phys. Lett.* **1986**, *126*, 209.

(21) Li, Y.; Liu, T.; Liu, H.; Tian, M.; Li, Y. *Acc. Chem. Res.* **2014**, *47*, 1186.

(22) Birks, J. B. *Photophysics of Aromatic Molecules*; Wiley, London, 1970.

(23) Forster, T.; Kasper, K. *Phys. Chem.* **1954**, *1*, 275.

(24) Jelley, E. E. *Nature.* **1936**, *138*, 1009.

(25) Scheibe, G. *Angew. Chem.* **1936**, *49*, 563.

(26) Mizutani, F.; Iijima, S.-i.; Tsuda, K. *Bull. Chem. Soc. Jpn.* **1982**, *55*, 1295.

(27) Chen, Z.; Lohr, C. R.; Saha-Moller; Wurthner, F. *Chem. Soc. Rev.* **2009**, *38*, 564.

(28) Kalisky, Y.; Williams, D. J. *Chem . Phys. Lett.* **1982**, *86*, 100.

(29) Das, S.; Thanulingam, T. L.; Thomas, K. G.; Kamat, P. V.; George, M. V. *J. Phys. Chem.* **1993**, *97*, 13620.

(30) Wurthner, F.; Thalacker, C.; Diele, S.; Tschierske, C. *Chem. Eur. J* **2001**, *7*, 2245.

(31) Brooker, L. G. S.; White, F. L.; Heseltine, D. W.; Keyes, G. H.; Dent, S. G.; VanLare, E. J. *J. Photogr. Sci.* **1953**, *1*, 173.

(32) McRae, E. G.; Kasha, M. J. *J. Chem. Phys* **1958**, *28*, 721.

(33) Kasha, M.; Rawis, H. R.; El-Bayoumi, M. A. *Pure. Appl. Chem.* **1965**, *11*, 371.

(34) Qin, A.; Tang, B. Z. *Aggregation-Induced Emission: Fundamentals.*, First ed.; John Wiley & Sons, Ltd., 2013.

(35) Broglia, M. F.; Bertolotti, S. G.; Previtali, C. M. *J. Photochem. Photobiol. A: Chem.* **2005**, *170*, 261.

(36) Islam, S. D.-M.; Fujitsuka, M.; Ito, O. *Phys. Chem. Chem. Phys.* **1999**, *1*, 3737.

(37) Broglia, M. F.; Bertolotti, S. G.; Previtali, C. M.; Montejano, H. A. *J. Photochem. Photobiol. A: Chem.* **2006**, *180*, 143.

(38) Gomez, M. L.; Avila, V.; Montejano, H. A.; Previtali, C. M. *Polymer.* **2003**, *44*, 2875.

(39) Gomez, M. L.; Previtali, C. M.; Montejano, H. A. *Spectrochim. Acta (Part A).* **2004**, *60*, 2433.

(40) Rosenberg, L. *J. Bone Joint Surg Am.* **1971**, *53*, 69.

(41) Sarkar, D.; Das, P.; Girigoswami, A.; Chattopadhyay, N. *J. Phys. Chem. A*. **2008**, *112*, 9684.

(42) Ganguly, P. *J. Mol. Liq.* **2010**, *151*, 67.

(43) Patra, A.; Hebalkar, N.; Sreedhar, B.; Sarkar, M.; Samanta, A.; Radhakrishnan, T. P. *Small.* **2006**, *2*, 650.

(44) Xiao, D.; Xi, L.; Yang, W.; Fu, H.; Shuai, Z.; Fang, Y.; Yao, J. *J. Am. Chem. Soc.* **2003**, *125*, 6740.

(45) Kanaparthi, R. K.; Sarkar, M.; Samanta, A. *J. Phys. Chem. B* **2009**, *113*, 15189.

(46) Saikia, P. M.; Dutta, R. K. *Indian Journal of Chemistry* **2001**, *40A*, 396.

(47) Saha, S.; Samanta, A. *J. Phys. Chem. A*. **1998**, *102*, 7903.

(48) Huang, C.; Li, Y.; Song, Y.; Li, Y.; Liu, H.; Zhu, D. *Adv. Mater.* **2010**, *22*, 3532.

(49) Ganeev, R. A.; Kamanina, N. V.; Kulagin, I. A.; Ryasnyansky, A. I.; Tugushev, R. I.; Usmanov, T. *Quantum Electron.* **2002**, *32*, 781.

Chapter 4

Cyanine Dye Induced Fluorescence Quenching of an Oligo(p-phenylene vinylene)-based Self-Assembly: Presence of Multiple Aggregates

Fluorescence quenching of an oligo(p-phenylene vinylene) (OPV) self-assembly/self-aggregates by a cyanine dye, oxatricarbocyanine (OCY), has been investigated using steady-state and time-resolved fluorescence techniques. A decrease in fluorescence intensity of the OPV self-assembly accompanied by an enhancement of the emission intensity of OCY has been observed indicating possible occurrence of Förster Resonance Energy Transfer (FRET) between the self-assembly and dye. However, the time-resolved studies reveal that fluorescence quenching proceeds via a static interaction between the two. Careful analysis of the steady-state and time-resolved spectral data and morphological changes with gradual increase of the cyanine concentration suggests that quenching is not only triggered by static interactions, but it also involves partial quenching of only one of the two distinct types of aggregates in the OPV self-assembly. These results point out the importance of a deeper analysis of the fluorescence quenching and aggregation behavior in self-aggregates to avoid erroneous conclusions.

4.1. Introduction

Organogels, which prevent the flow of entrapped solvents, have attracted tremendous interest over the past decade due to their potential applications in

organic electronics.[1-4] Among the numerous examples, the cholesterol and lecithin based organogels find wide applications in drug delivery, the thienylene vinylenes based gels are used in organic solar cells and the perylene bisimide- and phthalocyanine- based fluorescent organogels are widely employed in sensing and photovoltaic applications.[5-9] π-conjugated electron rich systems like oligophenylene vinylenes (OPVs) and oligophenylene ethynylenes (OPEs) have been studied extensively owing to their attractive fluorescence properties as well as ordered arrangement of the molecules in the gel state, which facilitates efficient energy migration.[10-12] The formation of 3D networks of fibrils in organogels is facilitated by self-assembly of molecules through non-covalent interactions like π-π stacking, hydrogen bonding, and van der Waal's interactions.[13] The nature of packing of molecules in the self-assemblies plays a key role in determining the photoluminescence properties of the gels. Extensive studies on tuning the fluorescence properties of the organogels by changing solvents, end-functional groups and alkyl chain lengths of monomers, thereby changing the intermolecular interactions which pave the way for gelation, have been reported.[14-16]

Linear π-conjugated systems, particularly the OPVs, are of particular interest owing to their efficient energy migration and intramolecular electron transfer properties.[10,17] Detailed studies on exploration of the structural aspect in self-assembly, energy migration, FRET, and molecular sensing properties of OPVs have been carried out by several groups among which those of Heegar, Bazan, Swager, and Ajayaghosh are noteworthy.[12,18-25] Meijer and Wurthner have studied the energy transfer process in H-bonded self-assemblies[26,27] and OPV-perylenebisimide co-assemblies.[28,29] Armaroli and Martin studied the electron

transfer in OPV-ferrocene[30] and OPV-fullerene dyads.[31] Recently, OPV-based systems have been used as passivating/stabilizing ligands for quantum dots to effectively tune their photophysical properties.[32,33]

Although majority of the studies have focused on the application of OPVs in the gel state,[12,24,25,34,35] the nature of aggregation in the self-assembly and the mechanism of fluorescence quenching observed in OPV aggregates by organic dyes remains poorly understood. The exact nature of aggregation of OPV remains a matter of debate as a red-shifted shoulder in the absorption spectrum of the self-assembly compared to the monomer indicates J-type aggregation. However, a decrease in fluorescence quantum yield and an overall blue-shift of the absorption spectra of the self-assembly compared to monomer suggests H-type aggregation.[36-39] Different types of aggregations like β-sheet motif, J or H-aggregation, and pseudo J or H-aggregation have been reported for the self-assembly of various OPV derivatives considering only their prominent optical properties.[36-39]

In the present work we have attempted to explain the presence of multiple aggregates in a bis alcohol derivative of OPV[12-14,36] by studying its interaction with an organic dye, DOTC iodide[40,41] also known as oxatricarbocyanine, OCY (Figure 4.1). Several factors have to be considered while selecting the solvent for studies involving interactions between self-assemblies and dyes as: (i) both the systems used should be dispersed in a suitable solvent in order to obtain a homogenous solution, (ii) the components must be stable under the experimental conditions, (iii) the critical gelation concentration of the gelator in the chosen

solvent should not be too high or it can cause inner filter effects and (iv) the resulting dye-organogel pair should be optically transparent for the photophysical characterization. Keeping these factors in view, we chose benzonitrile as solvent to study the interaction between OPV self-assembly and OCY. Figure 4.1 shows an overlap between the long wavelength region of the emission spectrum of OPV self-assembly and the absorption spectrum of OCY, indicating the possibility of FRET in the present system. The fluorescence quenching of OPV aggregates by OCY is studied in detail which will be presented in the following sections.

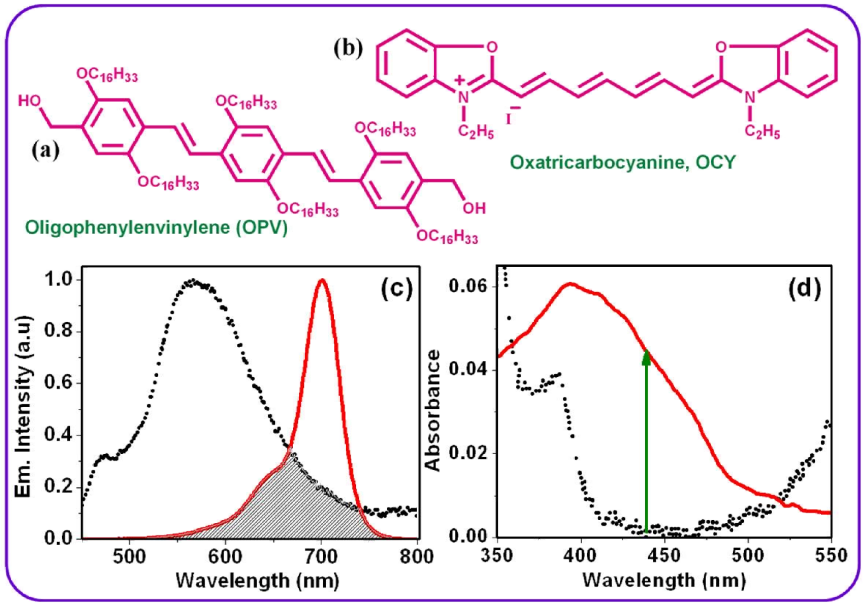

Figure 4.1. Structures of (a) OPV and (b) OCY. (c) Shaded area shows the spectral overlap between the emission spectrum of the OPV self-assembly (·····) and the absorption spectrum of OCY (——). (d) Comparison of the absorption spectra of 10 μM solutions of OCY (·····) and OPV (——) in benzonitrile highlighting the difference in OD at λ_{exc} = 439 nm.

4.2. Results and Discussion

4.2.1. Steady-state and time-resolved measurements

OPV self-aggregates in solvents like cyclohexane, dodecane, benzonitrile etc and exists as monomer in chloroform. The absorption and emission spectra of OPV in its self-assembled form (benzonitrile) and its monomeric form (chloroform) are shown in Figure 4.2 for comparison. In chloroform, the λ_{abs}^{max} is observed at ~410 nm, whereas in benzonitrile, the spectrum of the self-aggregates appears broader with a blue-shift of the absorption maxima and a shoulder appearing at ~497 nm. This spectral behavior is consistent with the literature of OPV self-aggregates.[13] The blue-shift of the absorption maxima compared to the monomer is an indication of H-aggregation.[39] On the other hand, a new shoulder appearing at the red end of the self-aggregate spectrum suggests J-aggregation.[38]

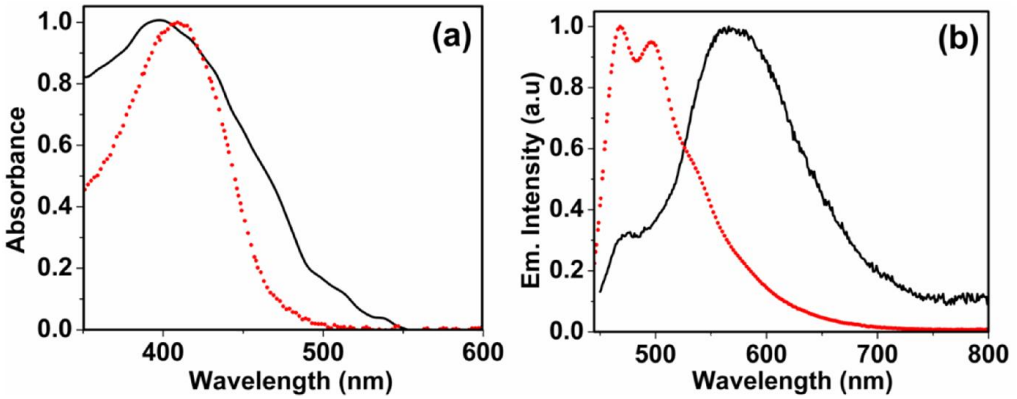

Figure 4.2. Normalized (a) absorption and (b) emission spectra of OPV in benzonitrile (——) and chloroform (·····), λ_{exc} = 439 nm.

OPV in the monomeric form exhibits structured emission with distinct peaks at ~468 and ~497 nm and a shoulder at around ~540 nm. But, compared to monomer, the emission spectrum of OPV self-aggregates is much broader and red-shifted due to aggregation.[24]

Emission properties of OPV in its monomeric form (chloroform) are independent of the excitation wavelength (λ_{exc}). However, emission behavior of OPV self-aggregates is found to depend on the excitation wavelength as shown in Figure 4.3. When λ_{exc} is varied from 350 to 390 nm, OPV self-assembly exhibits structured emission spectra between 400-500 nm and a broad band with peak at 550 nm. As λ_{exc} exceeds 400 nm, the peaks at lower wavelengths vanish and the long wavelength peak at 551 nm intensifies and exhibits gradual red-shift resulting in an emission at 577 nm.

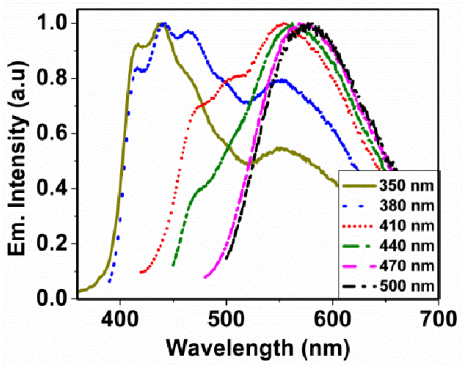

Figure 4.3. Excitation wavelength dependent emission of OPV in benzonitrile at 25 °C.

It is to be noted that, the peaks at 469 and 497 nm are due to the presence of monomeric form of OPV. The excitation wavelength dependent emission

behavior of OPV aggregates clearly suggests that the broad emission observed for OPV self-aggregates in benzonitrile is a combination of emission from monomer and self-aggregates.

4.2.2. Quenching studies

To get a better insight into the optical properties of OPV self-aggegrates, we have studied the quenching of the OPV fluorescence by an organic dye, OCY. The choice of the quencher was guided by our interest on the selective quenching of the emission of any one type of aggregates in the OPV self- assembly from the other aggregate/aggregates present, if any. Therefore the quencher absorption spectrum has spectral overlap with only the higher wavelength region of the emission spectra of OPV self-aggregtaes. The effective quenching of the emission of OPV gel by rhodamine B was studied by Ajayaghosh and coworkers. They attributed the quenching to FRET.[13,24] Even though this study helped in designing flexible (gel film) light harvesting devices, the time-resolved fluorescence measurements in support of the mechanism of fluorescence quenching of OPV self-aggregates by organic dyes were lacking.

The steady-state and time-resolved fluorescence quenching experiments have been performed by exciting the samples at 439 nm, where OPV self-assembly absorbs much more strongly compared to OCY, as shown in Figure 4.1. This ensures that the exciting light is primarily absorbed by the prospective donor, a condition ideally suited for energy transfer experiments. Moreover the emission of OCY[40-42] is well separated from that of OPV.

The concentration of OCY was varied from 10-100 μM for the quenching studies. It is to be noted that at these concentrations OCY remains in the monomer state. The effect of addition of OCY (10-100 μM) to OPV self-aggregates (10 μM) is shown in Figure 4.4. A significant decrease in the emission intensity of OPV self-aggregates along with an enhancement in the emission intensity of OCY is observed. Considerable narrowing of the emission band of OPV aggregates is also observed with increase in quencher concentration. No change was observed for the short wavelength fluorescence component (470 nm), which corresponds to the monomer emission (as mentioned earlier). Excitation of the dye solutions of same concentration at 439 nm in the absence and presence of OPV aggregates shows that, the emission intensity is slightly higher for the latter (inset Figure 4.4) indicating possibility of FRET.

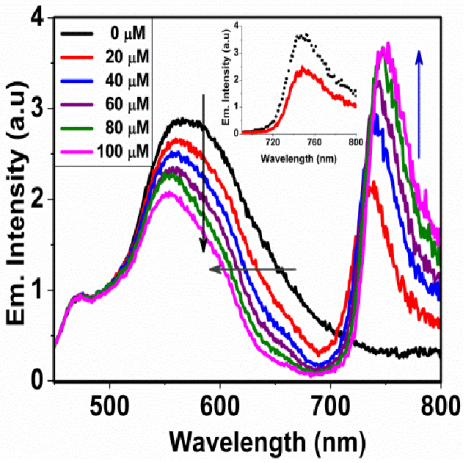

Figure 4.4. Quenching of the emission of OPV self-aggregates (10 μM) in benzonitrile with increasing concentrations of OCY (10-100 μM). Inset compares the emission of OCY (100 μM) in the absence (——) and presence (·····) of OPV, λ_{exc} = 439 nm.

To understand the exact mechanism of fluorescence quenching, time-resolved fluorescence is of eminent importance. The fluorescence decay of OPV aggregates in presence of various concentrations of OCY were monitored at 555 and 745 nm. OPV in chloroform (monomer) exhibits a single exponential fluorescence decay behavior with a lifetime of 1.5 ns. But in benzonitrile (self-aggregates), the fluorescence decay kinetics of OPV can be best represented by a sum of two exponentials of the form, $I(t) = a_1 \exp(-t/\tau_1) + a_2 \exp(-t/\tau_2)$ consisting of a major (77%) long-lived (1.95 ns) component and a minor short-lived (0.7 ns) component. The fluorescence lifetime data for OPV self-assembly in benzonitrile for different concentrations of OCY is presented in Table 4.1.

In general, if FRET occurs, the fluorescence lifetime of the donor should decrease. Also a growth component (with negative relative contribution) for the acceptor emission can be noticed in FRET, due to the sudden increase in the excited state population of acceptor. But in this study, we have not observed any considerable change in the fluorescence lifetime of the OPV self-aggregates, thereby ruling out the possibility of dynamic quenching. Moreover, no growth component was observed for the acceptor emission when monitored at 745 nm, indicating that the fluorescence quenching of OPV self-aggregates is not due to FRET.

Table 4.1. Time-resolved decay parameters of OPV self-assembly (10 μM) for various concentrations of OCY [λ_{exc} = 439 nm, emission collected at 555 nm].

OCY(mM)	τ_1(ns)	b_1	τ_2 (ns)	b_2	$\tau_{i.ave}$(ns)
0	0.73	23.08	1.95	76.92	1.66
0.02	0.76	25.63	2.00	74.37	1.68
0.04	0.75	25.80	1.93	74.20	1.63
0.06	0.74	26.38	1.93	73.62	1.62
0.08	0.76	28.48	1.91	71.52	1.58
0.1	0.75	28.83	1.93	71.17	1.59

Therefore, the selective quenching of emission intensity of OPV self-aggregates at the longer wavelength region of the spectra (575-625 nm) by OCY, is static in nature. The rate constant for the static quenching, estimated from the Stern-Volmer plot (Figure 4.5) based on steady-statefluorescence intensities, is 6.13×10^{12} M^{-1} s^{-1}.

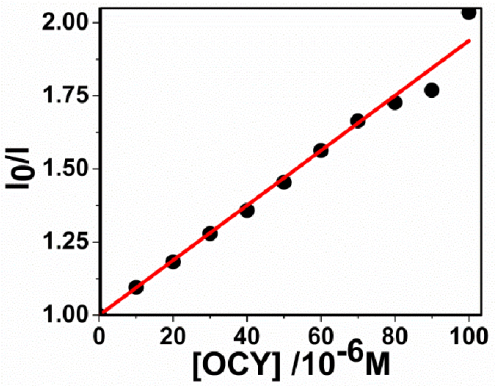

Figure 4.5. Stern-Volmer plot based on the fluorescence intensity measured at 605 nm.

In addition to the fluorescence quenching, another aspect which cannot be ignored, is the progressive narrowing of the fluorescence spectra of OPV self-

aggregates with increasing addition of OCY. A close look at the spectral behavior of OPV aggregates reveals, relatively higher extent of quenching at around 610 nm compared to 550 nm on addition of OCY. This suggests that the broad emission spectrum of the OPV self-assembly is due to the presence of two closely emitting species; one of which has emission maxima around 550 nm and the other emits at ~610 nm along with the monomer emission (470 nm). On addition of OCY, only long wavelength emission of OPV gets quenched selectively, due to the selective complex formation between one of the two types of aggregates present in OPV self-assembly (emitting at ~610 nm) and OCY, resulting in static quenching.

As the emissions of OPV self-assembly is due to the presence of two type of aggregates and the monomer, to understand the spectral behavior better, both the absorption and emission spectra of OPV self-assembly were deconvoluted as shown in Figure 4.6. The deconvolution of the absorption and emission spectra into overlapping Lorentzian curves were done using the MS Origin 7 fitting algorithm to obtain the minimum number of reproducible absorbing and emitting components using the adjustable parameters of the center, width and amplitude for the resolved bands. Multiple attempts were made to fit the data with different initial parameters and from a set of different deconvolutions of an overall spectrum, a "good fit" was then judged by a minimum in the goodness of fit parameter χ^2.

The deconvolution of absorption spectra yields three peaks: a central band around 410 nm, a blue-shifted 365 nm band and a red-shifted band around 465 nm (Figure 4.6). As already mentioned, the absorption maximum around 410 nm

corresponds to the monomer absorption (as observed in chloroform). According to literature the red-shifted shoulder around 470 nm seen for OPV self-assembly in non-polar solvents is due to aggregation.[24] The blue-shift to form a band at 365 nm cannot be due to the polarity change, as benzonitrile is more polar in nature than chloroform.

Emission spectra of OPV self-aggregates were also deconvoluted, to yield two peaks, one at ~ 560 nm and the other at ~615 nm. These peaks match well with the emission maxima observed after addition of OCY. This further suggests that OPV self–assembly consists of two different types of aggregates. Since, the monomer peak is separated (470 nm) from the aggregates; it is not specifically shown in the deconvoluted emission spectra.

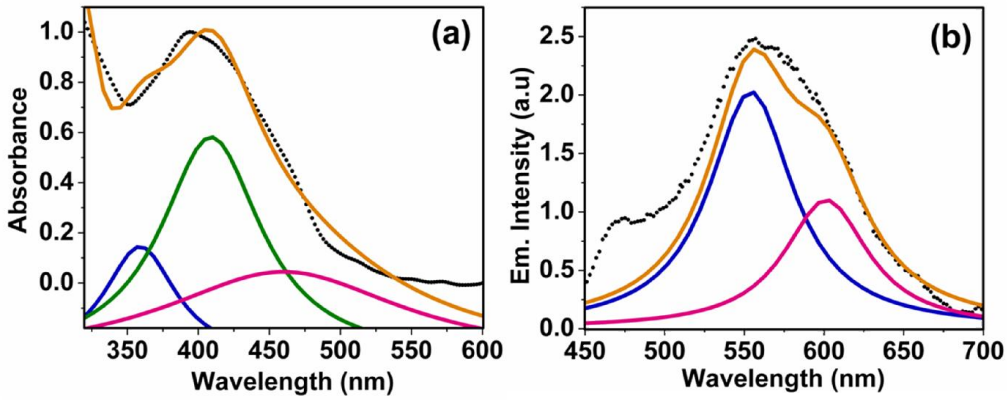

Figure 4.6. Deconvoluted (a) absorption and (b) emission spectrum of OPV self-assembly in benzonitrile.

4.2.3. Morphology

4.2.3.1. Scanning electron microscopy

The fibrillar morphology of the OPV self-assembly is well known.[24] In benzonitrile, OPV self-assembles into entangled nanostructures of approximately 100-200 nm width. Several studies on the interaction of OPVs with other organic molecules have been reported.[24,36] No change in the morphology of OPV self-assembly were reported in those cases. But we observed a change in the fibrillar morphology of OPV aggregates to sheet structures on addition of OCY.

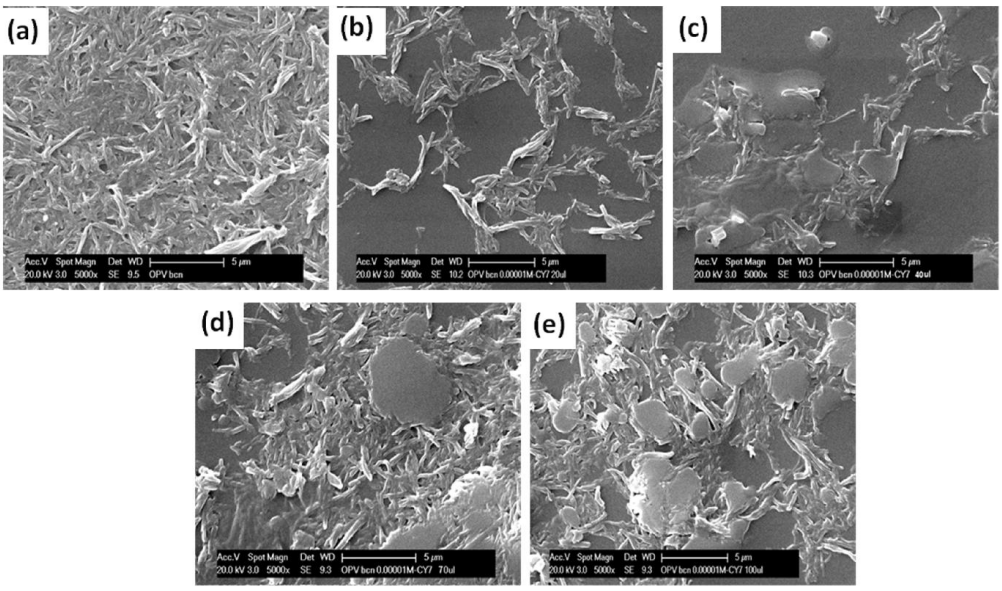

Figure 4.7. SEM images of OPV in benzonitrile (10 µM) with different concentrations of OCY (a) 0 µM (b) 20 µM, (c) 40 µM, (d) 70 µM and (e) 100 µM. The scale bar is 5 µm for all images.

Figure 4.7 depicts the SEM images of OPV self-assembly in benzonitrile highlighting the change in morphology on gradual addition of OCY. However, we observed drastic change in the morphology of OPV self-assembly, indicating an interaction between OPV and OCY at the molecular level.

The transition from fibrillar to sheet morphology with increasing concentrations of OCY can be understood as follows: in the beginning, when OCY concentration is zero, OPV shows fibrillar morphology as expected. With 20 μM concentration of OCY, the self-assembly is disturbed and as a result fibril clusters could be observed. As the concentration of OCY increases to 40 μM, sheet like structures could be observed along with the initial fibrillar morphology. This indicates that at 20 μM concentration of OCY, OPV self- assembly could not form any sheets, but instead interacts with the dye which hinders the formation of self-assembly and results in the formation of OPV fibril clusters. When concentration of OCY is further increased to 70 μM, sheets can be clearly observed which is due to enhanced interaction of OPV self-assembly with the dye molecules thereby hindering the forces responsible for the formation of fibrils. At 100 μM concentration well separated sheets and fibrils can be seen which shows that OCY forms a complex with only the one type of OPV aggregates and the other fibrils which are part of the second type of aggregates remain unaffected in morphology even after the interaction with OCY.

4.2.3.2. Confocal fluorescence microscopy

In order to correlate the emission properties and morphology of OPV aggregates, confocal fluorescence microscopy experiments, where the emission

spectra of a particular nano/micro particle can be recorded, were carried out. OPV fibrils are not clearly visible by confocal microscopy due to the lower resolution of the instrument. However, the same sample is used for all the morphological analysis. Figure 4.8 shows the transformation of fluorescent OPV fibrils to non fluorescent sheets with increasing concentrations of OCY. The sheet morphology with fibrils at the edges and on the surface of the sheets, earlier observed in the SEM images are now visible more clearly.

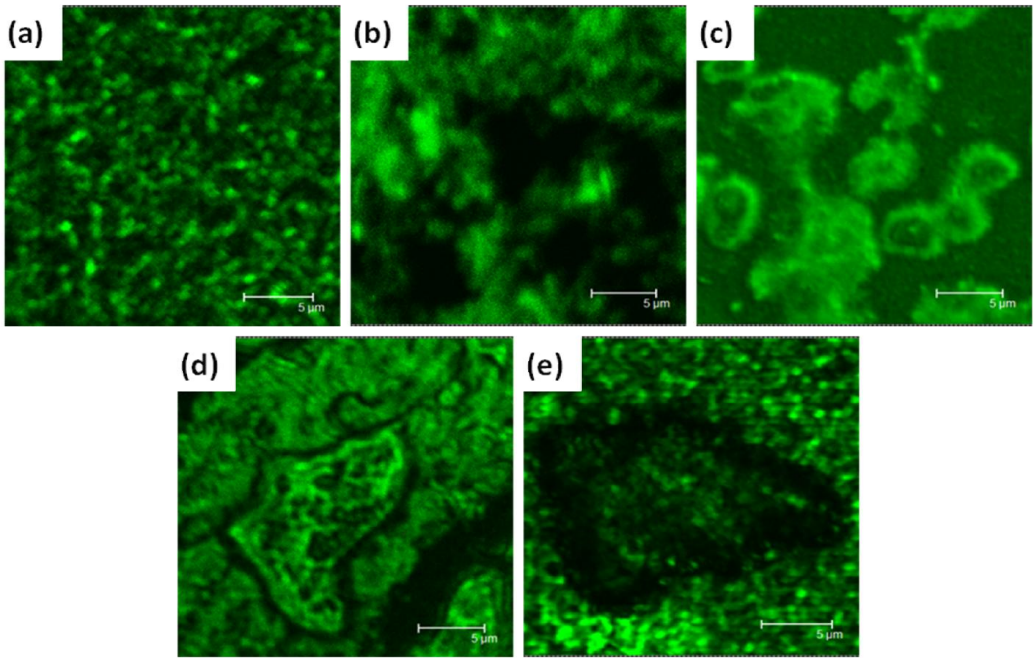

Figure 4.8. Confocal fluorescence images of OPV in benzonitrile (10 µM) with different concentrations of OCY (a) 0 µM (b) 20 µM, (c) 40 µM, (d) 70 µM and (e) 100 µM. The scale bar is 5 µm for all images.

The emission spectra from OPV aggregates were plotted and found exactly match with the emission properties in the solution. Figure 4.9 (a) shows that the broad emission for OPV self-assembly (drop casted on cover slip and vacuum dried) in the 500-700 nm region is very similar to that in the solution. The fibrillar regions at the edges of the sheets visible on addition of OCY, emits at around 550 nm which corresponds to the emission maximum of OPV at the highest concentration of OCY (as found in the quenching studies in solution) (Figure 4.9 (b)). Therefore, these studies confirm the presence of two types of aggregates, where the type which emits at longer wavelength is quenched by OCY and forms non fluorescent sheets where as the other type which emit at 550 nm is not influenced by OCY, and hence, retains original fibrillar morphology.

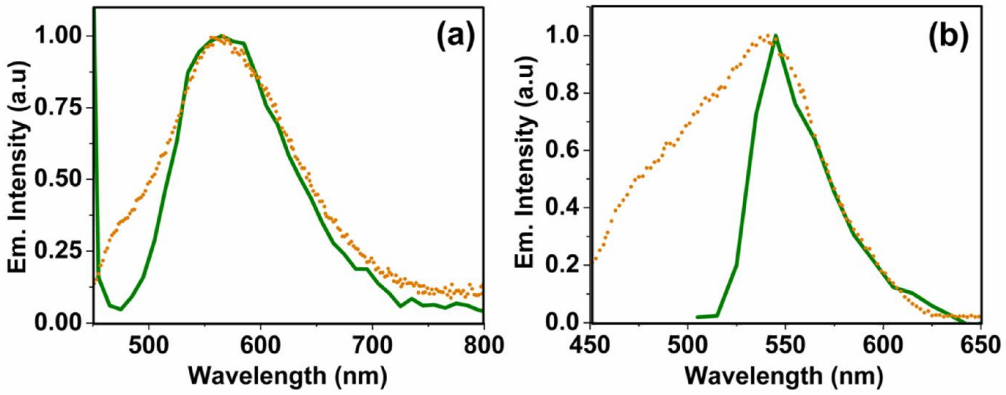

Figure 4.9. Comparison of emission spectra of OPV in benzonitrile (——) from confocal fluorescence microscope technique with that of the solution state (·····), (a) in the absence of OCY and (b) in the presence of 100 μM OCY.

4.2.4. Quenching studies of OPV gel with OCY

The nature of aggregation is the foundation for the formation of gel. Therefore, the results in the self-assembled state and gel state should ideally match. In this context, fluorescence quenching experiments were carried out in the gel state of OPV. It is to be noted that the critical gelation concentration (CGC) was calculated to be 2.8 mM for OPV in benzonitrile. The results observed in the gel matches very well with that observed in OPV self-aggregates which further proves the presence of two types of aggregates in OPV self-assembly (Figure 4.10). It is worth noticeable that the complete quenching of OPV occurs in the gel state even at lower concentrations of OCY. When the quencher concentration exceeds 0.05 mM, gel formation itself does not occur at all, which indicates that the equilibrium between the various forces responsible for gelation is disturbed in presence of OCY. This in turn corroborates the interaction between OPV and OCY at the molecular level.

The concept of H and J-aggregation based on the distinct changes in the absorption spectra of aggregates as compared to the monomeric species have been proposed by Jelley and coworkers.[43,44] Accordingly, the absorption spectra and quantum yields give us a clear idea on the type of aggregates present in the self-assembly.[5,45]

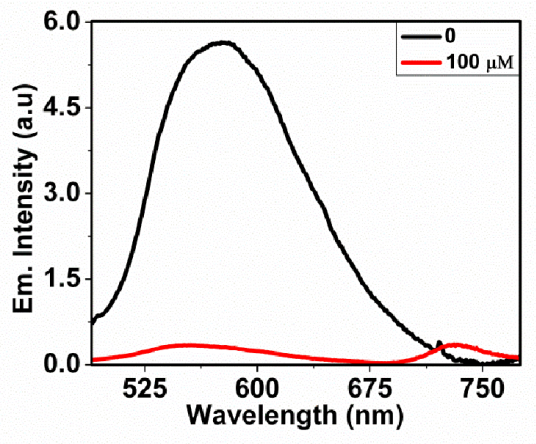

Figure 4.10. Comparison of the emission spectra of OPV gel in the absence and presence of OCY (100 µM). The concentration of OPV used is the CGC.

J-aggregation results in a red-shifted absorption with increase in quantum yield (compared to monomer), where as a blue-shifted, diminished emission indicates H-aggregation. But in case of OPV, the longer wavelength shoulder at ~497 nm in the absorption spectra indicates J-type aggregation, whereas decrease in the quantum yield values in comparison to the monomer and the overall blue-shifted absorption indicates H- type aggregation.[37-39] The deconvoluted emission spectrum of OPV aggregates in benzonitrile indicates the presence of two peaks with maxima at 550 and 610 nm which might be due to the emission from H and J-aggregates respectively. Therefore, the longer wavelength emitting species (~ 610 nm) that undergoes static quenching is, in all probability, a J-aggregate and the lower wavelength emitting species (~ 550 nm) which does not interact with OCY is the H-aggregate. The overall broad emission of OPV in non polar solvents can then be explained considering the overlap between the emission of H and J-aggregates.

In presence of OCY, a change in the morphology of OPV self-assembly and the disruption of the gel network have been observed as discussed in the previous sections which clearly indicate that OCY and OPV undergo chemical interaction thereby explaining the fluorescence quenching mechanism of OPV self-assembly. This is anomalous with the previous quenching studies of OPV[36] and could be explained from the energy optimized molecular structure of OCY. As shown in Figure 4.11, OCY is planar in nature with an approximate length and width of 20.64 Å and 5.2 Å respectively. These dimensions are comparable to the length (20 Å) and width (5.6 Å) of OPV core.

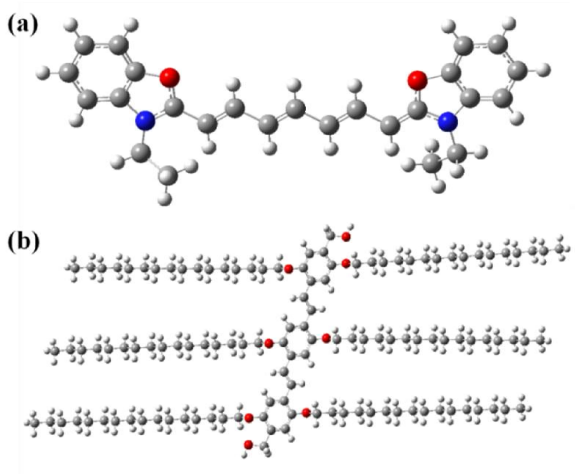

Figure 4.11. Optimized molecular structures of (a) OCY and (b) OPV

OCY also has good conjugation and therefore, when both OPV and OCY are present, they can undergo comprehensive π-π stacking thereby disturbing the hydrogen bonding interaction between the components involved in aggregation. Also OCY has two nitrogen atoms which can form hydrogen bonds with OPV

thereby disturbing the gel formation. Since hydrogen bonding is mainly responsible for the J-aggregation in OPV self-assembly, the selective interaction with OCY affects the J-aggregates only, which explain the selective static quenching of the longer wavelength J-aggregate emission. Based on the results of our studies, we can conclude that OPV self-aggregates in benzonitrile contains both H and J-aggregates, with J-aggregates selectively interacting with OCY *via* hydrogen bonding.

4.3. Conclusions

The fluorescence quenching of OPV self-assembly by an organic dye OCY was used as a tool to unveil the aggregation nature of OPV self-assembly. Even though the steady-state experiments show that the quenching could be due to FRET, a careful analysis of the time-resolved fluorescence data proves that the quenching proceeds via static process. Further morphological investigations indicate the presence of two types of aggregates in OPV self-assembly. Deeper analysis of the SEM, confocal fluorescence data and the gel state spectral studies shows that the fluorescence quenching was due to the formation of less fluorescent complex between J-aggregates of OPV and OCY. H-aggregates do not interact with OCY, thereby retaining their morphology. Moreover, OPV failed to form gel in presence of high concentrations of OCY which indicates that the gelation in OPV therefore depends heavily on the interaction between H and J-aggregates. These results also prove that interpretation and analysis of quenching data of the organogels are crucial and negligence would tend to end up in an incorrect picture on the mechanism of quenching as well as the nature of aggregation in the self-assembly.

REFERENCES

(1) Meijer, E. W.; Schenning, A. P. H. J. *Nature* **2002**, *419*, 353.

(2) Carroll, R. L.; Gorman, C. B. *Angew. Chem., Int. Ed.* **2002**, *41*, 4378.

(3) Hoeben, F. J. M.; Jonkheijm, P.; Meijer, E. W.; Schenning, A. P. H. J. *Chem. Rev.* **2005**, *105*, 1491.

(4) Meijer, E. W.; Schenning, A. P. H. J. *Chem. Commun* **2005**, 3245.

(5) Li, Q., X; Zhang, X.; Ghosh, S.; Wurthner, F. *Chem. Eur. J* **2008**, *14*, 8074.

(6) Prasanthkumar, S.; Gopal, A.; Ajayaghosh, A. *J. Am. Chem. Soc.* **2010**, *132*, 13206.

(7) Prasanthkumar, S.; Saeki, A.; Seki, S.; Ajayaghosh, A. *J. Am. Chem. Soc.* **2010**, *132*, 8866.

(8) van Esch, J. H.; Feringa , L. B. *Angew. Chem., Int. Ed.* **2000**, *39*, 2263.

(9) Van Nostrum, C. F.; Picken, S.; Schouten, A.-J.; Nolte, R. J. M. *J. Am. Chem. Soc.* **1995**, *117*.

(10) Babu, S. S.; Kartha, K. K.; Ajayaghosh, A. *J. Phys. Chem. Lett* **2010**, *1*, 3413.

(11) Sudeep, P. K.; James, P. V.; George Thomas, K.; Kamat, P. V. *J. Phys. Chem. A* **2006**, *110*, 5642.

(12) Vijayakumar, C.; Praveen, V. K.; Kartha, K. K.; Ajayaghosh, A. *Phys. Chem. Chem. Phys.* **2011**, *13*, 4942.

(13) George, S. J.; Ajayaghosh, A. *Chem. Eur. J.* **2005**, *11*, 3217.

(14) Dasgupta, D.; Srinivasan, S.; Rochas, C.; Ajayaghosh, A.; Guenet, J. M. *Soft Matter* **2011**, *7*, 9311.

(15) Dasgupta, D.; Srinivasan, S.; Rochas, C.; Thierry, A.; Schroder, A.; Ajayaghosh, A.; Guenet, J. M. *Soft Matter* **2011**, *7*, 2797.

(16) Praveen, V. K.; George, S. J.; Ajayaghosh, A. *Macromol. Symp* **2006**, *241*, 1.

(17) Wielopolski, M.; Atienza, C.; Clark, T.; Guldi, M. D.; Martin, N. *Chem. Eur. J* **2008**, *14*, 6379.

(18) Stork, M.; Gaylord, B. S.; Heeger, A. J.; Bazan, G. C. *Adv. Mater* **2002**, *14*, 361.

(19) Gaylord, B. S.; Heeger, A. J.; Bazan, G. C. *J. Am. Chem. Soc.* **2003**, *125*, 896.

(20) Liu, B.; Gaylord, B. S.; Wang, S.; Bazan, G. C. *J. Am. Chem. Soc.* **2003**, *125*, 6705.

(21) Wang, S.; Gaylord, B. S.; Bazan, G. C. *J. Am. Chem. Soc.* **2004**, *126*, 5446.

(22) McQuade, D. T.; Hegedus, A. H.; Swager, T. M. *J. Am. Chem. Soc.* **2000**, *122*, 12389.

(23) Zheng, J.; Swager, T. M. *Chem. Commun* **2004**, 2798.

(24) Ajayaghosh, A.; George, S. J.; Praveen, V. K. *Angew. Chem., Int. Ed.* **2003**, *42*, 332.

(25) Kartha, K. K.; Babu, S. S.; Srinivasan, S.; Ajayaghosh, A. *J. Am. Chem. Soc.* **2012**, *134*, 4834.

(26) Beckers, E. H. A.; van Hal, P. A.; Schenning, A. P. H. J.; El-ghayoury, A.; Peeters, E.; Rispens, M. T.; Hummelen, J. C.; Meijer, E. W.; Janssen, R. A. J. *J. Mater. Chem* **2002**, *12*, 2054.

(27) Hoeben, F. J. M.; Herz, L. M.; Daniel, C.; Jonkheijm, P.; Schenning, A. P. H. J.; Silva, C.; Meskers, S. C. J.; Beljonne, D.; Phillips, R. T.; Friend, R. H.; Meijer, E. W. *Angew. Chem., Int. Ed.* **2004**, *43*, 1976.

(28) Wurthner, F. *Chem. Commun* **2004**, 1564.

(29) Wurthner, F.; Chen, Z.; Hoeben, F. J. M.; Osswald, P.; You, C.-C.; Jonkheijm, P.; van Herrikhuyzen, J.; Schenning, A. P. H. J.; van der Schoot, P. P. A. M.; Meijer, E. W.; Beckers, E. H. A.; Meskers, S. C. J.; Janssen, R. A. J. *J. Am. Chem. Soc.* **2004**, *126*, 10611.

(30) Figueira-Duarte, T. M.; Rio, Y.; Listorti, A.; Delavaux-Nicot, B.; Holler, M.; Marchioni, F.; Ceroni, P.; Armaroli, N.; Nierengarten, J. F. *New. J. Chem* **2008**, *32*, 54.

(31) Gegout, A.; Delgado, J., L; Nierengarten, J. F.; Delavaux-Nicot, B.; Listorti, A.; Chiorboli, C.; Belbakra, A.; Armaroli, N. *New. J. Chem* **2009**, *33*, 2174.

(32) Sudeep, P. K.; Emrick, T. *Acs Nano* **2009**, *3*, 4105.

(33) Sudeep, P. K.; Early, K. T.; McCarthy, K. D.; Odoi, M. Y.; Barnes, M. D.; Emrick, T. *J. Am. Chem. Soc.* **2008**, *130*, 2384.

(34) Ajayaghosh, A.; Praveen, V. K.; Vijayakumar, C. *Chem. Soc. Rev.* **2008**, *37*, 109.

(35) Ajayaghosh, A.; Praveen, V. K.; Srinivasan, S.; Varghese, R. *Adv. Mater.* **2007**, *19*, 411.

(36) Praveen, V. K.; George, S. J.; Varghese, R.; Vijayakumar, C.; Ajayaghosh, A. *J. Am. Chem. Soc.* **2006**, *128*, 7542.

(37) Ajayaghosh, A.; Vijayakumar, C.; Varghese, R.; George, S. J. *Angew. Chem. Int. Ed.* **2006**, *45*, 456.

(38) Hulvat, F. J.; Sofos, M.; Tajima, K.; Stupp, I. S. *J. Am. Chem. Soc.* **2005**, *127*, 366.

(39) Wall, D. B.; Zhou, Y.; Mei, S.; Ardona, M. A. H.; Ferguson, L. A.; Tovar, D. J. *Langmuir.* **2014**, *30*, 375.

(40) Iwata, K.; Weaver, W. L.; Gustafson, T. L. *J. Phys. Chem.* **1992**, *96*, 10219.

(41) Oulianov, D. A.; Dvornikov, A. S.; Rentzepis, P. M. *Optics Communications* **2002**, *205*, 427.

(42) Netzel, T. L.; Nafisi, K.; Zhao, M. *J. Phys. Chem.* **1995**, *99*, 17936.

(43) Jelley, E. E. *Nature* **1936**, *138*, 1009.

(44) Scheibe, G. *Angew. Chem.* **1936**, *49*, 563.

(45) Wu, H.; Xue, L.; Shi, Y.; Chen, Y.; Li, X. *Langmuir* **2011**, *27*, 3074.

Chapter 5

Contrasting Fluorescence Response of Two Dipolar Probe Molecules in a Leucine-based Organogel and Its Implications

Fluorescence behavior of two frequently used dipolar probe molecules, coumarin 153 (C153) and 4-aminophthalimide (AP), has been studied in an organogel comprising a leucine-derivative as gelator and toluene as solvent to probe the various microenvironments of the medium. The steady-state emission data clearly suggests different locations of the two probe molecules. While AP is found to be located close to the hydroxyl moieties of the gelator and engaged in hydrogen bonding interactions, C153 is found in bulk toluene-like regions. In contrast to C153, the emission behavior of AP is observed to be excitation wavelength dependent indicating that all hydrogen-bonded AP molecules are not energetically similar. The time-resolved fluorescence behavior of the two systems is found to be consistent with this picture. Unlike C153, AP exhibits a biexponential fluorescence decay behavior in gel. Time-resolved fluorescence anisotropy study of the rotational behavior of the molecules reveals strong association of only the AP molecules with the gelator. Unlike C153, AP is also found to influence the critical gelation concentration of the gel thus suggesting its direct participation in the gel formation process. The present results highlight the importance of intermolecular interactions between the gelator and guest molecules in gels encapsulated with guest molecules.

5.1. Introduction

Gels are three dimensional cross-linked network structures made up of one dimensional nanofibers capable of trapping large quantities of solvent and

preventing its flow. These have attracted considerable interest in recent years due to their potential applications in optoelectronics, drug delivery and photovoltaics, and as light harvesting systems, and sensors.[1-5] Gels possess the characteristics of both liquids and solids.[6] Because of the ease of preparation of the gels and pH or temperature dependent conversion to sol,[7-9] which allows controlled release of guest molecules, low molecular weight organogels (LMWOGs) have gained precedence in recent years over the more common polymer gels.[10,11] The formation of entangled networks of fibers in LMWOGs is facilitated by the self-assembly of molecules through non-covalent interactions like π-π stacking, hydrogen bonding, co-ordination bonding, and van der Waals interactions.[12] The packing of molecules in the self-assembly plays a key role in determining various properties of the gels.[13] Even though considerable attention has been given towards designing the structure, tuning of properties and applications of hydro and organogels as a medium,[12,14-17] studies dealing with the structure of the gels at the microscopic level and understanding of the specific interactions between the gelators and guest molecules, if any, in hydrogels are sparse.[18-20]

Fluorescence techniques are routinely used for the exploration of complex media[21-33] and the study of the gels is no exception. Bhattacharyya and coworkers observed excitation wavelength dependent emission of AP in polyacrylamide (PAA) hydrogel and attributed it to the existence of water pools of different sizes in the gel and distribution of the probe molecule in these pools.[18] Mukhopadhyay et al. observed two-component rotational diffusion for 8-anilino-1-naphthalene sulfonic acid (ANS) in a low molecular weight hydrogel.[20] Interestingly, for 1,6-diphenylhexatriene (DPH), only one rotational component could be observed.[20]

Recently, Tahara and coworkers investigated the local environments of three hydrogels, poly-(2-acrylamido-2-methylpropanesulfonic acid) (PAMPS), poly-acrylamide (PAA) and mixed double-network hydrogel of PAMPS and PAA using Coumarin 6H as the fluorescence probe.[34] They found that the probe molecules reside in the solvent pools of the gel and experience a bulk solvent like environment thus suggesting the pool sizes to be much bigger compared to the probe size. These studies were carried out in hydrogels, where the interaction between the probe and water molecules dominated, which made it difficult to detect the influence of interaction between the probe and gelator molecules, if any. It is for this specific reason we have taken up this work in an organogel comprising a solvent incapable of entering into strong hydrogen bonding interaction with the probe molecule.

The organogel chosen in this study is a thermo-reversible and non-fluorescent one developed by Maruyama and coworkers and is based on gelator, OG-leucine (Chart 5.1), which is considered to be a novel class of gelator capable of trapping water, organic solvents and also the ionic liquids.[35] The unique gel formation ability of OG-leucine with various solvents is attributed to the presence of the amide functionality, hydrophobic tail and polyol hydrophilic moiety, which balance its solubility in a broad range of solvents. OG-leucine molecules self-assemble in toluene with the non-polar tail exposed to the solvent. These self-assemblies then form nanofibrils, which crosslink and entangle to form a three-dimensional network structure.[35] As specific interactions between the gelator molecules play a crucial role in self-aggregation, the primary step in the process

of gelation, it is important to find out whether the guest molecules in low concentration can influence these interactions and affect the process of gelation.

In this study, we have employed two dipolar fluorescence probes, AP and C153 (Chart 5.1) in OG-leucine organogel using toluene as the solvent. This choice of ours has been guided by the fact that both the probes are of comparable sizes[36] and exhibit fluorescence properties, which are highly sensitive to the environment due to intramolecular charge transfer (ICT) nature of the emitting state and also, hydrogen bonding interactions.[37-45] Of the two molecules, the fluorescence properties of AP are more sensitive towards the hydrogen-bonding interaction compared to C153.[44,45] Toluene is used as the solvent in this study as OG-leucine forms stable gel in toluene and does not have strong hydrogen bonding ability with the probe molecules. The concentrations of C153 and AP in gel were maintained at 15 and 75 μM, respectively.

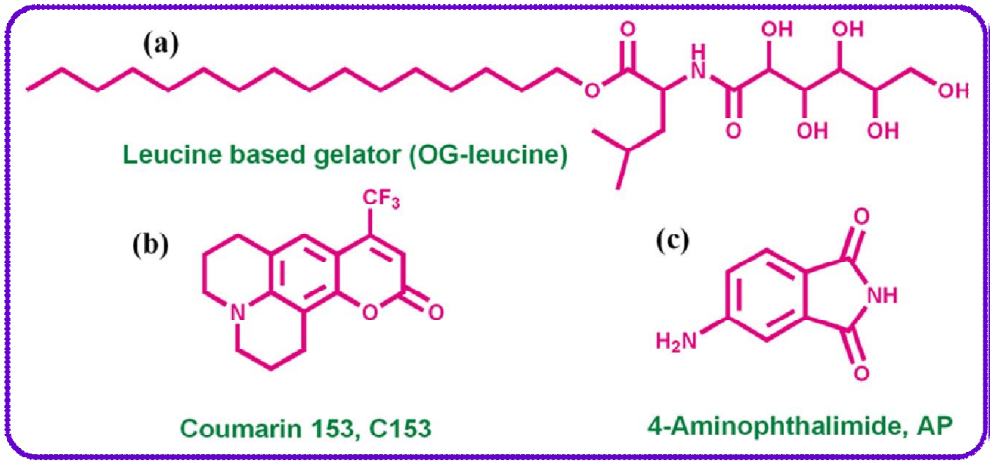

Chart 5.1. Chemical formula of the gelator and probes. (a) Leucine based gelator (OG-leucine), (b) coumarin 153 (C153) and (c) 4-aminophthalimide (AP).

5.2. Results

5.2.1. Steady-state measurements

The fluorescence spectra of AP (λ_{exc} = 375 nm) in gel and in toluene are shown in Figure 5.1 for comparison. The spectrum in gel is found to be broader and the peak position (λ_{em}^{max} = 452 nm) appears red-shifted by ~28 nm compared to toluene. The peak position of AP in gel is found comparable to that of the molecule in acetonitrile (458 nm).[38,39] Thus, it is evident that AP molecules are not located in the solvent pools comprising toluene; but are present in a polar environment of the gel.

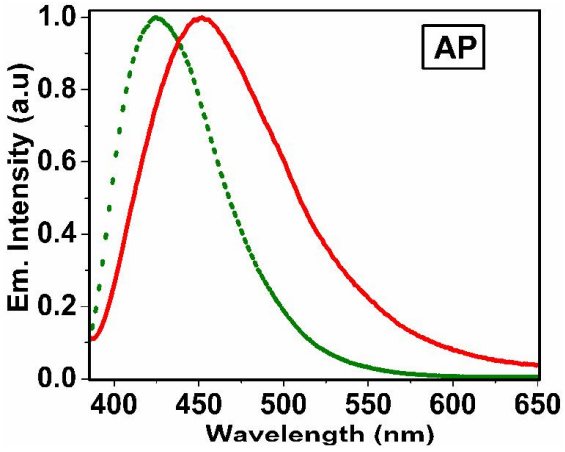

Figure 5.1. Emission spectra of AP (λ_{exc}= 375 nm) in toluene (····) and gel (—), normalized to the peak intensity.

A similar study on C153, however, reveals almost identical fluorescence spectra of the molecule in toluene and gel (Figure 5.2). Considering that any hydrogen bonding interactions of C153 with the hydroxylated gelator molecules

could have resulted in a Stokes shift[42-46] of its λ_{em}^{max} (albeit smaller in magnitude compared to AP), we infer that a toluene-like environment is experienced by the C153 molecules. It essentially means that C153 molecules are located in regions filled by the solvent molecules (i.e. in the solvent pools).

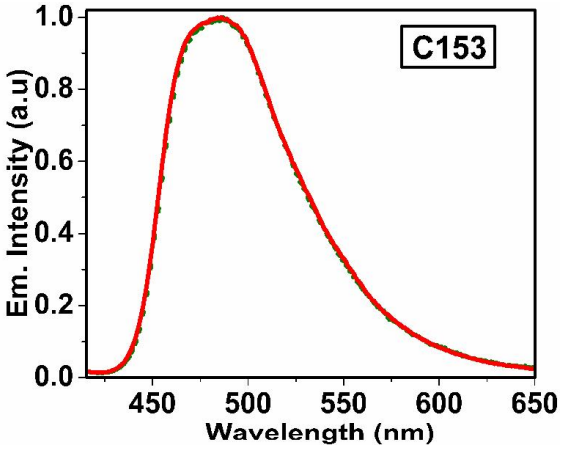

Figure 5.2. Emission spectra of C153 (λ_{exc} = 405 nm) in toluene (····) and gel (——), normalized to the peak intensity.

In common solvents like toluene, the emission properties of AP and C153 are independent of the excitation wavelength. However, a careful study of the emission behavior of the two systems in gel reveals that the fluorescence spectrum of AP is dependent on the excitation wavelength (λ_{exc}), when the latter exceeds 380 nm (Figure 5.3). We observed that for a change of λ_{exc} from 380 to 420 nm, λ_{em}^{max} shifts from 452 to 511 nm (i.e. 59 nm). Interestingly, in the case of C153, no excitation wavelength dependence could be observed in this gel.

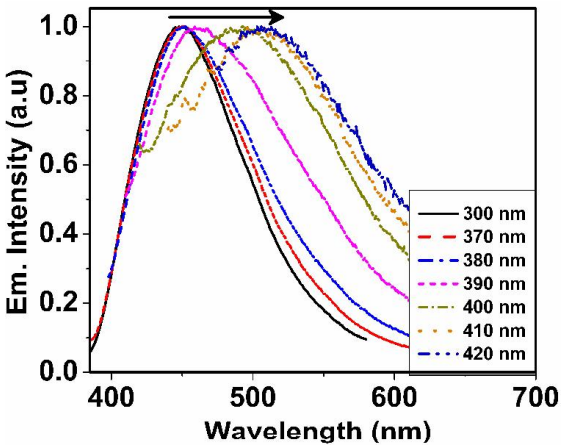

Figure 5.3. Excitation wavelength dependence of the emission spectra (normalized to the peak intensity) of AP in gel at 25 ^{0}C.

As can be seen from Figure 5.4, the change in the spectral behavior with increase of temperature is negligible as long as the gel state is retained. Significant changes are, however, observable from the gel melting temperature of 70 ^{0}C onwards. The spectra not only broadened considerably towards the longer wavelengths but more importantly, the λ_{em}^{max} value shifts from 452 to ~511 nm, which corresponds closely to the reported emission maxima of AP in propanol (518 nm).[48] Interestingly, the emission spectrum of C153 is found largely independent of temperature.

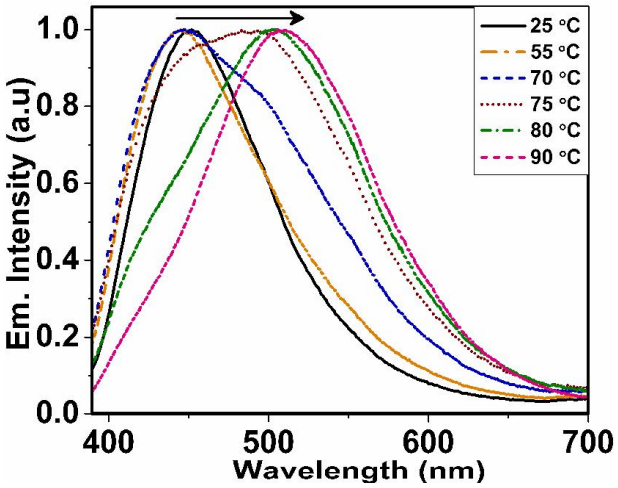

Figure 5.4. Temperature dependence of the emission spectrum (normalized to the peak intensity) of AP in gel (λ_{exc} = 375 nm).

5.2.2. Time-resolved measurements

As the fluorescence lifetime (τ_f) of AP and C153 are also sensitive to the environment,[24,38-45,49,50] we have measured the τ_f values of the two systems at different temperatures. These values are collected in Table 5.1. Unlike in conventional solvents, the fluorescence decay kinetics in gel at 25 and 70 ^{0}C is best represented by a sum of two exponentials of the form, $I(t) = a_1 \exp(-t/\tau_1) + a_2 \exp(-t/\tau_2)$ consisting of a major (90-95%) long-lived (12.7–11.0 ns) component and a minor short-lived (1.5-3.4 ns) component. Interestingly at temperature (90 ^{0}C) above the GTT, AP exhibits a single exponential decay behavior with a lifetime of 8.9 ns, which is comparable to the lifetime of AP in

ethanol (9.5 ns). Unlike AP, the decay profiles of C153 in gel are found to be single exponential throughout the entire temperature range of 25-90 ^{0}C with a lifetime between 4.0-4.9 ns.

Table 5.1. Fluorescence lifetime (in ns) of AP (λ_{exc} = 375 nm) and C153 (λ_{exc} = 405 nm) in gel at different temperatures.

	AP			C153	
T [^{o}C]	**λ_{em} (nm)**	**τ_1 (a_1)**	**τ_2 (a_2)**	**λ_{em} (nm)**	**τ_f**
25	450	3.35 (0.10)	12.61 (0.90)	485	4.87
70	500	1.47 (0.05)	10.99 (0.95)	485	4.71
90	525	8.85		485	4.02

In order to obtain additional information on the microenvironment of the two probe molecules, we have studied their rotational diffusion by measuring the fluorescence anisotropy as a function of time. The time-resolved fluorescence anisotropy, r(t), is calculated using the following equation,

$$r(t) = \frac{I_{II}(t) - GI_{\perp}(t)}{I_{II}(t) + 2GI_{\perp}(t)}$$

where, I_{II} *(t)* and $I_{\perp}$ *(t)* are the observed emission intensities for parallel and perpendicular orientations of the emission polarizer with respect to the polarization of the excitation light, respectively. G is the correction factor for the detector sensitivity to the polarization direction of the emission, which depends on both the excitation source and monitoring wavelength. For the present systems, the estimated G factors are found to lie between 0.53 and 0.57. The initial

anisotropies, r_0, are found to be within the limiting value of 0.4 for both the probe molecules. The time dependence of the measured anisotropy profiles can reasonably be described by a single exponential function. A bi-exponential fit to the anisotropy data did not improve the quality of fitting and also, the average rotational time thus estimated was found to be identical with that obtained from the single exponential fit. A representative plot of fluorescence anisotropy vs. time in gel (λ_{exc} = 375 nm) at 25 ^{0}C is shown in Figure 5.5.

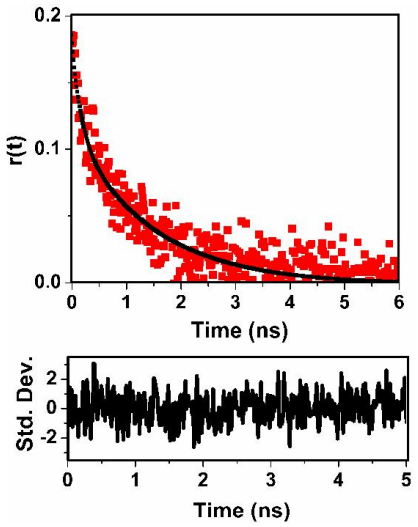

Figure 5.5. Fluorescence anisotropy decay profiles of AP in gel (λ_{exc} = 375 nm) at 25 ^{0}C. Solid line is the single exponential fit to data.

The rotational diffusion times of AP and C153 in toluene are found to be 63 and 68 ps, respectively. These values are consistent with similar sizes of these molecules.[36] At 25 ^{0}C the rotational time of AP in gel is estimated to be ~1300 ps. This value is ~20-fold higher than its measured rotational time in toluene. At the gel to sol transition temperature of 70 ^{0}C, a small decrease of the rotational

time is observed, but the value is still much higher than that in toluene. Even at 90 ^{0}C, the rotational time of AP (685 ps) is ~10-fold higher than its value in toluene. Interestingly, the rotational time of C153 in gel (117 ps) at 25 ^{0}C is higher than in toluene by a factor of only two. When the temperature is increased further, the rotational time decreases and the value reaches similar to that in toluene. The measured rotational times of the molecules are presented in Table 5.2.

Table 5.2. Rotational diffusion time of AP and C153 in gel at different temperatures

T	AP			C153		
[°C]	λ_{em} [nm]	τ_{rot} [ps]	χ^2	λ_{em} [nm]	τ_{rot} [ps]	χ^2
25	450	1295	1.0	485	117	1.0
70	500	1143	1.0	485	76	1.0
90	525	685	1.2	485	50	1.1

5.2.3. Gelation properties of AP and C153 doped organogels

The gelation property of OG-leucine in toluene was assessed in the presence of small amounts (75 μM) of the probe molecules, AP and C153. For this purpose, the gelator and the stock solution of the probe in toluene were heated in a sealed sample vial until the gelator dissolved completely. The solution was then allowed to cool down to room temperature and the formation of gel was confirmed by the failure of the transparent soft mass to flow by inverting the vial. The CGC of OG-leucine gel is reported to be 2 wt% in toluene.[35] In presence of AP and C153, the gelation was studied as a function of varying amounts of OG-

leucine. Interestingly, we found that the gelation occurs with 1 wt % of OG-leucine in presence of AP, which implies reduction of the CGC value by nearly half. However, no change in gelation behavior of OG-leucine was observed in presence of C153.

5.3. Discussion

Both steady-state and time-resolved fluorescence data suggests that the environments experienced by C153 and AP in OG-leucine organogel are very different. While C153 senses a toluene-like environment, AP is clearly located in a much polar environment of the gel.

The excitation wavelength dependence of the emission of AP in gel is an interesting observation, which suggests that even though AP molecules are in polar locations, they all are not in an identical environment. We note that excitation wavelength dependent emission of AP has been observed in the past, though only in hydrogels, and the observation is attributed to the existence of water pools of different sizes in the gel into which the probe molecules are distributed.[18] As the present gel does not contain any water pool, a different explanation is needed to account for the excitation wavelength dependence.

The influence of hydrogen bond donating solvents on the emission behavior of AP has been studied extensively in the past.[38,39,50,51] As hydrogen bonding interaction leads to a significant Stokes shift of the emission maxima of AP, we can conclude that the polar environment sensed by AP molecules is the result of hydrogen bonding interaction of the molecule with the hydroxyl moieties of the gelator. The excitation wavelength dependence of the emission spectrum of AP is

then must be a consequence of the existence of a distribution of AP molecules (all are in the vicinity of the hydroxyl group and hydrogen bonded to the hydroxyl moieties) which differ in the nature and strength of hydrogen bonding interaction.

Considering this picture, the effect of temperature on the fluorescence spectra of AP can be explained as follows. In the gel state, due to rigidity of the medium the hydrogen bonding interaction between the probe and gelator molecules is not fully optimized, and the molecules do not emit from the states that are stabilized to the maximum extent through hydrogen bonding interactions. When gel is transformed to sol at higher temperatures, the probe and gelator molecules can arrange themselves in a more favorable configuration to achieve maximum stabilization of the emitting state of AP. This explains why the emission peak shifts from 452 nm in the gel state to 513 nm in the sol state.

Fluorescence lifetime of AP is quite sensitive to the environment and it decreases significantly in hydrogen bond donating solvents.[24,38,39,51] A biexponential fluorescence decay behavior of AP and the individual lifetime components in gel at various temperatures are consistent with the fact that all AP molecules are not hydrogen bonded in an identical manner. The long-lived (10.99-12.61 ns) dominant contribution presumably arises from those molecules, which are not so well stabilized by the hydrogen bonding interactions compared to the other set of molecules. A single exponential fluorescence decay behavior of AP with a lifetime of 8.85 ns in the sol state suggests that all AP molecules are strongly associated with the hydroxyl groups of the gelator molecules and senses an alcohol-like environment. As fluorescence decay profile of C153 is single exponential with a lifetime between 4.9 and 4.0 ns throughout the entire

temperature range of 25-90 ^{0}C, not much information can be extracted from this data. However, the fact that fluorescence lifetime of C153 in toluene is comparable to the values estimated in the gel under different conditions does not contradict the view that these molecules are placed in the toluene pools.

The hydrogen-bond mediated association of the AP molecules with the hydroxyl group(s) of the gelator and its influence in the gel formation process is substantiated by the measured rotational times of the system. A ~20-fold increase in rotational time of the molecule in gel compared to toluene suggests that AP molecules are strongly associated with the hydroxyl groups of the gelator. Even at the gel transition temperature (70 ^{0}C), when the medium has softened, a decrease in the rotational time is observed, but the molecules are still found to be associated. The rotational diffusion time of AP at 90 ^{0}C, when the system is in the sol state, is still higher than that in toluene by nearly a factor of 10 indicating the dominance of the hydrogen bonding interaction. Likely location of AP molecules and its interaction with the gelators at different temperatures are illustrated in Scheme 5.1.

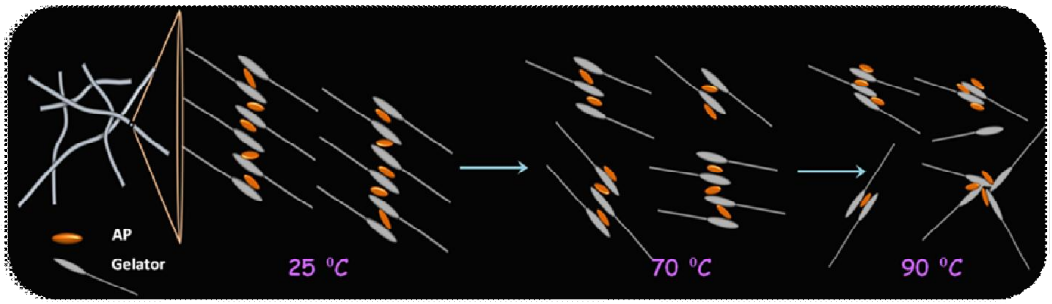

Scheme 5.1. Possible locations of AP molecules and its interactions with the gelators.

The two-fold enhancement in the rotational time of C153 at 25 ^{0}C compared to toluene is clearly a reflection of the viscosity of the medium. The value suggests, however, that the microviscosity around C153 is significantly lower than the rigidity of the gel. As AP and C153 have similar size,[36] the influence of viscosity on the rotational diffusion of the probe molecules would have been similar had they been positioned in similar locations. The huge difference in the rotational diffusion times of two probes of similar sizes in the gel substantiates their different locations in the medium and the interactions experienced by them. The measured rotational times of C153 clearly indicate that it is not associated through hydrogen bonding interactions and hence, occupies the toluene filled pools.

5.4. Conclusions

This study reveals the importance of interactions between the guest and gelator in gels encapsulated with guest molecules. It is commonly taken for granted that a guest molecule in a gel resides in the solvent pools; it does not interact with the gelator and hence, does not influence the gelation process. Though this assumption is largely valid for hydrogels, the present results clearly show that as far as organogels are concerned, the intermolecular interactions between a gelator and a probe molecule can be an important factor in not only determining the location of the probe in a gel, but also influencing the process of gelation.

REFERENCES

(1) Aratani, N.; Kim, D.; Osuka, A. *Acc. Chem. Res.* **2009**, *42*, 1922.

(2) Carrasco-Orozco, M.; Tsoi, W. C.; O'Neill, M.; Aldred, M. P.; Vlachos, P.; Kelly, S. M. *Adv. Mater.* **2006**, *18*, 1754.

(3) Kartha, K. K.; Babu, S. S.; Srinivasan, S.; Ajayaghosh, A. *J. Am. Chem. Soc.* **2012**, *134*, 4834.

(4) Pisal, S. S.; Paradkar, A. R.; Mahadik, K. r.; Kadam, S. S. *Int J Pharm.* **2004**, *270*, 37.

(5) Warman, J. M.; Piris, J.; Pisula, W.; Kastler, M.; Wasserfallen, D.; Mullen, K. *J. Am. Chem. Soc.* **2005**, *127*, 14257.

(6) Osada, Y.; Kajiwara, K. *Gels Handbook: The Fundamentals.* ; Academic Press., 2001; Vol. 1.

(7) Prasanthkumar, S.; Gopal, A.; Ajayaghosh, A. *J. Am. Chem. Soc.* **2010**, *132*, 13206.

(8) Krieg, E.; Shirman, E.; Weissman, H.; Shimoni, E.; Wolf, S. G.; Pinkas, I.; Rybtchinski, B. *J. Am. Chem. Soc.* **2009**, *131*, 14365.

(9) Komatsu, H.; Matsumoto, S.; Tamaru, S.; Kaneko, K.; Ikeda, M.; Hamachi, I. *J. Am. Chem. Soc.* **2009**, *131*, 5580.

(10) Robinson, R. C. *Bull. Sch. Med. Univ. Md.* **1955**, *40*, 86.

(11) Kawata, M.; Suzuki, T.; Kim, N. S. *J. Pharm. Sci.* **1991**, *80*, 1072.

(12) Vintiloiu, A.; Leroux, J. C. *Journal of Controlled Release* **2008**, *125*, 179.

(13) Weiss, R. G. *J. Am. Chem. Soc.* **2014**, *136*, 7519.

(14) Hanabusa, K.; Fukui, H.; Suzuki, M.; Shirai, H. *Langmuir.* **2005**, *21*, 10383.

(15) Dong, X.; Wang, H.; Fang, F.; Li, X.; Yang, Y. *Electrochimica Acta.* **2010**, *55*, 2275.

(16) Kawaguchi, H. *J. Oleo Sci.* **2013**, *62*, 865.

(17) Tellis, C. J.; Christopher, A.; Myers, M. M.; Kneas, A. K. *Anal. Chem.* **2011**, *83*, 928.

(18) Datta, A.; Das, S.; Mandal, D.; Pal, S. K.; Bhattacharyya, K. *Langmuir.* **1997**, *13*, 6922.

(19) Grant, D. C.; DeRitter, R. M.; Steege, E., K.; Fadeeva, A. T.; Castner, W. E. *Langmuir.* **2005**, *21*, 1745.

(20) Mukhopadhyay, S.; Ira.; Krishnamoorthy, G.; Maitra, U. *J. Phys. Chem. B.* **2003**, *107*, 2189.

(21) Kalyanasundaram, K. *Photochemistry in Microheterogeneous Systems*; Academic Press INC. (London) Ltd., 1987.

(22) Lakowicz, J. R. *Principles of Fluorescence Spectroscopy*, Second ed.; Kluwer Academic/Plenum Publishers, 1999.

(23) Ramamurthy, V. *Photochemistry in Organized and Constrained media*; VCH Publishers, 1991.

(24) Soujanya, T.; Krishna, T. S. R.; Samanta, A. *J. Phys. Chem.* **1992**, *96*, 8544.

(25) Khara, D. C.; Samanta, A. *Phys. Chem. Chem. Phys.* **2010**, *12*, 7671.

(26) Samanta, A. *J. Phys. Chem. Lett.* **2010**, *1*, 1557.

(27) Samanta, A. *J. Phys. Chem. B.* **2006**, *110*, 13704.

(28) Karmakar, R.; Samanta, A. *J. Phys. Chem. A.* **2002**, *106*, 6670.

(29) Karmakar, R.; Samanta, A. *J. Phys. Chem. A.* **2003**, *107*, 7340.

(30) Jin, H.; Li, X.; Maroncelli, M. *J. Phys. Chem. B.* **2007**, *111*, 13473.

(31) Sen, P.; Ghosh, S.; Sahu, K.; Mondal, S. K.; Roy, D.; Bhattacharyya, K. *J. Chem. Phys.* **2006**, *124*, 204905 (1.

(32) Cross, J. A.; Fleming, R. G. *Biophys. J.* **1986**, *50*, 507.

(33) Ho, C.; Williams, W. B.; Stubbs, D. C. *Biochim. Biophys. Acta.* **1992**, *1104*, 273.

(34) Hattori, T.; Ishii, K.; Tominaga, T.; Osada, Y.; Tahara, T. *Chem. Phys.* **2013**, *419*, 172.

(35) Minakuchi, N.; Hoe, K.; Yamaki, D.; Ten-no, S.; Nakashima, K.; Goto, M.; Mizuhata, M.; Maruyama, T. *Langmuir.* **2012**, *28*, 9259.

(36) Ito, N.; Arzhantsev, S.; Maroncelli, M. *Chem. Phys. Lett.* **2004**, *396*, 83.

(37) Samanta, A.; Fessenden, R. W. *J. Phys. Chem. A.* **2000**, *104*, 8577.

(38) Soujanya, T.; Fessenden, R. W.; Samanta, A. *J. Phys. Chem.* **1996**, *100*, 3507.

(39) Soujanya, T.; Krishna, T. S. R.; Samanta, A. *J. Photochem. Photobiol. A: Chem.* **1992**, *66*, 185.

(40) Dobek, K.; Karolczak, J. *J. Fluoresc.* **2012**, *22*, 1647.

(41) Dobek, K.; Karolczak, J.; Kubicki, J. *Dyes and Pigments* **2014**, *100*, 222.

(42) Jones II, G.; Jackson, W. R.; Choi, C., Y; Bergmark, W. *J. Phys. Chem.* **1985**, *89*, 294.

(43) Knut, R.; Spieles, M. *Anal. Chem.* **2011**, *83*, 1232.

(44) Krolicki, R.; Jarzeba, W.; Mostafavi, M.; Lampre, I. *J. Phys. Chem. A*. **2002**, *106*, 1708.

(45) Maroncelli, M.; Fleming, R. G. *J. Chem. Phys.* **1987**, *86*, 6221.

(46) Wagner, D. B. *Molecules*. **2009**, *14*, 210.

(47) Perrin, D. D.; Armerego, W. L. F.; Perrin, D. R. *Purification of Laboratory Chemicals.*; Pergamon Press: Newyork., 1980.

(48) Durantini, M. A.; Falcone, D. R.; Anunziata, D. J.; Silber, J. J.; Abuin, B. E.; Lissi, A. E.; Correa, M. N. *J. Phys. Chem. B*. **2013**, *117*, 2160.

(49) Dobek, K. *Photochem.Photobiol. Sci.* **2008**, *7*, 361.

(50) Khara, D. C.; Banerjee, S.; Samanta, A. *Chem Phys Chem.* **2014**, *15*, 1793.

(51) Krystkowiak, E.; Dobek, K.; Maciejewski, A. *J. Photochem. Photobiol. A: Chem.* **2006**, *184*, 250.

Chapter 6

Förster Resonance Energy Transfer in Agarose Hydrogel

Förster resonance energy transfer (FRET) from coumarin 102 (C102) to rhodamine 6G (Rh6G) is studied in agarose gel using steady-state and time-resolved fluorescence measurements. These studies have been carried out in gels comprising 0.075 and 0.3 weight percent (wt%) of agarose in 20% v/v ethanol-water mixture. The convincing evidence of FRET is provided by the rise time of the acceptor emission. The donor-acceptor distances in the gel, calculated using the Förster theory, are found to be 45 and 52 Å in 0.075 and 0.3 wt% agarose gel, respectively. FRET efficiency is high in 0.3 wt% agarose gel due to the reduced pore size. This work emphasizes the use of gels as efficient medium for FRET as the same donor-acceptor pair does not exhibit FRET in the bulk solvent medium and also the application of FRET to estimate the pore dimensions of the gel.

6.1. Introduction

In recent years, FRET has gained remarkable interest in nanoparticles based sensors, light harvesting systems, supramolecular aggregates, gels, vesicles and polymers.[1-7] FRET is a phenomenon which occurs between a donor in the excited state and acceptor in the ground state which are separated by distances 10-100 Å.[8-10] The rate of energy transfer mainly depends upon the extent of the spectral overlap [$J(\lambda)$], the quantum yield of the donor, the relative orientation (κ^2) of the donor and acceptor transition dipoles, and the distance between the donor and

acceptor molecules (R_{DA}).[8-10] The most common application of FRET is to measure the distances between donor and acceptor residing at two different sites on macromolecules, polymer films, vesicles etc.[8-10]

According to the Förster theory, the rate of FRET is inversely proportional to the sixth power of the donor-acceptor distance.[8,10,11] The distance at which FRET is 50% efficient is called as Förster distance and is typically 20-60 Å.[8,10] Confining the donor and acceptor molecules within the Forster distance helps in enhancing the rate of FRET.[2,3,12-14] In general, heterogeneous media are employed to confine the donor-acceptor molecules to enhance FRET efficiency.[8,10] Ultrafast FRET in heterogeneous media like micelles, mixed micelles and room temperature ionic liquids have been investigated in detail by Bhattacharyya and coworkers.[3,12-16] To determine the size and dynamics of the unfolded proteins, Eaton and coworkers studied, combining single molecule lifetime and intensity FRET measurements along with molecular simulations.[17]

In the present work, we have investigated FRET in the well known biopolymer hydrogel agarose and used it to understand the average pore dimensions of the gel. Agarose is a polysaccharide consisting of 1,3-linked β-D-galactopyranose-D-galactopyranose (Scheme 6.1).[18] This basic agarobiose unit repeats to form long chains with an average molecular mass of 1,20,000 daltons, representing about 400 agarobiose units.[18] The mechanism for gelation of agarose was first suggested by Rees and later demonstrated by Arnott et al.[19,20] Agarose exists as random coils in solution (Figure 1.4). In the initial stages of gelation, random coils change to double helices which link in three dimensions by

zones/junctions. Then they form bundles of double helices which entangled at junctions to form gel. The gelation process of agarose is thermo reversible in nature.[21] The average pore size typically varies from 10-1100 nm and depends on concentration and type of agarose.[19,20,22]

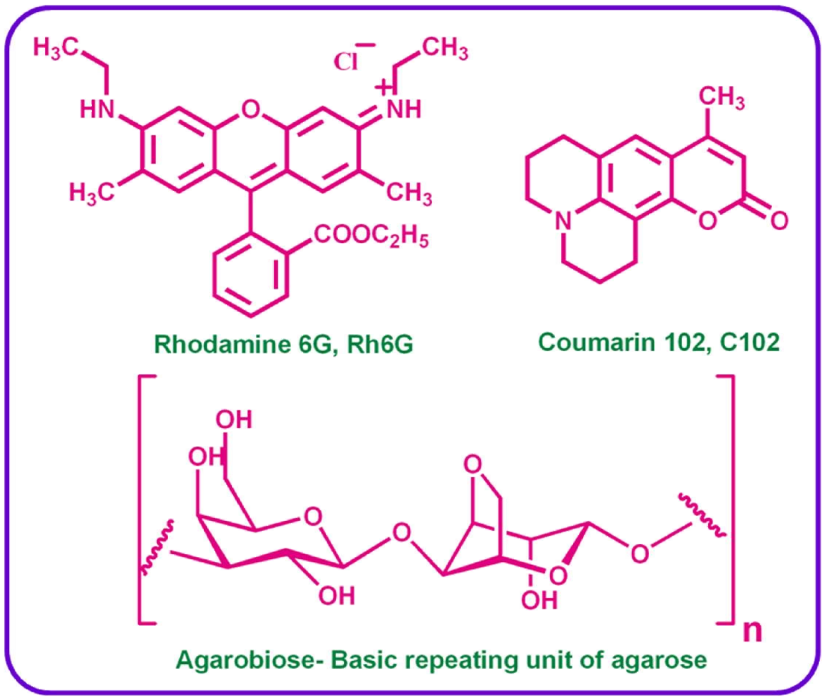

Scheme 6.1. Structures/Abbreviations of the dyes employed in the present study.

Agarose gel was chosen particularly for our studies as it is well known that its pore size depends highly on external factors like monomer concentration and solvent.[22] FRET can be used as an effective tool to calculate the donor-acceptor distance within the gels prepared using different concentrations of the monomer which should ideally give us some information about the pore size. In general, the

heterogeneous media used (micelles or ionic liquids) for the FRET studies cause spectral shifts in the donor and acceptor thereby changing the overlap integral.[14,16] Hence, it is confusing that the increase in the rate of FRET in confined environment is due to the decreased donor-acceptor distance or due to the increase in overlap integral. In agarose gel, no spectral changes were observed for both the donor and acceptor with respect to the bulk solvent thereby making sure that the rate of FRET could only be dependent on donor-acceptor distance.

Coumarins and rhodamines are well known FRET pairs in heterogeneous media like micelles and vesicles.[2,3,12-15] However, in aqueous solution no FRET takes place between these molecules.[14] In our study, we have used coumarin 102 (C102) as the donor and rhodamine 6G (Rh6G) as the acceptor. Agarose gels with two different concentrations of monomers (0.075 and 0.3 wt%) were prepared for the studies. 20% v/v ethanol-water mixture was used to prepare agarose hydrogel, as it is known that ethanol in lower percentages makes agarose hydrogel more stable and compact.[23] Moreover to the best of our knowledge pore size of agarose hydrogel in 20% v/v ethanol-water mixture has not been explored yet. As higher quantities of ethanol hinder gel formation, we have used an optimum 20% v/v ethanol-water mixture to prepare the gels.

6.2. Results and Discussion

6.2.1. Studies in 0.075 wt% agarose gel

The λ_{abs}^{max} of C102 and Rh6G in gel are 403 and 529 nm, respectively. C102 and Rh6G exhibits λ_{em}^{max} at 489 and 562 nm, respectively in the gel medium. The

absorption and emission spectra of C102 and Rh6G in agarose gel appear almost at the same as that in the bulk solvent. This indicates that the dyes experience a bulk solvent like environment in gel and are presumably located in the solvent filled regions of the gel. The emission spectra of the dyes are found to be independent of the excitation wavelength (Figure 6.1). This indicates that all the dye molecules experience more or less uniform microenvironment in the gel.[27]

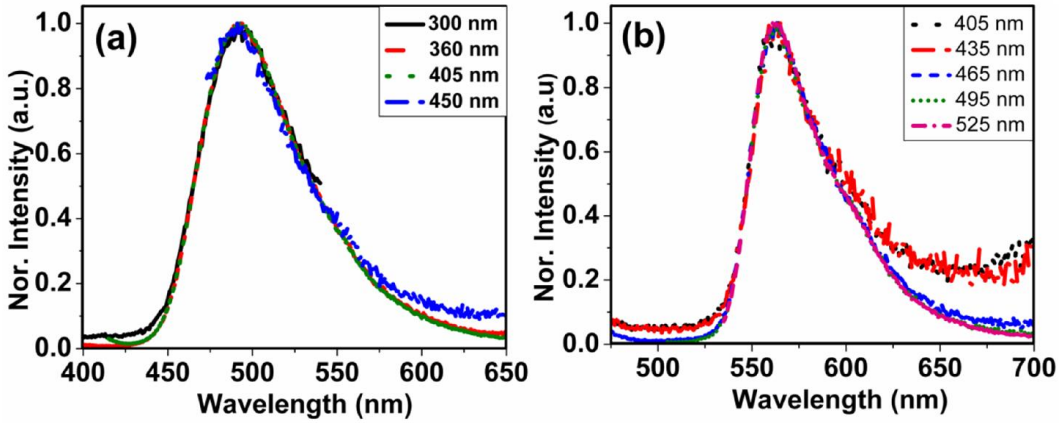

Figure 6.1. Excitation wavelength dependence of the emission spectra (normalized to the peak intensity) of (a) C102 and (b) Rh6G in gel at 25 °C.

Figure 6.2 shows the overlap between the emission spectrum of C102 (donor) and absorption spectrum of Rh6G (acceptor) in gel. The spectral overlap integral [J(λ)], in this gel calculated using Förster theory, is 3.7×10^{15} $M^{-1}cm^{-1}nm^4$. In this study, the concentration of the donor is maintained as 20 μM and the acceptor concentration was varied between 4-40 μM. The energy transfer study was carried out by exciting the samples at 405 nm at which the absorption due to the donor

(C102) is much higher than that of the acceptor (Rh6G), one of the ideal conditions for FRET.

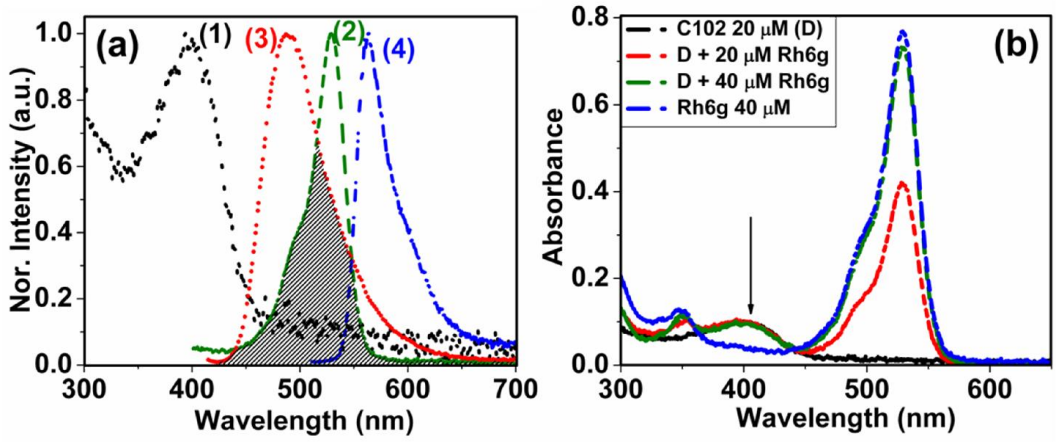

Figure 6.2. (a) Absorption spectra of C102 (1), Rh6G (2) and emission spectra of C102 (3) and Rh6G (4) in agarose gel (0.075 wt%) in 20% v/v ethanol-water mixture. (b) Absoprtion spectra of C102 in 0.075 wt% percent agarose gel with various concentrations of Rh6G and only Rh6G spectra (40 μM), highlighting the difference of OD at the excitation wavelength, 405 nm.

Figures 6.2 (b) and 6.3 (a) show the changes in the absorption and emission of C102 respectively, with gradual increase in the concentration of Rh6G in this medium. It is clearly visible that the OD of the donor at the excitation wavelength (405 nm) does not change considerably even after the addition of the acceptor. The observed quenching of C102 fluorescence accompanied by an enhancement in Rh6G emission suggests the involvement of FRET between C102 and Rh6G. The efficiency of FRET (E_{FRET}) is calculated to be ~60% in this medium (Table 6.2), by using, $E_{FRET} = 1-(I_{DA}/I_D)$, where I_{DA} and I_D are the steady-state emission

intensities of the donor in the presence and in the absence of acceptor, respectively.

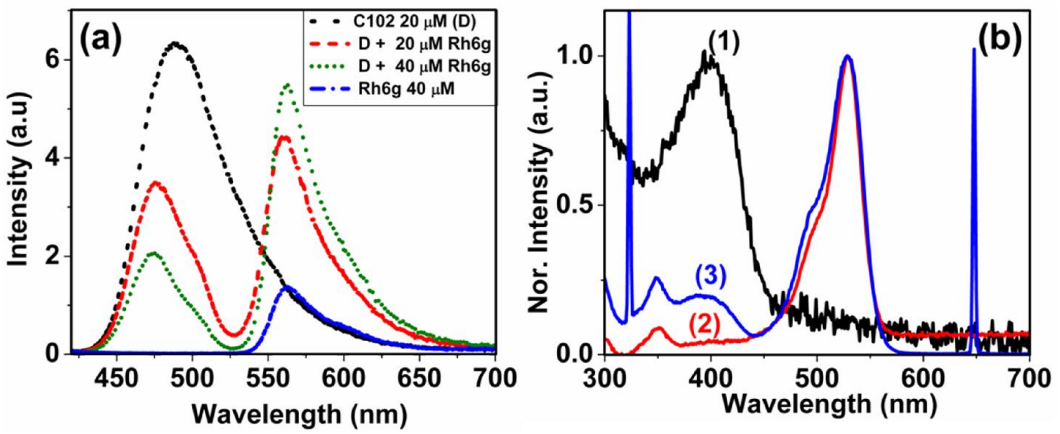

Figure 6.3. Quenching of the emission of C102 (20 μM) in 0.075 wt% gel with increasing concentrations of Rh6G (4-40 μM). The emission spectrum of Rh6G in gel is also shown (blue). (b) Comparison of absorption spectra of C102 (1) and Rh6G (2) in gel with the excitation spectra of a mixture of C102 (20 μM) and Rh6G (40 μM) monitored at 650 nm (3).

The energy transfer process is substantiated from the excitation spectra[28] of a sample containing 20 μM C102 and 40 μM Rh6G in gel as shown in Figure 6.3 (b). When monitored at 650 nm, where C102 does not emit, a peak at ~ 400 nm corresponding to the absorption of C102 is observed along with that of Rh6G absorption. This clearly indicates that energy is transferred from the excited state of C102 to Rh6G in the ground state thereby resulting in an enhanced emission of the acceptor compared to that of the direct excitation.

In order to further investigate the FRET process, the time-resolved fluorescence measurements have been performed. The fluorescence decay profiles of the donor and the acceptor at different emission wavelengths were monitored for various acceptor concentrations. Both C102 and Rh6G separately exhibit a single exponential decay behavior in this gel with fluorescence lifetimes of 5.9 and 4.6 ns, respectively. These values are identical with the lifetime observed for these dyes in 20% v/v ethanol-water mixture. FRET is commonly monitored by decrease of the donor lifetime in presence of the acceptor. However, in this case, on addition of the acceptor, no such decrease of the donor lifetime was observed at 460 nm, where C102 emission predominates. This is a common phenomenon observed in heterogeneous media like micelles and gels due to the presence of more number of unquenched donors as the donors and acceptors are not equally distributed in the solvent pools present in the medium.[3,15,29] This can be elaborated as follows. The probability that every donor present in a solvent pool has an acceptor molecule as the nearest neighbor is less than unity. Thus all C102 molecules are not effective donors and the integrated fluorescence intensity decreases. But the lifetime of the donor in the presence of varying concentrations of the acceptor does not show significant decrease since we measure mostly the lifetime of donor molecules which does not participate in FRET.[3,15,29]

The components of FRET can be determined by monitoring the rise of the acceptor emission. For this purpose, the fluorescence lifetime was monitored at the acceptor emission (560 nm), where the contribution of the quenched donor emission is negligible. We were not able to monitor the emission at wavelengths higher than 560 nm as the medium scatters light considerably in compared to

homogenous bulk solvents. Table 6.1 shows the fluorescence decay parameters of the system for various concentrations of Rh6G. In 0.075 wt% agarose gel, the time-resolved fluorescence data clearly manifests a ~3 ns rise time (Figure 6.4) of the acceptor with a relative contribution of 34% at the highest acceptor concentration (40 μM), followed by a decay of 4.6 ns which is well matched with the single exponential decay of Rh6G in gel. As FRET between donor and acceptors residing at different pools would have given rise to multiple rise times,[3,14,30] it can be concluded that in agarose gel, FRET mainly happens between the donor and acceptor present in the same pool. Therefore the rise component can be attributed to FRET between donor and acceptor residing at a close proximity within the same solvent pool.[3,14,30]

Table 6.1. Time-resolved fluorescence parameters of the system (λ_{em} = 560 nm) for various concentrations of Rh6G.

Agarose wt%	Sample	τ_1 (ns)	a_1	τ_2(ns)	a_2	χ^2	τ_{av} (ns)
0.075	C102-20 μM	3.09	-0.31	4.68	0.131	1.06	
	C102-40 μM	3.18	-0.34	4.77	0.134	1.06	
	40 μM Rh6G	4.65				1.15	4.65
0.03	C102-20 μM	3.28	-0.38	4.58	0.138	1.12	
	C102-40 μM	3.52	-0.49	4.52	0.149	1.09	
	40 μM Rh6G	4.77				1.21	4.77

The time-resolved fluorescence data clearly established FRET as the reason behind fluorescence quenching of C102 in presence of Rh6G. The Förster distance, R_0 and the distance between donor and acceptor, r, were calculated and

listed in Table 6.2. In 0.075 wt% gel the average donor-acceptor distance were calculated to be 45 Å.

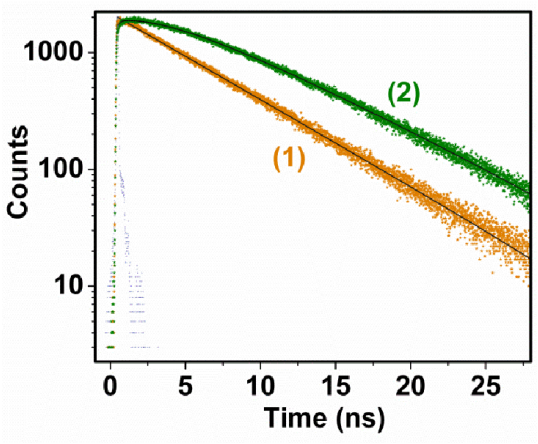

Figure 6.4. Fluorescence decay profiles of the system monitored at (1) 460 nm and (2) 560 nm, respectively in 0.075 wt% agarose gel.

In ethanol-water mixture, FRET between C102 and Rh6G was not observed.[14] As the overlap integral remains same, the efficient FRET in gel medium perhaps could be due to the confinement of the donor-acceptor molecules in the solvent pools of the gel. The preferential interaction of the dye with the solvent molecules, may act in competition with the FRET process. Moreover, in bulk solvent, all the solvent molecules are free to interact with the dyes. But, in gel, water molecules are known to cocrystallise with agarose helical chains in the fibrils thereby decreasing the concentration of solvent molecules available to interact with the dye molecules in the solvent pool of the gel.[21,31]

6.2.2. Studies in 0.3 wt% agarose gel

In order to understand the effect of gelator concentration on the pore size of agarose gel, the quenching studies in 0.3 wt% agarose gel were carried out. No changes in the spectral properties of the dyes are observed with increasing concentration of agarose used for gel preparation. As there is no considerable change in the spectral properties of the dyes in the two different agarose gel samples, there is only a small change in J(λ) in these gels. The overlap integral, J(λ), in this gel is calculated to be 4.3×10^{15} $M^{-1}cm^{-1}nm^4$. The quenching of C102 fluorescence with gradual increase in the concentration of Rh6G is monitored as shown in Figure 6.5.

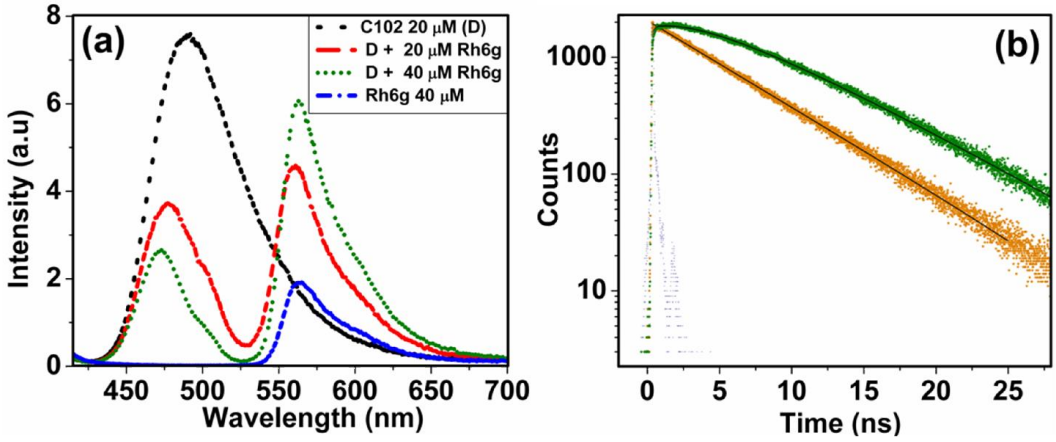

Figure 6.5. Quenching of the emission of C102 (20 μM) in 0.03 wt% gel with increasing concentrations of Rh6G (4-40 μM). The emission spectrum of Rh6G in gel is also shown (blue). (b) Fluorescence decay profiles of the system monitored at (1) 460 and (2) 560 nm, respectively in 0.3 wt% agarose gel.

The quenching of C102 was more efficient in 0.3 wt% agarose gel compared to 0.075 wt% gels, thereby increasing the efficiency of FRET to be ~65 %. In this case also, no shortening of fluorescence lifetime of C102 was observed in the presence of Rh6G.[3,15,29] Rise time of the acceptor emission was found be similar to that observed in 0.075 wt% gels, but with higher amplitude (0.49) for the rise time, thereby resulting in an efficient FRET. Single rise time indicates the occurrence of FRET between donor and acceptor present in the same solvent pool. The distance between the donor and acceptor in 0.3 wt% gel was found to be 52 Å. All the parameters of FRET were listed in Table 6.2.

Table 6.2. Energy Transfer Parameters for C102-Rh6G pair in agarose gel.

Agarose wt %	J(λ) ($M^{-1}cm^{-1}nm^4$)	R_0 (Å)	E_{FRET} (%)	r (Å)
0.075	3.7×10^{15}	55	60	45
0.3	4.3×10^{15}	50	65	52

From the analysis of FRET studies, it could be understood that 4 times increase in the concentration of gelator causes small change in the pore size. As the average distance between donor and acceptor present in the same pool varies from 45 to 52 Å, the pool size could be more than 45 and 52 Å in the 0.075 and 0.3 wt% gels, respectively. Thus it is evident that presence of ethanol decreases the pool size of agarose gel as the pool size of the gels made using same concentrations of monomer in water is found to be ~150 Å. [22] Moreover we could not observe FRET in agarose hydrogel made using water (data not shown). This indicates that addition of ethanol varied the pool size of the gel as FRET is

observed in gels prepared using 20% v/v ethanol-water mixture. The effect of pool size on the FRET efficiency is further proved by increasing the agarose monomer concentration, where efficiency is found to be enhanced.

6.3. Conclusions

In this work, we have studied FRET between C102 and Rh6G in agarose gels made using two different monomer concentrations. The distance between donor and acceptor can be calculated from FRET studies thereby understanding the solvent pool size of the gels. Single rise time for FRET indicates that the donor and acceptor are residing at the same solvent pool. Four times increase in the concentration of the monomer resulted in a very small change in the pool size. This study clearly shows the effect of confinement in FRET as it does not occur in the bulk solvent even with the same spectral overlap integral. The results points to the applications of gels as efficient FRET medium without varying other parameters necessary for FRET.

REFERENCES

(1) Cotlet, M.; Vosch, T.; Habuchi, S.; Weil, T.; Mullen, K.; Hofkens, J.; De Schryver, F. *J. Am. Chem. Soc.* **2005**, *127*, 9760.

(2) Das, A. K.; Mondal, T.; Sasmal, D. K.; Bhattacharyya, K. *J. Chem. Phys.* **2011**, *135*, 074507.

(3) Ghosh, S.; Dey, S. A., A; Mandal, U.; Bhattacharyya, K. *J. Phys. Chem. B.* **2007**, *111*, 7085.

(4) Goldman, E. R.; Medintz, I. L.; Whitley, J. L.; Hayhurst, A.; Clapp, A. R.; Uyeda, H. T.; Deschamps, J. R.; Lassman, M. E.; Mattoussi, H. *J. Am. Chem. Soc.* **2005**, *127*, 6744.

(5) Jordanides, X. J.; Scholes, G. D.; Fleming, G. R. *J. Phys. Chem. B.* **2001**, *105*, 1652.

(6) Jordanides, X. J.; Scholes, G. D.; Shapley, W. A.; Reimers, J. R.; Fleming, G. R. *J. Phys. Chem. B.* **2004**, *108*, 1753.

(7) Srinivas, G.; Yethiraj, A.; Bagchi, B. *J. Phys. Chem. B.* **2001**, *105*, 2475.

(8) Lakowicz, J. R. *Principles of Fluorescence Spectroscopy*, Second ed.; Kluwer Academic/Plenum Publishers, 1999.

(9) van der Meer, B. W. Förster Theory, in FRET - Förster Resonance Energy Transfer: From Theory to Applications; Medintz, I., Hildebrandt, N., Eds.; Wiley-VCH Verlag GmbH & Co. KGaA, Weinheim, Germany., **2013**.

(10) Valeur, B. *Resonance Energy Transfer and Its Applications, in Molecular Fluorescence: Principles and Applications*; Wiley-VCH Verlag GmbH, Weinheim, FRG., **2001**.

(11) Yun, C. S.; Javier, A.; Jennings, T.; Fisher, M.; Hira, S.; Peterson, S.; Hopkins, B.; Reich, N. O.; Strouse, G. F. *J. Am. Chem. Soc.* **2005**, *127*, 3115.

(12) Adhikari, A.; Das, D. K.; Sasmal, D. K.; Bhattacharyya, K. *J. Phys. Chem. A.* **2009**, *113*, 3737.

(13) Das, D. K.; Das, A. K.; Mondal, T.; Mandal, A. K.; Bhattacharyya, K. *J. Phys. Chem. B.* **2010**, *114*, 13159

(14) Sahu, K.; Ghosh, S.; Mondal, S. K.; Ghosh, B. K.; Sen, P.; Roy, D.; Bhattacharyya, K. *J. Chem. Phys.* **2006**, *125*, 044714.

(15) Mandal, A. K.; Das, A. K.; Mojumdar, S. S.; Bhattacharyya, K. *J. Indian. Chem. Soc.* **2011**, *88*, 1917.

(16) Mondal, S. K.; Ghosh, S.; Sahu, K.; Mandal, U.; Bhattacharyya, K. *J. Chem. Phys.* **2006**, *125*, 224710.

(17) Merchant, K. A.; Best, R. B.; Louis, J. L.; Gopich, I. V.; Eaton, W. A. *Proc.Natl. Acad. Sci. U.S.A.* **2007**, *104*, 1528.

(18) Rochas, C.; Lahaye, M. *Carbohydrate Polymers.* **1989**, *10*, 289.

(19) Arnott, S.; Fulmer, A.; Scott, W. E. *J. Mol. Biol.* **1974**, *90*, 269.

(20) Rees, D. A. *Biochem. J.* **1972**, *126*, 257.

(21) Itagaki, H.; Fukiishi, H.; Imai, T.; Watase, M. *Journal of Polymer Science: Part B: Polymer Physics* **2005**, *43*, 680.

(22) Narayanan, J.; Xiong, J. Y.; Liu, X. Y. *J. Phys: Conf. Ser.* **2006**, *28*, 83.

(23) Bulone, D.; Newman, J.; San Biagio, P. L. *Biophysical Journal Volume* **1997**, *72* 388.

(24) Perrin, D. D.; Armerego, W. L. F.; Perrin, D. R. *Purification of Laboratory Chemicals.*; Pergamon Press: Newyork., 1980.

(25) Nowakowska, J. The Refractive Indices of Ethyl Alcohol and W ater Mixtures. Master' s Theses Paper 668., Loyola University, Chicago, 1939.

(26) Byron, M. L.; Variano, E. A. *Exp Fluids.* **2013**, *54*.

(27) Grant, D. C.; DeRitter, R. M.; Steege, E., K.; Fadeeva, A. T.; Castner, W. E. *Langmuir.* **2005**, *21*, 1745.

(28) Hoffman, J. B.; Choi, H.; Kamat, P. V. *J. Phys. Chem. C* **2014**, *118*, 18453.

(29) Kenney-Wallace, G. A.; Flint, J. H.; Wallace, S. C. *Chem. Phys. Lett.* **1975**, *32,*, 71.

(30) Mandal, U.; Ghosh, S.; Das, D. K.; Adhikari, A.; Dey, S.; Bhattacharyya, K. *J. Chem. Sci.* **2008**, *120*, 15.

(31) Ramzi, M.; Rochas, C.; Guenet, J. M. *Int. J. Biol. Macromol.* **2000**, *27*, 163.

Chapter 7

Concluding Remarks

This chapter summarizes the results of the investigations presented in this thesis. The scope of further studies based on the findings of the present work is also outlined.

7.1. Overview

This thesis is devoted to the study of two classes of promising materials, organic nanoparticles (ONPs) and gels. The main focus is to explore the photophysical properties and morphology of ONPs prepared using inverse reprecipitation technique and to compare their utility with the self-assembled dye aggregates. For this purpose, we have prepared the ONPs of three phenazenium dyes using reprecipitation method, characterized their morphology and studied the linear and non-linear optical behavior. A fluorescent gelator has been chosen, to study its fluorescence quenching in self- assembled and gel state using organic dyes. Low molecular weight non-fluorescent gelators which can form stable gels with organic solvents were employed to understand the interactions of guest molecules incorporated in gels with the gelator by monitoring the spectral properties of the fluorescent guest molecules. Förster resonance energy transfer (FRET) is explored in a non-fluorescent polymer gel for estimation of the donor-acceptor distance, which in turn helps in providing information on the pore size of the gel.

While the dyes, safranin O, safranin T, phenosafranin, oxatricarbocyanine, 4-aminophthalimide, coumarin 153, coumarin 102, rhodamine 6G and gelator, agarose were procured from commercial sources. The low molecular weight compounds used for the preparation of gels, oligophenylenevinylene and leucine based organogelator were synthesized, purified and characterized for the studies.

Several methods and instrumental techniques, which include NMR for compound characterization, TEM, SEM and AFM for morphology identifications of ONPs and gel, femtosecond Z-scan setup for the non-linear optical measurements, UV-vis spectrophotometer, steady-state and time-resolved fluorescence techniques for the ensemble photophysical studies, and time-resolved confocal fluorescence microscope for fluorescence measurements at single particle level have been employed for carrying out the work presented here. The results of the finding are summarized below.

Though many studies on the photophysical properties of aggregates have been carried out, understanding of the morphology, linear and nonlinear optical properties of dye nanoparticles prepared by induced aggregation has not explored. To compare the optical properties of dye nanoparticles with the self aggregates formed at higher dye concentrations, ONPs of three phenazenium dyes, safranin O (SFO), safranin T (SFT) and phenosafranin (PSF) were prepared using inverse reprecipitation method. It was found that the morphology of the aggregates can be tuned by controlling the concentration of the stock solution injected during the preparation of ONPs. A J-type interaction is indicated by the spectral data. A four-fold enhancement in the fluorescence quantum yield and considerable

increase in fluorescence lifetime with increasing particle size is observed. The Z-scan studies indicated a five-fold enhancement in the nonlinearity for the colloids. Thus, careful induced aggregation of phenazenium dyes particularly to form J-type aggregates resulted in the enhancement of optical properties in comparison to monomer. But the same "self aggregates" formed by increasing dye concentration quenched the dye fluorescence due to H aggregate formation.

Oligophenylenevinylenes (OPVs) are fluorescent gelator molecules which self aggregate to form fibrils in the initial stage, which then entangle to form gels. To understand the fluorescence quenching mechanism of OPVs with organic dyes, steady-state and time-resolved spectral properties of OPV in presence of oxatricarbocyanine (OCY) has been investigated in benzonitrile. It is observed that even though the spectral data of the two interacting partners indicate the possibility of FRET, the quenching is not dynamic in nature. The morphological investigations revealed the presence of two types of aggregates in OPV self-assembly. The analysis of the spectral data showed that the fluorescence quenching of OPV self-assembly was only due to the static quenching of one type of aggregates. The other aggregate does not take part in quenching thereby maintaining its fibrillar morphology. Moreover, OPV could not gelate in presence of OCY which supports the interactions between OPV and OCY. This study suggests that the gelation in OPV is actually a balance between the interactions between two types of aggregates.

4-Aminophthalimide (AP) and coumarin 153 (C153) are two dipolar fluorescence probes of comparable sizes which exhibit fluorescence properties,

highly sensitive to the environment due to intramolecular charge transfer (ICT) nature of the emitting state and also, hydrogen bonding interactions. Of the two molecules, the fluorescence properties of AP are more sensitive towards the hydrogen-bonding interaction compared to C153. To understand the interaction between the guest molecules and the gelator, we have encapsulated these probes (separately) in a leucine based organogel. The steady-state and time-resolved fluorescence measurements reveal that the C153 molecules are present in the solvent filled regions of the gel whereas AP molecules are located close to the gelator. Measurement of rotational times of the probes using fluorescence anisotropy experiments indicated specific interactions between AP molecules and gelator. It is commonly believed that the guest molecule in a gel resides in the solvent pools; it does not interact with the gelator and hence, does not influence the gelation process. Though this assumption is largely valid for the hydrogels, the present results clearly show that as far as the organogels are concerned, the intermolecular interactions between a gelator and a probe molecule can be an important factor in not only determining the location of the probe in a gel, but also influencing the process of gelation.

FRET between Coumarin 102 (C102) and rhodamine 6G (Rh6G) has been studied in agarose gel in 20% v/v ethanol-water mixture. C102 and Rh6G do not undergo FRET in bulk solvent, but are well known FRET pairs in heterogeneous media. FRET measurements have been carried out in gels using two different concentrations of agarose. The calculated donor-acceptor distance helps in the estimation of pore size of the gel as a function of agarose concentrations used for gel preparation. The convincing evidence of FRET is provided by the rise time of

the acceptor emission. The calculated donor-acceptor distance is found to be 45 and 52 Å for 0.075 and 0.3 weight percent agarose gels, respectively. These indicate that the pool size of the gel could be more than 52 Å. Thus it is evident that presence of ethanol decreases the pool size of agarose gel as the pool size of the gels made using same concentrations of monomer in water is ~150 Å.

7.2. Future scope

Spectral properties of self-aggregates have been explored extensively since early 1930's. Self-aggregates formed at higher dye concentrations are undesirable as they quench the fluorescence. This is why fluorescence measurements are carried out using dilute solutions. However, in heterogeneous media like cell membranes and vesicles, even when dilute solutions are used, due to the heterogeneity in the media, the molecules are forced to be dispersed in a particular region depending upon the polarity of the microenvironment. This results in aggregation of molecules and fluorescence quenching in these media is observed even when the solutions are dilute. Therefore molecules whose fluorescence properties enhance upon aggregation are ideally suited for probing heterogeneous media. In this context, we have investigated the linear and non-linear optical properties of phenazenium dye aggregates prepared by inverse reprecipitation method to compare their properties with that of the self-assemblies formed at higher concentrations of the dye. We could clearly see the enhancement in the optical properties of the dye nanoparticles prepared using inverse reprecipitation when compared to monomer. As the specific fabrication of J-aggregates does not follow any thumb rule, it is important to explore the various fabrication methods

to tune the interactions between molecules to enhance the properties of aggregates. As research on enhancing linear and non linear optical properties of the aggregates by simply varying the experimental conditions like temperature, pH, concentration/quantity of stock solutions injected during aggregate preparation are not well understood, one can explore this aspect.

Gels are formed by the self aggregation of molecules to form fibrils which entangle to form networks which can trap solvents. Therefore the properties of the self aggregates dictate the properties of gel. Earlier reports on the steady-state fluorescence quenching of OPV by organic dyes suggested FRET between OPV and dyes. However, by investigating the time-resolved fluorescence measurements we could understand that fluorescence quenching of OPV self aggregates in presence of cyanine dye, OCY is static in nature. Moreover, the spectral and morphological studies indicate the presence of multiple aggregates in OPV self assembly. Like OPVs, which are one of the important classes of gelators used, there are many other gelators whose nature of aggregation remains unexplored. These studies are important as gels are extensively employed in day-to-day applications.

Gels are well known for many applications owing to their semisolid nature which helps in the easy storage and transport. Gels are widely used in day-to-day needs like tooth paste, hair gel, sanitary napkins, baby wipes, cosmetics etc. The common belief is that, molecules encapsulated in gels reside in the solvent pools of the gel. But gelation itself is a balance between various intermolecular forces between the gelator molecules. Therefore it is expected that any other

intermolecular interactions induced in the media will affect gelation. But these studies in low molecular weight organogels have not been explored yet. We have conclusively established the importance of intermolecular interactions between gelator and guest molecules incorporated in the gel. However, since the interactions depend highly on the structures/functional groups of the gelator and guest molecules, there is a lot more to understand about specific interactions in various gels. This will also help us tuning the utility of various gels according to their specific interactions.

Photophysical processes in gel gained great attention recently due to the increased use of gels in various applications. But the use of photophysical processes for the characterization of gels is not a very commonly explored area of research. Even though gels are widely used in various applications, the basic understanding of the gel medium remains cumbersome. We have used FRET to obtain an idea about the pool size in the gel. Similarly, by employing various photophysical processes, characterizations of various properties of gels like microviscosity and micro polarity can be explored.